AD-A073 378 FLIGHT DYNAMICS RESEARCH CORP VAN NUYS CALIF F/G 21/5
HIGH SPEED EJECTORS.(U)
MAY 79 M ALPERIN, J WU F33615-77-C-3160
UNCLASSIFIED FDRC-3160-12-78 AFFDL-TR-79-3048 NL

| OF |
AD
A073378

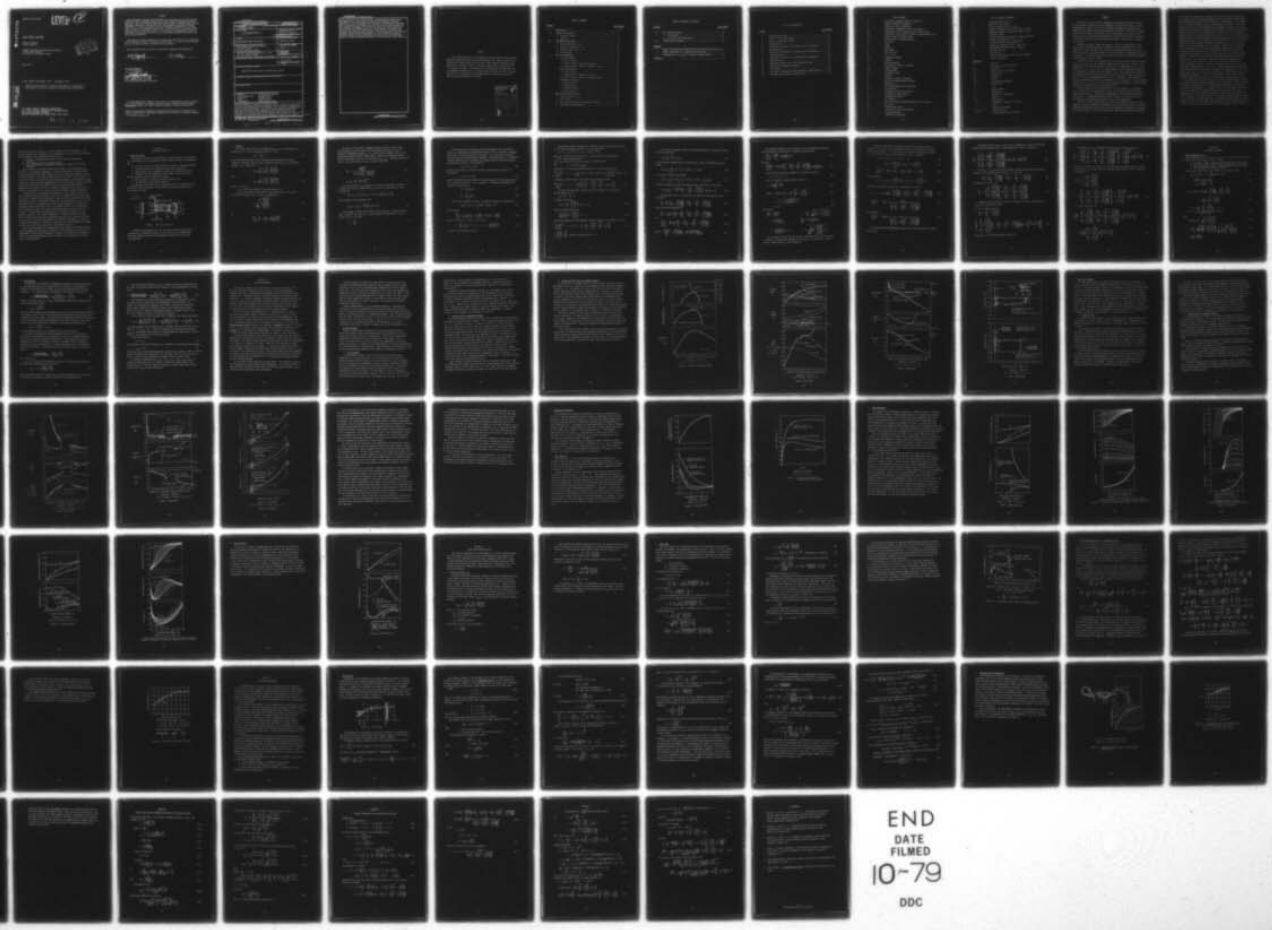

END
DATE
FILMED
10-79
DDC

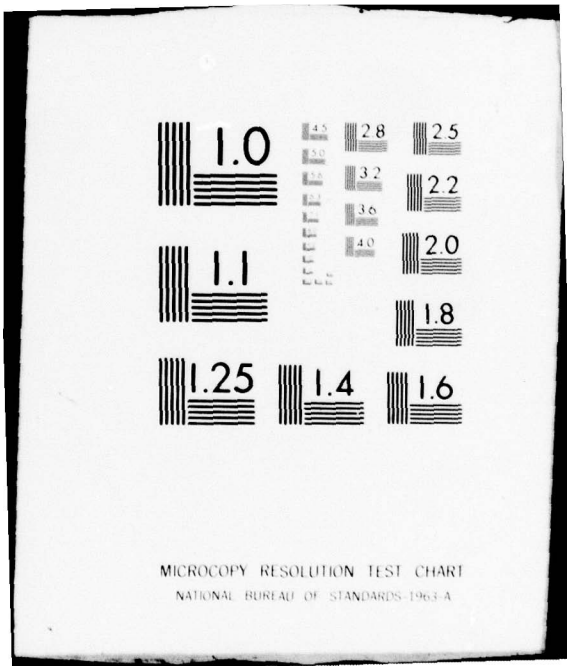
1.0
1.1
1.25
1.4
1.6
2.0
2.2
2.5
2.8
3.2
3.6
4.0
4.5
5.0
MICROCOPY RESOLUTION TEST CHART
NATIONAL BUREAU OF STANDARDS-1963-A

AFFDL-TR-79-3048

LEVEL II (2)

HIGH SPEED EJECTORS

Morton Alperin
Jiunn-Jenq Wu

Flight Dynamics Research Corporation
15809 Stagg Street
Van Nuys, California 91406

May 1979

Final Report September 1977 - December 1978

Approved for public release; distribution unlimited

AIR FORCE FLIGHT DYNAMICS LABORATORY
AIR FORCE WRIGHT AERONAUTICAL LABORATORIES
AIR FORSE SYSTEMS COMMAND
WRIGHT-PATTERSON AIR FORCE BASE, OHIO 45433

NOTICE

When Government drawings, specifications, or other data are used for any purpose other than in connection with a definitely related Government procurement operation, the United States Government thereby incurs no responsibility nor any obligation whatsoever; and the fact that the government may have formulated, furnished, or in any way supplied the said drawings, specifications, or other data, is not to be regarded by implication or otherwise as in any manner licensing the holder or any other person or corporation, or conveying any rights or permission to manufacture, use, or sell any patented invention that may in any way be related thereto.

This report has been reviewed by the Information Office (OI) and is releasable to the National Technical Information Service (NTIS). At NTIS, it will be available to the general public, including foreign nations.

This technical report has been reviewed and is approved for publication.

K. S. Hafarah

Rick Lindley

FOR THE COMMANDER

PETER J. BUTKEWICZ, Col, USAF
Chief, Aeromechanics Division
Air Force Flight Dynamics Laboratory

"If your address has changed, if you wish to be removed from our mailing list, or if the addressee is no longer employed by your organization please notify AFFDL/FXM *, W-PAFB, OH 45433 to help us maintain a current mailing list".*

Copies of this report should not be returned unless return is required by security considerations, contractual obligations, or notice on a specific document.

AIR FORCE/56780/14 August 1979 — 230

(9) Final rept. Sep 77 - Dec 78

UNCLASSIFIED

SECURITY CLASSIFICATION OF THIS PAGE (When Data Entered)

(17) **REPORT DOCUMENTATION PAGE**

READ INSTRUCTIONS BEFORE COMPLETING FORM

1. REPORT NUMBER (18) AFFDL-TR-79-3048	2. GOVT ACCESSION NO.
3. RECIPIENT'S CATALOG NUMBER	
4. TITLE (and Subtitle) (6) HIGH SPEED EJECTORS	5. TYPE OF REPORT & PERIOD COVERED Technical-Final Sept 1977 - Dec 1978
(14)	6. PERFORMING ORG. REPORT NUMBER FDRC-3160-12-78
7. AUTHOR(s) (10) Morton Alperin and Jiunn-Jeng Wu	8. CONTRACT OR GRANT NUMBER(s) (15) F33615-77-C-3160
9. PERFORMING ORGANIZATION NAME AND ADDRESS Flight Dynamics Research Corporation 15809 Stagg Street Van Nuys, California 91406	10. PROGRAM ELEMENT, PROJECT, TASK AREA & WORK UNIT NUMBERS (16) 2404-10-31 (11) 10
11. CONTROLLING OFFICE NAME AND ADDRESS Air Force Flight Dynamics Laboratory (FXM) Air Force Systems Command Wright-Patterson Air Force Base, Ohio 45433	12. REPORT DATE (11) May 1979
	13. NUMBER OF PAGES 79 (12) 92 p.
14. MONITORING AGENCY NAME & ADDRESS (if different from Controlling Office)	15. SECURITY CLASS. (of this report) Unclassified
	15a. DECLASSIFICATION/DOWNGRADING SCHEDULE

16. DISTRIBUTION STATEMENT (of this Report)

Approved for public release; distribution unlimited

17. DISTRIBUTION STATEMENT (of the abstract entered in Block 20, if different from Report)

18. SUPPLEMENTARY NOTES

19. KEY WORDS (Continue on reverse side if necessary and identify by block number)

Ejector	Boundary Layer Ingestion
Thrust Augmentation	Non-Uniform Flow
Propulsion	Thermal Mixing
Mixing	Kinetic Mixing
Jet-Diffusers	Translating Ejectors

20. ABSTRACT (Continue on reverse side if necessary and identify by block number)

The performance of solid and jet-diffuser ejectors in motion in their thrust direction was analyzed under the assumption that all fluids are compressible and have arbitrary properties. Two solutions to the equations representing the laws of mass flow and energy conservation and the momentum theorem were obtained. The solutions were examined and only those regions that were consistent with the Second Law of Thermodynamics were utilized. In these valid regions, three distinct characteristic points were observed, and chosen as criteria for classification of ejector performance. These characteristic points

DD FORM 1 JAN 73 1473 EDITION OF 1 NOV 65 IS OBSOLETE S/N 0102-014-6601

UNCLASSIFIED

SECURITY CLASSIFICATION OF THIS PAGE (When Data Entered)

determined which of nine possible ejector configurations provided optimal performance at any given flight and injected gas conditions. Detailed examination of the thermodynamic cycle was made for representative cases and data was presented to illustrate the influence of ejectors upon conventional gas generator performance. The influence of nozzle loss, skin friction and flow separation, incomplete kinetic and thermal mixing, and boundary layer ingestion were taken into consideration in the analysis. Correlation with existing stationary solid and jet-diffuser ejector experiments showed excellent agreement between theory and experiment. It has been shown that ejectors designed according th the methods described, can provide large improvement in propulsion system performance throughout the entire practical flight regime.

PREFACE

The research reported in this document was performed by Flight Dynamics Research Corporation during the period September 1977 through December 1978. Sponsorship was provided by the Air Force Flight Dynamics Laboratory under Contract No. F33615-77-C-3160. Technical coordination was provided by Dr. K.S. Nagaraja of AFFDL. The authors wish to acknowledge the foresight and encouragement provided by Dr. D. Zonars, Deputy Director of AFFDL (retired), and by Mr. P.P. Antonatos, Chief Aeromechanics Division AFFDL (retired), during the early phases of the effort.

TABLE OF CONTENTS

TABLE OF CONTENTS (Concluded)

LIST OF ILLUSTRATIONS

LIST OF SYMBOLS

A	duct area or parameter defined in Equation 35
B	parameter defined in Equation 36
a	primary jet area or thickness
C	coefficient or parameter defined in Equation 37
C_F	coefficient of skin friction (based on throat area)
C_f	coefficient of skin friction (based on wetted surface area)
c_v	specific heat at constant volume
c_p	specific heat at constant pressure
F	net thrust
f	force
ℓ	length
M	Mach number
$\dot{m}$	mass flow rate
n	$(= (\gamma - 1)/\gamma)$
P_o	stagnation pressure
p	pressure
q	dynamic pressure
R	gas constant, radius of curvature
Re_ℓ	Reynolds number
R_p	relative power
r	entrainment ratio
S	entropy
s	diffuser jet area or thickness
$\bar{\bar{s}}$	mass flow averaged specific entropy
T	temperature
$\bar{\bar{T}}_o$	mass flow averaged total temperature
t	jet thickness
U	secondary or mixed flow velocity
$\bar{U}$	averaged core flow velocity
U'	perturbation velocity
V	jet velocity
V'	jet velocity after lossless expansion from the plenum
X	duct width
$\tilde{X}$	effective duct width
x	coordinate in the thrust direction
y	lateral coordinate
z	longitudinal coordinate

α	inlet area ratio (= A_2/a_1)
β	diffuser jet exit angle
γ	ratio of specific heats (= c_p/c_v)
δ	geometric diffuser or outlet area ratio (= X_3/X_2)
δ^*	effective diffuser or outlet area ratio (= $\tilde{X}_3/X_2$)
η	efficiency factor
θ	diffuser jet angle with respect to thrust direction
ΔP	primary jet pressure rise (= $P_{or} - P_{o\infty}$)
ΔS	entropy production in the mixing duct
ΔT	primary jet temperature rise (= $T_{op} - T_{o\infty}$)
λ	non-dimensional mean velocity (= $\bar{U}/V_{pl}$)
μ	absolute viscosity
ρ	mass density
σ	effective diffuser area ratio of a jet-diffuser
ϕ	thrust augmentation

Subscripts

c	core flow
d	diffuser or ejector outlet duct
di	inlet drag
dj	diffuser jet or jet diffuser
e	ejector inlet
eff	effective
ej	ejector
exp	experimental measurement
i	induced flow
j	jet
N	primary nozzle
m	mixing duct
p	primary jet or propulsive
r	reservoir
ref	reference jet
o	unaugmented, stagnation or overall
T	total
t	stagnation or thermal
1,2,3,4,J	ejector stations
∞	undisturbed or ambient condition

SUMMARY

The effort was initiated by a mathematical treatment of the laws of mass flow and energy conservation and the momentum theorem as they apply to a model representing an ejector in which the processes of ingestion and mixing occur sequentially in separate and distinct regions of the duct. Injection is assumed to occur at the start of the mixing section, downstream of the ejector inlet. Mixing occurs in a constant cross-section duct after which the flow is exhausted in an outlet diffuser or nozzle to ambient pressure. Jet diffusion is applied if practical.

Injected and induced flows are assumed to consist of compressible, ideal fluids having arbitrary properties consistent with the perfect gas law. The losses due to inlet blockage, skin friction and incomplete thermal and kinetic mixing were taken into consideration in the formulation of the mathematical system of equations. In addition provision was made to assess the influence of boundary layer ingestion into the ejector.

Solutions of this set of equations were based upon assumed values of the area ratio α_∞ ($= X_2/a_\infty$), the environmental characteristics (U_e, p_∞, T_∞ and M_∞), the properties of the injected gas ($\dot{m}_p$, T_{op} and P_{or}), the magnitude of the loss coefficients (C_{di}, η_i, η_N, C_f, $\Delta\bar{s}$), the non-uniformity due to incomplete mixing and the pressure of the induced flow at Station 1 (p_1). With these given quantities, the characteristics of the flow at any station of the ejector and the outlet area ratio $\delta (= X_3/X_2)$ were determined from the set of equations. (The pressure, p_1, can be calulated by the same set of equations, if δ is specified). The performance parameters (ϕ, η_p, R_p, η_o, η_t) could then be evaluated in terms of the flow characteristics for any given set of input quantities.

When the density of the fluid does not vary with pressure or temperature (as in the case of an incompressible fluid) the ejector flow equations have a single valid solution. The functional dependence of density upon pressure and temperature in a compressible fluid however, results in a situation in which two solutions can represent physically realistic flow properties.

The first solution (under which the flow, after complete mixing, is always subsonic) provides information regarding the flow pattern, performance and ejector geometry corresponding to any given flight or operational condition and injected gas characteristics. Under this solution the resulting thermodynamic properties

of the mixed flow always are consistent with the mass flow and energy conservation laws and with the momentum theorem and the Second Law of Thermodynamics. An optimization procedure in which the value of the Mach Number of the induced flow at the start of mixing (M_1) was systematically varied over a wide range, indicated that the ejector performance was a maximum at one value of M_1 which depends upon the values of the other input parameters. Results of this numerical analysis indicated that the optimal value of M_1 under this first solution is always less than 1.0, but varied from values close to 1.0 to low subsonic values, depending upon the flight Mach Number and the characteristics of the injected gas. Ejector performance at this design point decreased from high values of thrust augmentation under stationary conditions to values close to 1.0 at the high subsonic flight Mach Numbers, when the injected, energized gas was unheated. With the injection of hot gas without mechanical compression, the ejector performance obtained from ejectors designed under this first solution with subsonic mixing remained very high over the entire range of practical flight Mach No's. Supersonic mixing provided high performance only at supersonic flight speeds. The injection of gases having high thermal and mechanical energy, as does the efflux from a turbo-jet, resulted in a decrease of ejector performance similar to that with unheated injected gas as the flight Mach Number varied from zero to about 0.5. Further increasing the flight Mach Number produced improved performance throughout the remainder of the practical flight speed range with ejectors designed under this first solution, with high temperature injected gas. Thus it is evident that at high flight speeds, ejectors operate effectively with hot gas injection under the first solution.

The second solution (under which the flow after complete mixing is always supersonic) provides information regarding the flow pattern, ejector performance and geometry corresponding to any given flight or operational condition and injected gas characteristics. Variation of M_1 over a wide range indicates that the total entropy of the completely mixed flow may be less than, equal to or greater than the sum of the total entropies of the primary and induced flows prior to mixing. Low subsonic values of M_1 generally produce negative changes of total entropy which increase as M_1 is increased, becoming greater than zero prior to $M_1 = 1.0$. Thus at some subsonic value of M_1 the entropy change $(S_2 - S_1)$ is zero. This point is chosen as one of two characteristic points under the

second solution. Continuing to increase M_1 results in positive entropy changes and in general, a functional dependence of thrust agumentation (ϕ) upon M_1 which has a local maximum at a value of M_1 which may be slightly less than 1.0, but which, in general, is greater than 1.0. This maximum ϕ is considered to be the second characteristic point under the second solution.

In general there are three distinct characteristic points, one which results from the use of the first solution and two of which result from the use of the second solution, all of which are consistent with the Second Law of Thermodynamics. The performance and the geometry of the ejector are determined by the flow characteristics at the design point or in other words ϕ, $\eta_{p,ej}$, $\eta_{t,ej}$, $\eta_{o,ej}$ are determined by the value of M_1(or p_1), the input quantities (α_∞, M_∞, $\Delta P/p_\infty$, $\Delta T/T_\infty$) and the calculated quantities (α, δ^*, λ_∞, λ_3, $V_{p\infty}/V_{p1}$).

Examples illustrating the dependence of ϕ upon M_1 are presented for both solutions at two operational conditions ($M_\infty = 0.3$ and $M_\infty = 2.0$) using injected gas characteristics corresponding to typical effluent gases from a fanjet at $M_\infty = 0.3$ and from a ramjet at $M_\infty = 2.0$, to illustrate the shape of the curves, the location of the three characteristic points and the criticality of the proper choice of M_1 or ejector configuration.

Ejector performance over the entire practical range of flight speeds is then presented for fanjet, ramjet, turbojet and rocket type gas generators at each of the three characteristic points, to illustrate the influence of combination thrusters on the performance of each type of gas generator acting as a free jet.

The use of a jet-diffuser modifies the set of equations since the flow does not return to ambient pressure at Station 3 as in the case when diffusion is accomplished by solid surfaces. The diffuser jet itself requires the injection of energized fluid whose momentum must be considered in the evaluation of ejector performance. The relationship among the diffuser jet slot thickness, angle of departure from the solid surface, the effective area ratio and the momentum requirement are presented for use in evaluating the performance of this type of ejector.

The real fluid effects and the influence of incomplete mixing are then discussed and compared with existing experiments performed under stationary conditions. The comparisons, using realistic values for the loss coefficients indicate agreement, proving the validity of the method and the relative unimportance of the requirement for complete mixing.

SECTION I

INTRODUCTION

Basically ejectors are suitably shaped ducts which are designed to capture ambient fluid and cause it to mix with a stream of energized fluid. This concept was first reduced to practice in the form of a pump which caused a large mass flow of essentially stationary fluid to flow against a small pressure head while being energized by a small mass flow of rapidly moving fluid. Recognition of the fact that the ejector process could provide an increase of momentum flux compared to that of the energized stream, stimulated the development of ejector thrust augmenters. Early theoretical analyses based upon the theory of flow of incompressible fluids appeared to indicate a large potential for augmenting the thrust of a fluid stream when the ambient fluid was induced to flow through the ejector from a stationary undisturbed state or when the ejector was at rest with respect to the undisturbed fluid. Motion of the ejector in its thrust direction appeared to result in a rapid decrease of net thrust with increasing ejector velocity. This observation, based upon some limited investigations which did not attempt to optimize the thrust augmentation by proper selection of ejector geometry and injected fluid characteristics, discouraged further attempts to utilize ejectors as thrust augmenters during translational motion. In addition, since the entrainment of ambient fluid was known to depend upon mixing of the energized stream with the ambient fluid, it was assumed that complete mixing was essential regardless of the cost. This assumption led to the design of ejectors having large cross-sections to capture large amounts of ambient fluid, and multiple injection jets of energized fluid to accelerate mixing. Further it was recognized that by incorporating a diffuser at the end of the mixing process, it was possible to reduce the throat pressure and to convert lost kinetic energy into useful energy thereby increasing the flow of ambient fluid per unit area and improving the propulsive efficiency. The use of diffusers however resulted in further increases in ejector length and diameter as well as the momentum loss due to skin friction and separation. Furthermore, if flow separation occurs in the diffuser, the diffuser area ratio is effectively reduced. As a matter of fact, without boundary layer control, effective

diffuser area ratios in excess of 2 do not exist in ejector technology. Thus ejector thrusters were considered to be impractical on the basis of three concepts derived primarily from incompressible flow theory.

1) Decrease of augmenting capability with increasing translational velocity.
2) Long length required for complete mixing.
3) Large transverse and longitudinal dimensions required for effective diffusion.

Recent advances in diffuser design have resulted in the development and testing of a jet-diffuser (Reference 1) which has the ability to achieve large diffuser area ratios with small lengths and lateral dimensions compared to those of solid diffusers. This concept involves the use of a high velocity thin jet of fluid, injected at the wall of the solid diffuser surface to avoid separation and to provide a curved jet sheet downstream of the solid surface to sustain a pressure gradient and thus extend the region in which the flow can diffuse and mix. Experiments have verified that solid surfaces downstream of the diffuser jet can diverge to half angles (β) at least as large as 60 degrees without separation.

Investigations of the optimized performance of solid diffuser ejectors in high speed motion in their thrust direction in an incompressible fluid have been carried out recently by FDRC (Reference 2) where it has been shown that the thrust augmentation does not necessarily decrease with increasing speed. In fact it has been shown that in an incompressible fluid, thrust augmentation increases with decreasing values of $q/\Delta P$, the ratio of the dynamic pressure to the pump head. Thus regardless of speed, the thrust augmentation remains constant when $q/\Delta P$ is constant. In other words if pump heads (ΔP) increases in proportion to the dynamic pressure (q), the thrust augmentation (ϕ) remains constant, provided other factors such as the inlet and diffuser area ratio are fixed and cavitation does not occur. This work was extended to include the jet-diffuser ejector and is reported in Reference 3, where it is shown that the thrust augmentation depends upon the ratio $q/\Delta P$ as in the case of a solid diffuser ejector.

With the background of the incompressible flow analyses, the effort reported in this document was undertaken to determine if the performance of ejectors in a compressible medium could be optimized in terms of the injected fluid characteristics so that high performance could be achieved at high speeds with selected types of gas generators.

SECTION II

TECHNICAL DISCUSSION

1. Analytical Model

The analysis of ejector flow properties and the evaluation of performance in a compressible fluid environment has been carried out under the assumptions that

1) All fluids involved in the processes are perfect, compressible gases.

2) Injected fluids are at arbitrary pressure and temperature.

3) Induced flow is at an arbitrary velocity and stagnation pressure.

4) Influences of inlet blockage or shock losses, skin friction and diffuser seperation are included in the analysis.

5) Mixing occurs in a region of constant cross-section.

6) Jet Diffusion is used where practical.

The schematic arrangement of this generalized ejector configuration with alternative inlets and outlets and the pertinent station designations are illustrated on Figure 1.

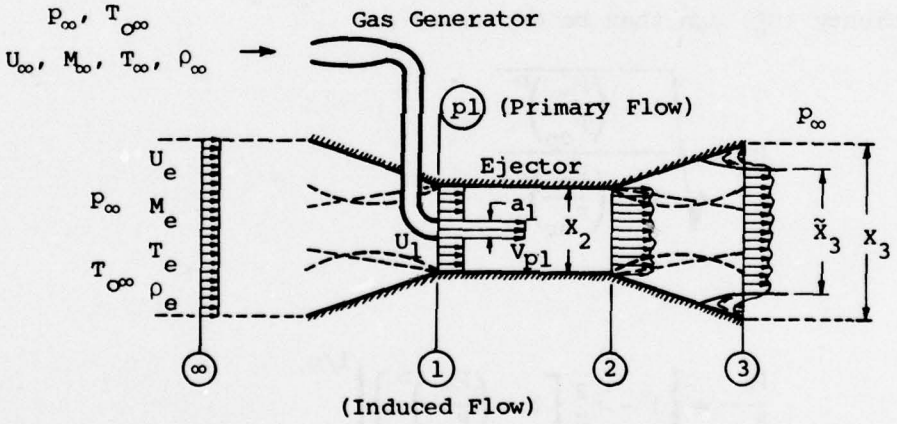

Figure 1. Generalized Ejectors

In general the equations of state, the laws of energy and mass flow conservation, the momentum theorem, and the Second Law of Thermodynamics have been imposed to obtain valid performance estimates and flow field configurations.

2. Analysis

The thrust efficiency of the primary nozzle (η_N) is represented by a reduction of the ideal, isentropic velocity. Thus

$$V_{p\infty} = \eta_N V_{p\infty}' \tag{1}$$

where the primed velocity is the velocity which would result from an isentropic expansion from the ideal stagnation pressure P_{or} to the ambient pressure (p_∞). Thus since

$$V_{p\infty}' = \sqrt{2c_p T_{op}\left[1 - \left(\frac{p_\infty}{P_{or}}\right)^n\right]} \tag{2}$$

and

$$V_{p\infty} = \sqrt{2c_p T_{op}\left[1 - \left(\frac{p_\infty}{P_{op}}\right)^n\right]} \tag{3}$$

where $n = (\gamma-1)/\gamma$

P_{or} is the ideal lossless reservior pressure and

P_{op} is the stagnation pressure of the primary nozzle (with loss).

The thrust efficiency (η_N) can then be expressed as

$$\eta_N = \sqrt{\frac{1 - \left(\frac{p_\infty}{P_{op}}\right)^n}{1 - \left(\frac{p_\infty}{P_{or}}\right)^n}} \tag{4}$$

or

$$\frac{p_\infty}{P_{op}} = \left\{1 - \eta_N^2\left[1 - \left(\frac{p_\infty}{P_{or}}\right)^n\right]\right\}^{1/n} \tag{5}$$

The inlet to the ejector is assumed to have a velocity U_e and a stagnation pressure P_{oe} which differ from the freestream velocity U_∞ and the isentropic stagnation pressure $P_{o\infty}$, as a result of the boundary layer or wave formation associated with the vehicle drag. However the stagnation temperature is identical to that of the freestream ($T_{oe} = T_{o\infty}$). Assuming the velocity ratio at the ejector inlet is U_e/U_∞, it can be shown that

$$M_e^2 = \frac{M_\infty^2\left(\frac{U_e}{U_\infty}\right)^2}{1 + \frac{\gamma-1}{2} M_\infty^2 \left[1 - \left(\frac{U_e}{U_\infty}\right)^2\right]} \tag{6}$$

$$P_{oe}/p_\infty = \left(1 + \frac{\gamma-1}{2} M_e^2\right)^{1/n} \tag{7}$$

The skin friction at the surfaces of the inlet of the ejector results in a further loss which is represented by an inlet loss coefficient C_{di} which is defined as

$$P_{oe} - P_{o1} = (\rho_1/2)U_1^2 C_{di} = (\gamma/\gamma-1)p_1 C_{di}\left[(P_{o1}/p_1)^n - 1\right]$$

which reduces to the convenient form

$$P_{oe}/p_1 = P_{o1}/p_1 + \frac{C_{di}}{n}\left[(P_{o1}/p_1)^n - 1\right] \tag{8}$$

This concept is useful when viscous drag is dominant. However when wave drag is dominant the inlet loss is more conveniently expressed as an inlet recovery factor (η_i) where

$$\eta_i = \frac{P_{o1}}{P_{oe}} \tag{9}$$

The mixing process is analyzed under the assumptions that the process occurs in a constant area duct between Stations 1 and 2, from known, uniformly distributed, arbitrary properties at Station 1 to a final state at Station 2 where the mixing is only partially completed. The mixing process is considered as being comprised of two processes; the thermal mixing in which the density distribution at Station 2 is described as

$$\rho_2(y) = \bar{\rho}_2 + \rho_2'(y) \tag{10}$$

and the kinetic mixing in which the velocity distribution at Station 2 is described as

$$U_2(y) = \bar{U}_2 + U_2'(y) \tag{11}$$

where the primed terms are assumed to be small compared to the average quantities. Pressure at Station 2 (p_2) is assumed to be uniformly distributed in a transverse direction, and

$$\bar{\rho}_2 = \frac{1}{X_2} \int_{X_2} \rho_2 dy \tag{12}$$

$$\bar{U}_2 = \frac{1}{X_2} \int_{X_2} U_2 dy \tag{13}$$

Under these conditions, the law of energy conservation is expressed as

$$T_{op}\dot{m}_p + T_{o\infty}\dot{m}_i = \int_{X_2} T_{o2} d\dot{m}_c = \bar{\bar{T}}_{o2}(\dot{m}_p + \dot{m}_i) \tag{14}$$

and therefore

$$\frac{\bar{\bar{T}}_{o2}}{T_{op}} = \frac{1}{\dot{m}_p + \dot{m}_i}\left(\dot{m}_p + \dot{m}_i \frac{T_{o\infty}}{T_{op}}\right) = \frac{1}{1 + r}\left(1 + r \frac{T_{o\infty}}{T_{op}}\right) \tag{15}$$

where if we define $\alpha = X_2/a_1 = (X_1 + a_1)/a_1$

$$r = \frac{\dot{m}_i}{\dot{m}_p} = \frac{\rho_1}{\rho_{p1}} (\alpha - 1)\ \lambda_1 = (\alpha - 1)\ \lambda_1 \frac{T_{p1}}{T_{op}} \frac{T_{op}}{T_{o\infty}} \frac{T_{o1}}{T_1} \tag{16}$$

in view of the equation of state.

The momentum theorem including the influence of a frictional force (f_m) due to skin friction between Stations 1 and 2 is expressed as

$$p_2 X_2 + \int_{X_2} \rho_2 U_2^2 dy + f_m = p_1 X_2 + \dot{m}_p V_{pl} + \dot{m}_i U_1 \tag{17}$$

where f_m = Force due to skin friction in the mixing duct (2-dimensional).

If ℓ_m = Length of mixing duct

and C_{fm} = Coefficient of skin friction in the mixing duct,

then

$$f_m = (\bar{\rho}_2/2)\bar{U}_2^2 C_{fm}(2\ell_m)$$

and Equation 17 is more conveniently written in a dimensionless form as

$$\frac{(p_2 - p_1)\alpha}{\rho_{pl} V_{pl}^2} = 1 + r\lambda_1 - \frac{1}{\dot{m}_p V_{pl}} \int (\bar{\rho}_2 + \rho_2')(\bar{U}_2 + U_2')^2 dy - C_{fm} \frac{\bar{\rho}_2 \bar{U}_2^2 X_2}{\rho_{pl} a_1 V_{pl}^2} (\ell_m/X_2) \tag{18}$$

Integration, neglecting the third order term, yields the result

$$\frac{(p_2 - p_1)\alpha}{\rho_{pl} V_{pl}^2} = 1 + r\lambda_1 - \frac{\bar{\rho}_2 \bar{U}_2^2 X_2}{\dot{m}_p V_{pl}} \left[1 + 2\frac{\overline{\rho_2' U_2'}}{\bar{\rho}_2 \bar{U}_2} + \frac{\overline{U_2'^2}}{\bar{U}_2^2} + C_{fm}(\ell_m/X_2) \right] \tag{19}$$

The mass flow continuity equation under the assumptions of incomplete mixing takes the form

$$\int_{X_2} \rho_2 U_2 dy = \dot{m}_p + \dot{m}_i$$

or after integration

$$\bar{\rho}_2 \bar{U}_2 X_2 \left(1 + \frac{\overline{\rho_2' U_2'}}{\bar{\rho}_2 \bar{U}_2} \right) = \dot{m}_p + \dot{m}_i = \dot{m}_c \tag{20}$$

and in a dimensionless form

$$\frac{\bar{\rho}_2 \bar{U}_2 X_2}{\rho_{pl} V_{pl} a_1} \left(1 + \frac{\overline{\rho_2' U_2'}}{\bar{\rho}_2 \bar{U}_2} \right) = 1 + r \tag{21}$$

which when combined with the momentum equation (Equation 19) provides the result

$$\frac{(p_2 - p_1)\alpha}{\rho_{pl} V_{pl}^2} = 1 + r\lambda_1 - (1 + r)\lambda_2 \left(1 + \frac{\overline{\rho_2' U_2'}}{\bar{\rho}_2 \bar{U}_2} + \frac{\overline{U_2'^2}}{\bar{U}_2^2} + \frac{1}{2} C_F \right) \tag{22}$$

if $\dfrac{\overline{\rho_2' U_2'}}{\bar{\rho}_2 \bar{U}_2}$; $\dfrac{\overline{U_2'^2}}{\bar{U}_2^2}$; and $C_F (= 2C_{fm}(\ell_m/X_2))$ are $\ll 1$.

To evaluate the pressure terms in the momentum equation, consider the total enthalpy at Station 2.

$$\frac{\gamma}{\gamma - 1}\frac{p_2}{\rho_2} + \frac{U_2^2}{2} = c_p T_{o2} \tag{23}$$

which when mass averaged over the cross-section, under the assumed conditions becomes

$$\frac{\gamma}{\gamma - 1} p_2 \int_{X_2} \frac{d\dot{m}}{\rho_2} + \frac{1}{2}\int (\bar{U}_2 + U_2')^2 d\dot{m} = c_p \int T_{o2} d\dot{m} \tag{24}$$

or since $d\dot{m} = \rho_2 U_2 dy$, this becomes

$$\frac{\gamma}{\gamma - 1} p_2 \int_{X_2} U_2 dy + \frac{1}{2}\int_{X_2} (\bar{\rho}_2 + \rho_2')(\bar{U}_2 + U_2')^3 dy = c_p \int_{X_2} T_{o2} d\dot{m} \tag{25}$$

and upon integration, neglecting third or higher order terms, this yields,

$$\frac{\gamma}{\gamma - 1} p_2 \bar{U}_2 X_2 + \frac{\bar{\rho}_2 \bar{U}_2^3 X_2}{2}\left(1 + 3\frac{\overline{U_2'^2}}{\bar{U}_2^2} + 3\frac{\overline{\rho_2' U_2'}}{\bar{\rho}_2 \bar{U}_2}\right) = c_p \bar{\bar{T}}_{o2}(\dot{m}_p + \dot{m}_i) \tag{26}$$

Using Equation 20 or 21 to eliminate the mass flow terms results in the expression

$$\frac{p_2}{p_\infty} = \frac{\bar{\bar{T}}_{o2}}{T_\infty}\frac{\bar{\rho}_2}{\rho_\infty}\left(1 + \frac{\overline{\rho_2' U_2'}}{\bar{\rho}_2 \bar{U}_2}\right)\left[1 - \frac{\lambda_2^2}{J}\left(1 + 3\frac{\overline{U_2'^2}}{\bar{U}_2^2} + 2\frac{\overline{\rho_2' U_2'}}{\bar{\rho}_2 \bar{U}_2}\right)\right] \tag{27}$$

which can also be expressed as

$$\frac{p_2}{p_\infty} = J\frac{1 + r}{\alpha\lambda_2}\left(\frac{T_{op}}{T_{p1}} - 1\right)\left[1 - \frac{\lambda_2^2}{J}\left(1 + 3\frac{\overline{U_2'^2}}{\bar{U}_2^2} + 2\frac{\overline{\rho_2' U_2'}}{\bar{\rho}_2 \bar{U}_2}\right)\right]\frac{p_1}{p_\infty} \tag{28}$$

or

$$\frac{p_2 \alpha}{\rho_{p1} V_{p1}^2} = \frac{nJ}{2}\frac{1 + r}{\lambda_2}\left[1 - \frac{\lambda_2^2}{J}\left(1 + 3\frac{\overline{U_2'^2}}{\bar{U}_2^2} + 2\frac{\overline{\rho_2' U_2'}}{\bar{\rho}_2 \bar{U}_2}\right)\right] \tag{29}$$

where $J = \dfrac{2c_p \bar{\bar{T}}_{o2}}{V_{p1}^2} = \dfrac{\bar{\bar{T}}_{o2}/T_{op}}{1 - T_{p1}/T_{op}} = \dfrac{1 + r(T_{o\infty}/T_{op})}{(1 + r)(1 - T_{p1}/T_{op})}$ (30)

The remaining pressure term in Equation 22 can be expressed conveniently using the equation of state and the enthalpy relationship as

$$\frac{p_1\alpha}{\rho_{p1}V_{p1}^2} = \frac{RT_{p1}\alpha}{V_{p1}^2} = \frac{n\alpha}{2(T_{op}/T_{p1} - 1)} \tag{31}$$

Therefore

$$\frac{(p_2-p_1)\alpha}{\rho_{p1}V_{p1}^2} = \frac{1+r}{\lambda_2}\frac{nJ}{2}\left[1 - \frac{\lambda_2^2}{J}\left(1 + 3\frac{\overline{U_2'^2}}{\bar{U}_2^2} + 2\frac{\overline{\rho_2' U_2'}}{\bar{\rho}_2 \bar{U}_2}\right)\right] - \frac{n\alpha}{2(T_{op}/T_{p1}-1)} \tag{32}$$

Using the above expression, Equation 22 reduces to the form,

$$A\lambda_2^2 - B\lambda_2 + C = 0 \tag{33}$$

This is a quadratic equation whose solution is

$$\lambda_2 = \frac{B \pm \sqrt{B^2 - 4AC}}{2A} \tag{34}$$

where $$A = \frac{\gamma+1}{2\gamma} + \frac{1}{2}C_F + \frac{3-\gamma}{2\gamma}\frac{\overline{U_2'^2}}{\bar{U}_2^2} + \frac{1}{\gamma}\frac{\overline{\rho_2' U_2'}}{\bar{\rho}_2 \bar{U}_2} \tag{35}$$

$$B = \frac{1 + r\lambda_1 + \dfrac{n\alpha}{2(T_{op}/T_{p1} - 1)}}{1+r} \tag{36}$$

$$C = nJ/2 \tag{37}$$

noting that,

$$\frac{T_{op}}{T_{p1}} = \left(\frac{P_{op}}{p_1}\right)^n \qquad \lambda_1 = \frac{U_1}{V_{p1}} = \sqrt{\frac{T_{o\infty}}{T_{op}}\frac{1 - (p_1/P_{o1})^n}{1 - (p_1/P_{op})^n}}$$

$$J = \frac{\bar{\bar{T}}_{o2}/T_{op}}{1 - T_{p1}/T_{op}} \qquad \frac{\bar{\bar{T}}_{o2}}{T_{op}} = \frac{1 + r\,T_{o\infty}/T_{op}}{1+r}$$

$$r = \frac{T_{op}}{T_{o\infty}}\left(\frac{P_{o1}}{P_{op}}\right)^n(\alpha-1)\lambda_1 \qquad \alpha = \alpha_\infty\sqrt{\left(\frac{p_1}{p_\infty}\right)^{2-n}\frac{\left(\frac{P_{op}}{p_1}\right)^n - 1}{\left(\frac{P_{op}}{p_\infty}\right)^n - 1}}$$

In the absence of skin friction and with complete mixing, the two solutions of Equation 34 provide Mach numbers (M_{2I} and M_{2II}) which correspond to those across a normal shock wave (see Appendix A).

In order to establish the validity of solutions and to evaluate the pressure ratio (p_2/p_3) for a non-uniform flow, it is necessary to consider the entropy equation. It is convenient to consider the entropy at Stations 1, 2 and 3 using the free stream entropy as a base. Therefore

$$S_1 - S_\infty = \dot{m}_p (s_{p1} - s_\infty) + \dot{m}_i (s_1 - s_\infty) \tag{38}$$

$$= \dot{m}_p c_v \ln \frac{p_1/p_\infty}{(\rho_{p1}/\rho_\infty)^\gamma} + \dot{m}_p r\, c_v \ln \frac{p_1/p_\infty}{(\rho_1/\rho_\infty)^\gamma} \tag{39}$$

or $$\frac{S_1 - S_\infty}{\dot{m}_p R} = \frac{1+r}{n\gamma} \ln \frac{p_1}{p_\infty} - \frac{1}{n}\left(\ln \frac{\rho_{p1}}{\rho_\infty} + r \ln \frac{\rho_1}{\rho_\infty} \right) \tag{40}$$

and at Station 2

$$S_2 - S_\infty = \int_{X_2} c_v \ln \frac{p_2/p_\infty}{(\rho_2/\rho_\infty)^\gamma}\, d\dot{m}_c = \int_{X_2} c_v \rho_2 U_2 \ln \frac{p_2/p_\infty}{(\rho_2/\rho_\infty)^\gamma}\, dy \tag{41}$$

which upon integration becomes, (see Appendix B for details)

$$S_2 - S_\infty = c_v \bar{\rho}_2 \bar{U}_2 X_2 \left(1 + \frac{\overline{\rho_2' U_2'}}{\bar{\rho}_2 \bar{U}_2}\right)\left[\ln \frac{p_2/p_\infty}{(\bar{\rho}_2/\rho_\infty)^\gamma} - \frac{\gamma}{2}\left(\frac{\overline{\rho_2'^2}}{\bar{\rho}_2^2} + 2 \frac{\overline{\rho_2' U_2'}}{\bar{\rho}_2 \bar{U}_2} \right)\right] \tag{42}$$

$$\frac{S_2 - S_\infty}{\dot{m}_p R} = \frac{1+r}{n\gamma} \ln \frac{p_2/p_\infty}{\left\{ \frac{\bar{\rho}_2}{\rho_\infty}\left[1 + \frac{1}{2}\left(\frac{\overline{\rho_2'^2}}{\bar{\rho}_2^2} + 2 \frac{\overline{\rho_2' U_2'}}{\bar{\rho}_2 \bar{U}_2} \right)\right]\right\}^\gamma} \tag{43}$$

and similarly

$$\frac{S_3 - S_\infty}{\dot{m}_p R} = \frac{1+r}{n\gamma} \ln \frac{1}{\left\{ \frac{\bar{\rho}_3}{\rho_\infty}\left[1 + \frac{1}{2}\left(\frac{\overline{\rho_3'^2}}{\bar{\rho}_3^2} + 2 \frac{\overline{\rho_3' U_3'}}{\bar{\rho}_3 \bar{U}_3} \right)\right]\right\}^\gamma} \tag{44}$$

The Second Law of Thermodynamics applied to the mixing process dictates that $S_2 \geq S_1$.

The pressure ratio p_2/p_3 (= p_2/p_∞) can be expressed in terms of the entropy change between Stations 2 and 3, using Equations 43 and 44, as follows.

$$\frac{p_2}{p_\infty} = \left\{ \frac{\bar{\rho}_2 \left[1 + \frac{1}{2} \left(\frac{\overline{\rho_2'^2}}{\bar{\rho}_2^2} + 2 \frac{\overline{\rho_2' u_2'}}{\bar{\rho}_2 \bar{u}_2} \right) \right]}{\bar{\rho}_3 \left[1 + \frac{1}{2} \left(\frac{\overline{\rho_3'^2}}{\bar{\rho}_3^2} + 2 \frac{\overline{\rho_3' u_3'}}{\bar{\rho}_3 \bar{u}_3} \right) \right]} \right\}^\gamma \exp \left(- \frac{n\gamma}{1 + r} \frac{\bar{\bar{s}}_3 - \bar{\bar{s}}_2}{\dot{m}_p R} \right) \tag{45}$$

Since $\bar{\bar{T}}_{o3} = \bar{\bar{T}}_{o2}$, the mass flow averaged enthalpy relationship described by Equation 27 can be expressed at Station 3 in the form,

$$1 = \frac{\bar{\bar{T}}_{o2}}{T_\infty} \frac{\bar{\rho}_3}{\rho_\infty} \left(1 + \frac{\overline{\rho_3' u_3'}}{\bar{\rho}_3 \bar{u}_3} \right) \left[1 - \frac{\lambda_3^2}{J} \left(1 + 3 \frac{\overline{u_3'^2}}{\bar{u}_3^2} + 2 \frac{\overline{\rho_3' u_3'}}{\bar{\rho}_3 \bar{u}_3} \right) \right] \tag{46}$$

dividing Eq. 27 by Eq. 46

$$\frac{p_2}{p_\infty} = \frac{\bar{\rho}_2}{\bar{\rho}_3} \frac{\left(1 + \frac{\overline{\rho_2' u_2'}}{\bar{\rho}_2 \bar{u}_2} \right) \left[1 - \frac{\lambda_2^2}{J} \left(1 + 3 \frac{\overline{u_2'^2}}{\bar{u}_2^2} + 2 \frac{\overline{\rho_2' u_2'}}{\bar{\rho}_2 \bar{u}_2} \right) \right]}{\left(1 + \frac{\overline{\rho_3' u_3'}}{\bar{\rho}_3 \bar{u}_3} \right) \left[1 - \frac{\lambda_3^2}{J} \left(1 + 3 \frac{\overline{u_3'^2}}{\bar{u}_3^2} + 2 \frac{\overline{\rho_3' u_3'}}{\bar{\rho}_3 \bar{u}_3} \right) \right]} \tag{47}$$

Combination of Equations 45 and 47 to eliminate $\bar{\rho}_2/\bar{\rho}_3$ and rearrangement to solve for λ_3, yields the result

$$\lambda_3^2 = \frac{J}{\left(1 + 3 \frac{\overline{u_3'^2}}{\bar{u}_3^2} + 2 \frac{\overline{\rho_3' u_3'}}{\bar{\rho}_3 \bar{u}_3} \right)} \times \left\{ 1 - \frac{\left(1 - \frac{1}{2} \frac{\overline{\rho_2'^2}}{\bar{\rho}_2^2} \right)}{\left(1 - \frac{1}{2} \frac{\overline{\rho_3'^2}}{\bar{\rho}_3^2} \right)} \left[1 - \frac{\lambda_2^2}{J} \left(1 + 3 \frac{\overline{u_2'^2}}{\bar{u}_2^2} + 2 \frac{\overline{\rho_2' u_2'}}{\bar{\rho}_2 \bar{u}_2} \right) \right] \left(\frac{p_\infty}{p_2} \right)^n \exp \left[\frac{n(\bar{\bar{s}}_3 - \bar{\bar{s}}_2)}{R} \right] \right\} \tag{48}$$

where p_2/p_∞ can be evaluated from Equation 28.

Elimination of p_2/p_∞ from Equation 45 and 47 provides the expression

$$\frac{\bar{\rho}_2}{\bar{\rho}_3}\,\frac{1+\dfrac{\overline{\rho_2' U_2'}}{\bar{\rho}_2\,\bar{U}_2}}{1+\dfrac{\overline{\rho_3' U_3'}}{\bar{\rho}_3\,\bar{U}_3}} = \left\{\frac{1-\dfrac{\lambda_2^2}{J}\left(1+3\,\dfrac{\overline{U_2'^2}}{\bar{U}_2^2}+2\,\dfrac{\overline{\rho_2' U_2'}}{\bar{\rho}_2\,\bar{U}_2}\right)}{1-\dfrac{\lambda_3^2}{J}\left(1+3\,\dfrac{\overline{U_3'^2}}{\bar{U}_3^2}+2\,\dfrac{\overline{\rho_3' U_3'}}{\bar{\rho}_3\,\bar{U}_3}\right)}\right\}^{\frac{1}{\gamma-1}}\left\{\frac{1-\frac{1}{2}\dfrac{\overline{\rho_2'^2}}{\bar{\rho}_2^2}}{1-\frac{1}{2}\dfrac{\overline{\rho_3'^2}}{\bar{\rho}_3^2}}\right\}^{\frac{\gamma}{\gamma-1}}\exp\left(\frac{\bar{\bar{s}}_3-\bar{\bar{s}}_2}{R}\right) \tag{49}$$

which is in a convenient form for use in evaluating the required effective outlet area ratio (δ^*) since from continuity applied between Stations 2 and 3, similarly to Equation 20,

$$\delta^* = \frac{\tilde{x}_3}{x_2} = \frac{\bar{\rho}_2\,\bar{U}_2\left(1+\dfrac{\overline{\rho_2' U_2'}}{\bar{\rho}_2\,\bar{U}_2}\right)}{\bar{\rho}_3\,\bar{U}_3\left(1+\dfrac{\overline{\rho_3' U_3'}}{\bar{\rho}_3\,\bar{U}_3}\right)}$$

$$= \frac{\lambda_2}{\lambda_3}\left\{\frac{1-\dfrac{\lambda_2^2}{J}\left(1+3\,\dfrac{\overline{U_2'^2}}{\bar{U}_2^2}+2\,\dfrac{\overline{\rho_2' U_2'}}{\bar{\rho}_2\,\bar{U}_2}\right)}{1-\dfrac{\lambda_3^2}{J}\left(1+3\,\dfrac{\overline{U_3'^2}}{\bar{U}_3^2}+2\,\dfrac{\overline{\rho_3' U_3'}}{\bar{\rho}_3\,\bar{U}_3}\right)}\right\}^{\frac{1}{\gamma-1}}\left\{\frac{1-\frac{1}{2}\dfrac{\overline{\rho_2'^2}}{\bar{\rho}_2^2}}{1-\frac{1}{2}\dfrac{\overline{\rho_3'^2}}{\bar{\rho}_3^2}}\right\}^{\frac{\gamma}{\gamma-1}}\exp\left(\frac{\bar{\bar{s}}_3-\bar{\bar{s}}_2}{R}\right) \tag{50}$$

or, since from Equation 48

$$\left(\frac{p_2}{p_\infty}\right)^n = \frac{\left(1-\frac{1}{2}\dfrac{\overline{\rho_2'^2}}{\bar{\rho}_2^2}\right)\left[1-\dfrac{\lambda_2^2}{J}\left(1+3\,\dfrac{\overline{U_2'^2}}{\bar{U}_2^2}+2\,\dfrac{\overline{\rho_2' U_2'}}{\bar{\rho}_2\,\bar{U}_2}\right)\right]}{\left(1-\frac{1}{2}\dfrac{\overline{\rho_3'^2}}{\bar{\rho}_3^2}\right)\left[1-\dfrac{\lambda_3^2}{J}\left(1+3\,\dfrac{\overline{U_3'^2}}{\bar{U}_3^2}+2\,\dfrac{\overline{\rho_3' U_3'}}{\bar{\rho}_3\,\bar{U}_3}\right)\right]}\exp\left[\frac{n(\bar{\bar{s}}_3-\bar{\bar{s}}_2)}{R}\right] \tag{51}$$

$$\delta^* = \frac{\lambda_2}{\lambda_3}\left(\frac{p_2}{p_\infty}\right)^{\frac{1}{\gamma}}\frac{\left(1-\frac{1}{2}\dfrac{\overline{\rho_2'^2}}{\bar{\rho}_2^2}\right)}{\left(1-\frac{1}{2}\dfrac{\overline{\rho_3'^2}}{\bar{\rho}_3^2}\right)}\exp\left[\frac{n(\bar{\bar{s}}_3-\bar{\bar{s}}_2)}{R}\right] \tag{52}$$

SECTION III

PERFORMANCE PARAMETERS

1. Thrust Augmentation (ϕ)

Thrust augmentation is defined as the ratio of the net thrust of an ejector to the net thrust of a reference "free" jet whose

a) Jet power is equal to that of the energized flow of the ejector
b) Mass flow is equal to that of the energized flow of the ejector
c) Ratio of mechanical energy to thermal energy is equal to that of the energized mass flow of the ejector.

Under these constraints, the net thrust of the reference jet is

$$F_{ref} = \dot{m}_p (V'_{p\infty} - U_\infty) = \dot{m}_p \left[(V_{p\infty}/\eta_N) - U_\infty \right] \tag{53}$$

and

$$\phi = \frac{\int \rho_3 U_3^2 dy - \dot{m}_i U_e - \dot{m}_p U_\infty}{\rho_{pl} a_1 V_{pl} \left(\frac{V_{p\infty}}{\eta_N} - U_\infty \right)} \tag{54}$$

$$\text{Since } \int \rho_3 U_3^2 dy = \bar{\rho}_3 \bar{U}_3^2 \tilde{X}_3 \left(1 + \frac{\overline{\rho'_3 U'_3}}{\bar{\rho}_3 \bar{U}_3} \right) \left(1 + \frac{\overline{\rho'_3 U'_3}}{\bar{\rho}_3 \bar{U}_3} + \frac{\overline{U'^2_3}}{\bar{U}_3^2} \right)$$

$$= \dot{m}_c \bar{U}_3 \left(1 + \frac{\overline{U'^2_3}}{\bar{U}_3^2} + \frac{\overline{\rho'_3 U'_3}}{\bar{\rho}_3 \bar{U}_3} \right) \tag{55}$$

$$\phi = \frac{(1 + r)\lambda_3 \left(1 + \frac{\overline{U'^2_3}}{\bar{U}_3^2} + \frac{\overline{\rho'_3 U'_3}}{\bar{\rho}_3 \bar{U}_3} \right) - r\,\lambda_e - \lambda_\infty}{(1/\eta_N)(V_{p\infty}/V_{pl}) - \lambda_\infty} \tag{56}$$

where

$$(1/\eta_N)(V_{p\infty}/V_{pl}) = \sqrt{\frac{1 - (p_\infty/P_{or})^n}{1 - (p_1/P_{op})^n}} \tag{57}$$

$$\lambda_\infty = \frac{U_\infty}{V_{pl}} = \sqrt{\frac{T_{o\infty}\left[1 - (p_\infty/P_{o\infty})^n \right]}{T_{op}\left[1 - (p_1/P_{op})^n \right]}} = \sqrt{\frac{\frac{\gamma-1}{2} M_\infty^2}{\frac{T_{op}}{T_\infty}\left[1 - \left(\frac{p_1}{p_{op}} \right)^n \right]}} \tag{58}$$

$$\lambda_e = \frac{U_e}{V_{pl}} = \left(\frac{U_e}{U_\infty} \right) \lambda_\infty \tag{59}$$

2. Propulsive Efficiency (η_p)

The propulsive efficiency of a free jet is commonly described as the ratio of the useful energy to the mechanical energy. Thus in general

$$\eta_p = \frac{\text{Thrust} \times \text{Velocity}}{\text{Mechanical Energy}} = \frac{\dot{m}_j (V_j - U_\infty) U_\infty}{(\dot{m}_j/2)(V_j^2 - U_\infty^2)} = \frac{2\, U_\infty}{V_j + U_\infty} \tag{60}$$

In the case of an ejector

$$\eta_{p,ej} = \frac{\dot{m}_p (V_{p\infty} - U_\infty) U_\infty \phi}{(\dot{m}_p/2)(V_{p\infty}^2 - U_\infty^2)} = \frac{2\phi\, U_\infty}{V_{p\infty} + U_\infty} \tag{61}$$

since the mechanical energy is that of its reference free jet whose mass flow, jet power and ratio of mechanical to thermal energy are equal to those of the ejector's energized flows, as in the reference jet used to describe thrust augmentation.

For non-air-breathing engines (rockets),

$$\eta_{p,\text{rocket}} = \frac{2\, U_\infty/V_j}{1 + (U_\infty/V_j)^2}, \text{ and, } \eta_{p,ej} = \phi\, \eta_{p,\text{rocket}} \tag{62}$$

3. Relative Power (R_p)

It is frequently of interest to compare thrusters on the basis of their power requirements when their net thrusts are equal. Since the equality of net thrust does not uniquely define the power relationship among thrusting systems it is necessary to impose additional constraints. In a system utilizing compressible fluids two additional constraints are required, and for purposes of the comparison of ejector systems with free jets these constraints are chosen to be the equality of energized mass flow and the equality of the ratio of mechanical to thermal energy. Thus

$$R_p = \frac{\text{Ejector Power}}{\text{Reference Jet Power}} = \frac{T_{op,ej} - T_{o\infty}}{T_{op,ref} - T_{o\infty}} \tag{63}$$

which in view of the constraints described above, reduces to the form

$$R_p = \frac{V_{p\infty}^2 - U_\infty^2}{V_{p\infty,ref}^2 - U_\infty^2} = \frac{V_{p\infty} + U_\infty}{\phi(V_{p\infty,ref} + U_\infty)} \tag{64}$$

since $F_{ej} = \dot{m}_p (V_{p\infty} - U_\infty)\phi = F_{ref} = \dot{m}_p (V_{p\infty,ref} - U_\infty)$

The equality of net thrusts and energized mass flows can be expressed as

$$\phi(V_{p\infty} - U_\infty) = V_{p\infty,ref} - U_\infty$$

or

$$V_{p\infty,ref} + U_\infty = \phi(V_{p\infty} + U_\infty) - 2(\phi - 1)U_\infty$$

and therefore

$$R_p = \frac{(V_{p\infty} + U_\infty)}{\phi^2(V_{p\infty} + U_\infty) - 2\phi(\phi - 1)U_\infty} = \frac{1}{\phi^2 - (\phi - 1)\eta_{p,ej}} = \frac{1}{\phi^2 - \phi(\phi - 1)\eta_{p,ref}} \quad (65)$$

since $\eta_{p,ej} = \phi\eta_{p,ref}$ as indicated by a comparison of Equations 60 and 61.

As can be observed from Equation 65, the ejector can be utilized to produce a given net thrust with a considerably smaller required jet power than that required by a free jet from a gas generator whose net thrust, mass flow and ratio of mechanical to thermal energies are equal to those of the ejector's injected jets. For example when $V_{p\infty} = U_\infty$, $R_p = 1/\phi$ and as in most application $V_{p\infty} >> U_\infty$ and $R_p \rightarrow 1/\phi^2$.

4. Efficiencies

To describe the performance of combination thrusters in which various types of gas generators are used in conjunction with ejectors, it is necessary to evaluate the influence of the ejector upon the cycle efficiencies of the gas generator. Thus conventionally, the propulsive efficiency of a free jet is

$$\eta_p = \frac{\text{Useful Energy}}{\text{Mechanical Energy}} = \frac{F_{p\infty}\, U_\infty}{\frac{1}{2}\dot{m}_p\,(V_{p\infty}^2 - U_\infty^2)} = \frac{2\,U_\infty}{V_{p\infty} + U_\infty} \tag{66}$$

and for an ejector, since $F_{ej} = \phi F_{ref}$, the propulsive efficiency referred to the injected mechanical energy

$$\eta_{p,ej} = \frac{2\phi U_\infty}{V_{p\infty} + U_\infty} \tag{67}$$

since the useful energy of the combination thruster is ϕ times the useful energy of its reference "free" jet which has the identical mechanical energy as that of the energized jet of the ejector. This definition of propulsive efficiency for ejectors is more useful than that which describes the ejector as a free jet. As a free jet if the ejector exhaust has a velocity U_3, its propulsive efficiency is

$$\eta'_{p,ej} = \frac{2\,U_\infty}{U_3 + U_\infty} \neq \eta_{p,ej} \tag{68}$$

since mechanical energy is not conserved in the ejector process.

Evaluation of propulsion system performance by means of the propulsive efficiency is unsatisfactory for comparison of various air breathing gas generator/ejector combination systems since defined in this manner useful energy is compared only to the jet mechanical energy; the thermal energy is neglected. Therefore the overall efficiency (η_o) is more appropriate for such comparisons. The overall efficiency is defined as the ratio of useful energy to the total jet energy

$$\eta_o = \frac{\text{Useful Energy}}{\text{Total Jet Energy}} = \frac{(V_{p\infty} - U_\infty)U_\infty}{c_p(T_{op} - T_{o\infty})} \tag{69}$$

for a "free" jet.

As in the definition of propulsive efficiency, the overall efficiency of a combination gas generator/ejector system is

$$\eta_{o,ej} = \phi\eta_o = \frac{\phi(V_{p\infty} - U_\infty)U_\infty}{c_p(T_{op} - T_{o\infty})} \tag{70}$$

since the useful energy is ϕ times that of the free reference jet and the total jet energy of the ejector is equal to that of its free reference jet.

Since the thermal efficiency (η_t) of a system is defined conventionally as the ratio of mechanical energy to total energy, it can be expressed for a "free" jet as

$$\eta_t = \frac{\text{Mechanical Energy}}{\text{Total Jet Energy}} = \frac{V_{p\infty}^2 - U_\infty^2}{2c_p(T_{op,ref} - T_{o\infty})} = \frac{F_{ref}(V_{p\infty} + U_\infty)}{2\dot{m}_p c_p(T_{op,ref} - T_{o\infty})} \quad (71)$$

This definition of thermal efficiency represents the distribution of the jet energy content, rather than the thermodynamic cycle efficiency. For example, an isentropically compressed jet (fanjet) contains 100% mechanical energy (100% conversion of mechanical energy to jet energy from any power source, such as jet engines, reciprocating engines, or electric motors), and has a 100% thermal efficiency as defined by Equation 71.

For an ejector in which the mass flow is augmented, the thermal efficiency is

$$\eta_{t,ej} = \frac{(\dot{m}_p + \dot{m}_i)(U_3^2 - U_\infty^2)}{2\dot{m}_p c_p(T_{op,ref} - T_{o\infty})} = \frac{F_{ref}(U_3 + U_\infty)}{2\dot{m}_p c_p(T_{op,ref} - T_{o\infty})} = \phi\eta_t \frac{U_3 + U_\infty}{V_{p\infty} + U_\infty} \quad (72)$$

$\eta_{t,ej}$ may be larger than or smaller than η_t depending upon the magnitude of the term $\phi(U_3 + U_\infty)/(V_{p\infty} + U_\infty)$. Examples illustrating the magnitude of the ratio $\eta_{t,ej}/\eta_t$, (mechanical energy output of ejector/mechanical energy output of reference jet) are presented in the following section.

Since for a free jet,

$$\eta_o = \eta_p \eta_t \quad (73)$$

by definition, the overall efficiency of a combined gas generator/ejector system is

$$\eta_{o,ej} = \phi\eta_o \quad (74)$$

indicating that the gas generator/ejector combination can produce ϕ times the useful work of that which can be produced by its reference "free" jet by virtue of its ability to convert lost mechanical and thermal energy to useful energy.

It should be emphasized that $\eta_{o,ej} = \eta'_{p,ej}\,\eta_{t,ej} \neq \eta_{p,ej}\,\eta_{t,ej}$ since the mechanical energy input does not equal the mechanical energy output of the ejector due to its intrinsic change of mechanical energy during mixing and the definition of $\eta_{p,ej}$ discussed previously.

SECTION IV

EJECTOR PERFORMANCE

The mixing of primary and induced flows in an ejector can result in two distinctly different conditions at the conclusion of the mixing process. Mathematically this is indicated by the quadratic nature of the equation for λ_2 (Equation 34). Physically this dual solution represents two different ejector geometries. It is shown in Appendix A that after complete mixing the Mach No. of the flow is less than 1.0 when using the negative sign in the solution of the quadratic equation and greater than 1.0 when the positive sign is used, and it is proven that, in the absence of skin friction, the two Mach No's are related by a normal shock wave relationship at the end of complete mixing.

The first solution corresponding to $M_2 < 1$ always represents a flow in which the total entropy change is greater than zero ($\bar{s}_2 \dot{m}_c > s_1 \dot{m}_i + s_{pl} \dot{m}_p$) and which therefore is consistent with the Second Law of Thermodynamics. The second solution is always consistent with the Second Law of Thermodynamics when $M_1 > 1$ (supersonic mixing), but at low subsonic values of M_1, it can result in mathematically correct solutions which represent a decrease of entropy or in which ($\bar{s}_2 \dot{m}_c < s_1 \dot{m}_i + s_{pl} \dot{m}_p$) across the mixing process, and which therefore is in violation of the Second Law of Thermodynamics. It therefore is essential to evaluate the entropy change before utilizing the results of these calculations.

A further characteristic of the solutions of the equations for the flow of a compressible fluid through an ejector is evidenced by regions where the solutions are complex. The limits of these regions are those points at which the discriminant in the solution of Equation 34 is zero. These two values represent a subsonic and a supersonic induced flow at Station 1. Values of M_1 between these limits produce complex solutions which indicate that the flow has become choked ($M_2 = 1.0$) at or prior to the completion of mixing. At the choking limits, the flow parameters are identical for each of the two solutions and the precise values of M_1 at which they occur depend upon the properties of the injected gas, the ejector geometry and the flight Mach number.

The solutions to these equations are also useful in the selection of ejector flow characteristics which produce optimum performance. In the regions where valid solutions are obtained, there are in general three distinct points or flow conditions which represent the best performance.

Extensive numerical analysis over large ranges of flight Mach No's. and injected gas characteristics have disclosed that in general the first solution represents a flow in which the maximum thrust augmentation occurs at subsonic values of M_1. The second solution represents a flow in which the maximum thrust augmentation exists at values of M_1 greater than, or slightly less than 1.0, and a limiting value of thrust augmentation at a subsonic value of M_1. This limiting value of thrust augmentation occurs at a point where the total entropy of the mixed flow at Station 2 is equal to the sum of the entropies of the unmixed primary and induced flows.

Further characterization of the functional dependence, limitations and optimization of the thrust augmentation under both solutions are discussed in terms of two specific examples to provide an indication of the method for optimal design of translating ejectors in a compressible medium. These calculations assume that the mixing is completed at Station 2, and that the flow is isentropic between Stations 2 and 3 ($\bar{\bar{s}}_3 = \bar{\bar{s}}_2$), and that $\eta_N = 1$, $C_{di} = C_F = 0$, $\delta^* = \delta$, $U_e = U_\infty$, $\gamma = 1.4$. In addition, the calculations were made for a fixed value of α_∞ to avoid variations of ejector size compared to primary jet size with variations of M_1.

1. Low speed example

During low speed flight, combination gas generator/ejector thrusters display good overall system characteristics when the gas generator is of the fanjet type or when the ejector is energized by a fluid which is mechanically compressed (isentropically) without the addition of heat energy. This is a result of the fact that at low flight speeds, high temperature jets have low thermal efficiencies. An example of the characteristics of the curves representing the ejector performance, flow properties, ejector geometry and thermodynamic cycles for both solutions during subsonic flight speeds are illustrated on Figure 2.

a. First solution

As illustrated on Figure 2, the first solution has a maximum thrust augmentation at a value of M_1 close to 1.0, at which point the transfer of mechanical energy from the reference jet to the ejector flow is also a maximum. The flow characteristics illustrated on Figure 2 indicate a maximum entrainment ratio and a minimum (but positive) entropy change during mixing. Temperatures and pressures at various stations within the ejector are also presented in a dimensionless form on this figure. The local Mach No's and the corresponding area ratios are also illustrated on Figure 2, where it can be observed that under the first solution the value of M_1 at the optimal point is large than the free

stream Mach No., thus requiring an accelerating inlet. The fact that M_3 is smaller than M_2 and that both are subsonic indicates a decelerating outlet or diffuser is required at the specified conditions, resulting in a conventional ejector design.

The Mollier Diagram illustrated on Figure 2 at this optimal point of the first solution describes the properties of the energized flow and the ejector mixing process. Since the primary injected gas and the induced flow are assumed to undergo isentropic processes from their undisturbed state to Station 1, in this example, their specific entropies at Station 1 are equal, thus $s_1 = s_{p1} = s_\infty$ and $T_1 = T_{p1}$. Mixing in this case results in an increased entropy for both streams and is concluded with a small increase in specific enthalpy at the point, where primary and induced flows are completely mixed. The recompression to ambient pressure is then assumed to be isentropic as indicated.

b. Second solution (supersonic mixing)

The second solution presents two distinct flow configurations which represent performance characteristics of interest. One of these occurs with supersonic mixing ($M_1 > 1$) and as shown on Figure 2, represents a situation in which the overall mechanical energy of the ejector flow, is a larger percentage of the mechanical energy of the reference jet than that at the optimal point of the first solution. The entropy change during mixing, the entrainment ratio and the pressures and temperature within the ejector are also described on Figure 2 for comparison with the first solution. As indicated, under the second solution, this optimal point has a positive but smaller entropy change and a smaller entrainment ratio than that of the optimal condition under the first solution. The Mach No's. and corresponding area ratios for this condition are presented on Figure 2 where it is evident that the inlet is accelerating and the outlet is decelerating. However since M_∞ is subsonic and M_1 is supersonic, the ejector inlet must have a converging/diverging De Lavel Nozzle, and since M_2 is supersonic, and M_3 is subsonic, the ejector outlet must be a converging/diverging De Laval Nozzle. The Mollier Diagram under this condition is presented on Figure 2.

Some additional features associated with this supersonic mixing point under the second solution include the facts that the thrust augmentation is only slightly dependent upon M_1 or outlet area ratio (δ) in this region and that the improved performance occurs with a smaller area ratio (δ) than that of the first solution.

c. Second solution (limit of subsonic mixing)

The other point of interest under the second solution provides a limiting performance within the Second Law of Thermodynamics which occurs during subsonic mixing ($M_1 < 1$). As indicated on Figure 2, this point represents the largest thrust augmentation among all three configurations of interest, a transfer of 100% of the mechanical energy of the reference jet to the ejector and as shown on Figure 2, zero total entropy change during mixing. The entrainment ratio is not a maximum at this point but is very close to that of the first solution. Temperatures and pressures are also indicated on Figure 2. The inlet of the ejector at this condition is accelerating and the outlet is a converging/diverging De Laval Nozzle providing a means for reduction of the Mach No. from a supersonic value at Station 2 to a subsonic value at Station 3 as indicated on Figure 2.

The Mollier Diagram for this cycle is presented on Figure 2 where it is shown to degenerate to a single isentropic line as a result of the assumption of isentropic compression and expansion and the selection of the point where the total entropy of the mixed flow is equal to the sum of the total entropies of the primary and induced flows. The loss of mechanical energy within the ejector in this case is zero.

It is of interest to note (Figure 2) that at this limiting point of subsonic mixing under the second solution the propulsive efficiency of the combined fanjet/ejector system can achieve values in the vicinity of 82% compared to 44% for the fanjet alone. This indicates a recovery, by the ejector, of a large percentage of the kinetic energy which is lost by the fanjet when operating as a free jet.

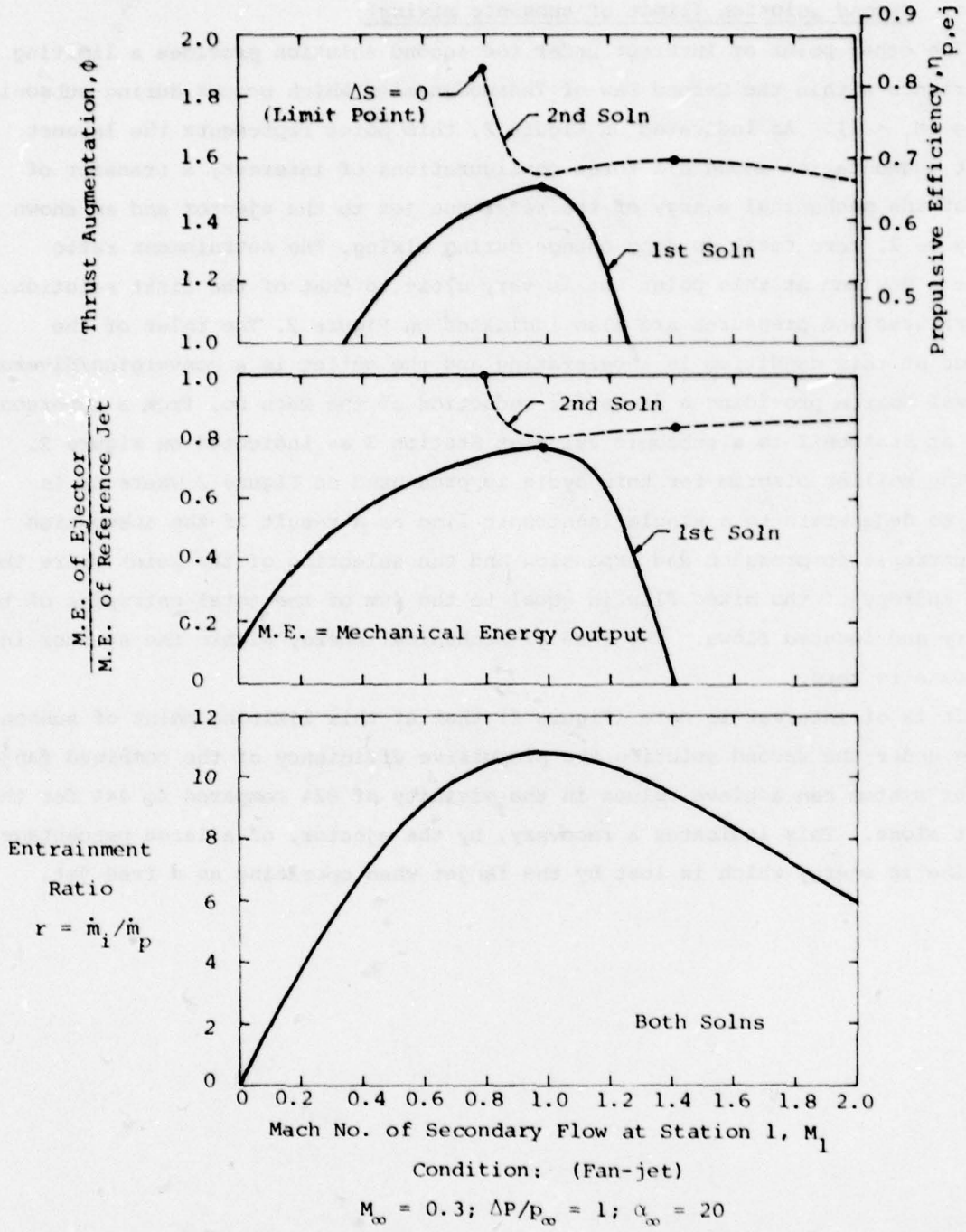

Condition: (Fan-jet)

$M_\infty = 0.3$; $\Delta P/p_\infty = 1$; $\alpha_\infty = 20$

Figure 2. Ejector in Low Speed Flight

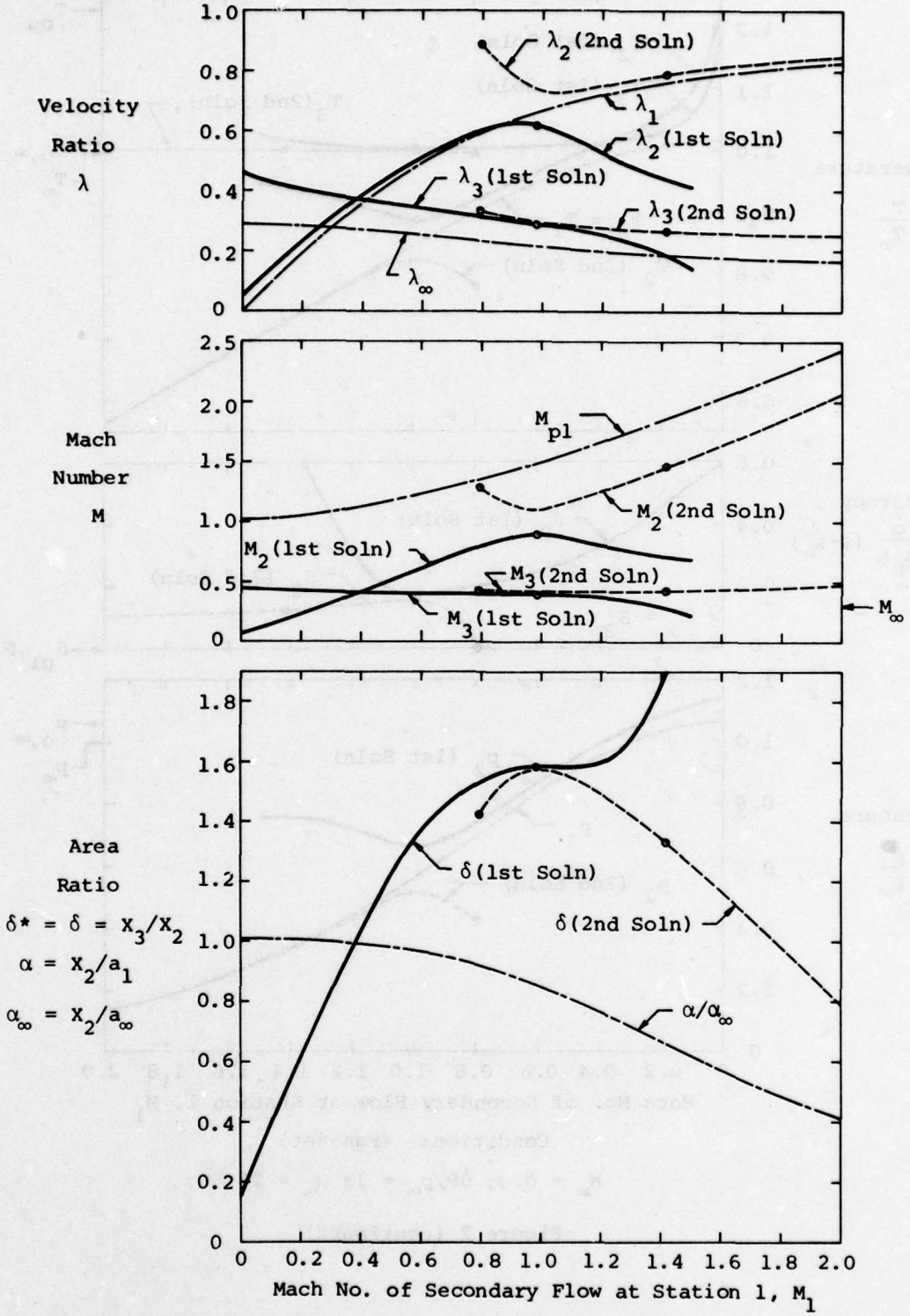

Condition: (Fan-jet)

$M_\infty = 0.3$; $\Delta P/p_\infty = 1$; $\alpha_\infty = 20$

Figure 2 (continued)

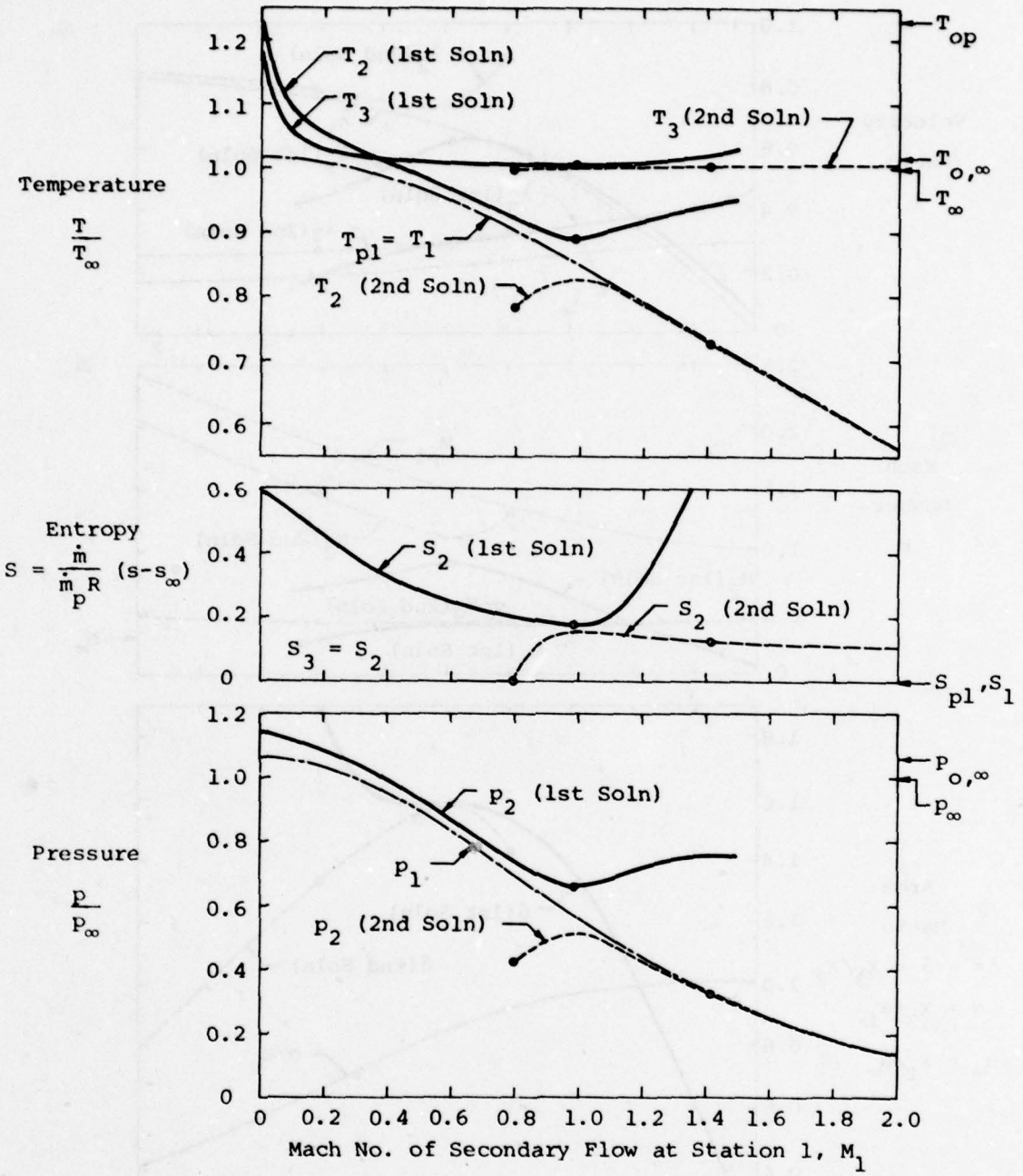

Condition: (Fan-jet)

$M_\infty = 0.3$; $\Delta P/p_\infty = 1$; $\alpha_\infty = 20$

Figure 2 (continued)

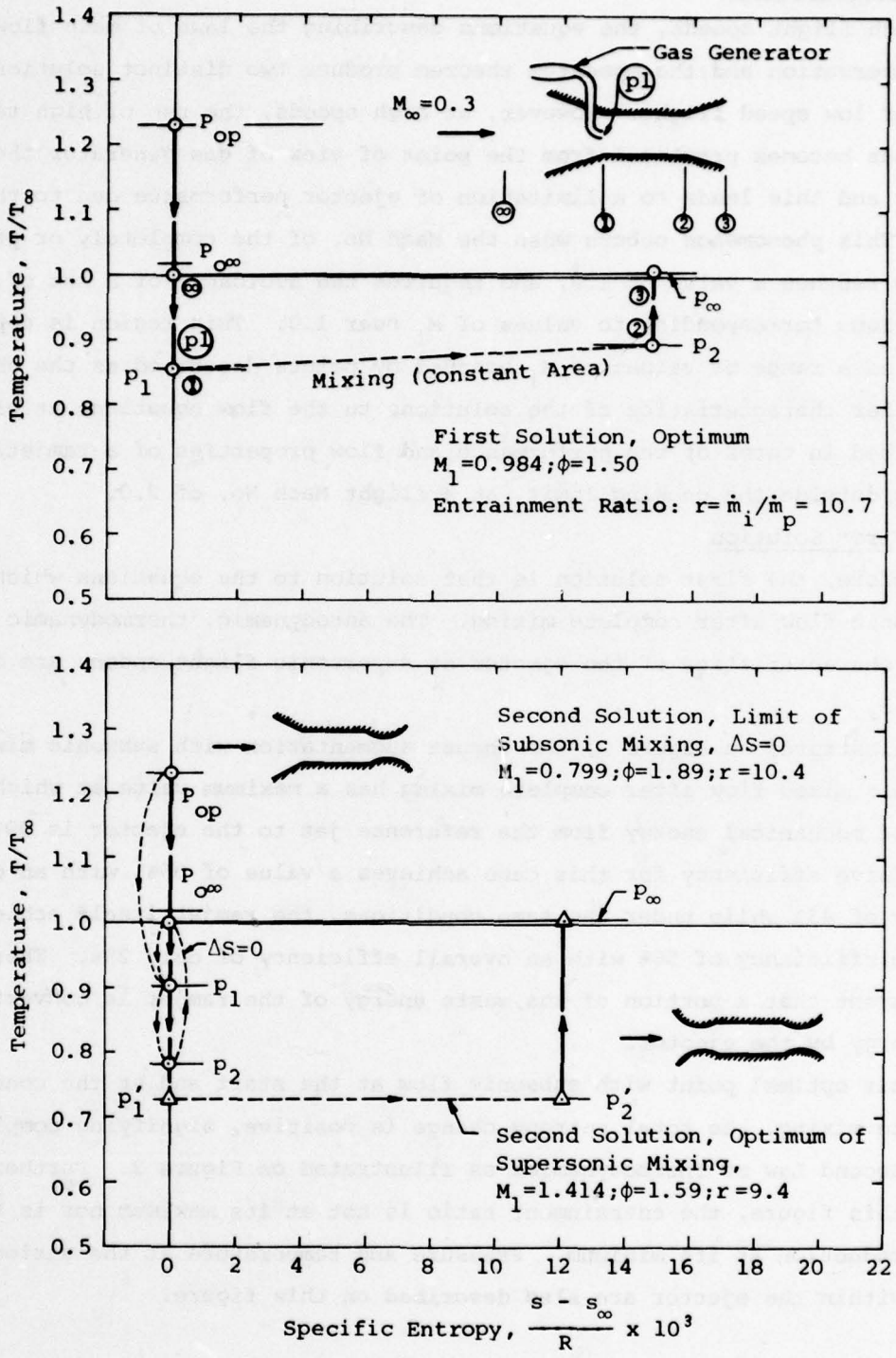

Condition: (Fan-jet)

M_∞ = 0.3; $\Delta P/p_\infty$ = 1; α_∞ = 20

Figure 2 (concluded)

2. High Speed Example

At high flight speeds, the equations describing the laws of mass flow and energy conservation and the momentum theorem produce two distinct solutions as in the case of low speed flight. However, at high speeds, the use of high temperature injected gas becomes practical from the point of view of gas generator thermal efficiency and this leads to a limitation of ejector performance due to thermal choking. This phenomenon occurs when the Mach No. of the completely or partially mixed flow reaches a value of 1.0, and requires the avoidance of a set of design configurations corresponding to values of M_1 near 1.0. This region is depicted on Figure 3, as a range of values of M_1 bounded by points described as the choking limit. Other characteristics of the solutions to the flow equations at high speeds are described in terms of the performance and flow properties of a ramjet/ejector in regions outside the choking limit, at a flight Mach No. of 2.0.

a. First Solution

As before, the first solution is that solution to the equations which result in a subsonic flow after complete mixing. The aerodynamic, thermodynamic and geometric characteristics of the ejector at supersonic flight speeds are described on Figure 3.

As illustrated on Figure 3, the thrust augmentation with subsonic mixing and subsonic mixed flow after complete mixing has a maximum value at which the transfer of mechanical energy from the reference jet to the ejector is 99%, and the propulsive efficiency for this case achieves a value of 96%, with an overall efficiency of 43% while under the same conditions, the ramjet itself achieves a propulsive efficiency of 56% with an overall efficiency of only 25%. Therefore it is apparent that a portion of the waste energy of the ramjet is converted to useful energy by the ejector.

At this optimal point with subsonic flow at the start and at the conclusion of complete mixing, the total entropy change is positive, signifying compliance with the Second Law of Thermodynamics as illustrated on Figure 3. Further as shown on this figure, the entrainment ratio is not at its maximum nor is the entropy production at its minimum. Pressure and temperature at the various stations within the ejector are also described on this figure.

The Mach No. and area ratios of the ejector flows are described on Figure 3. As illustrated, operation at this optimal point requires a converging/diverging, decelerating De Laval Nozzle at the inlet to the ejector and a converging/diverging, accelerating supersonic nozzle at the exit of the ejector. The area ratio of the converging/diverging, accelerating exit nozzle is 0.94, somewhat less than 1.0.

The Mollier Diagram showing the specific enthalpy vs. specific entropy changes occuring in the primary, energized flow and in the induced and mixed flows are presented on Figure 3. The large decrease in specific entropy and specific enthalpy of the primary flow and the corresponding small increase of these properties in the induced flow result in a net increase of the total entropy after mixing as a consequence of the large entrainment ratio. Thus the cycle at this optimal point is not in violation of the Second Law of Thermodynamics.

b. Second Solution (supersonic mixing)

The second solution, as before at low speeds, displays two distinct flow configurations of interest. One of these occurs with supersonic mixing and in this particular example is coincident with the first solution since the maximum thrust augmentation lies exactly at the supersonic choking limit.

As illustrated on Figure 3, the thrust augmentation and the transfer of mechanical energy are smaller than those with subsonic mixing but the advantage may result from the possibility of reduced inlet loss with supersonic values of M_1. Propulsive and overall efficiencies remain high compared to those of the ramjet alone.

Figure 3 indicates a positive change of total entropy and an entrainment ratio close to the maximum for this condition. Pressures and temperatures throughout the ejector are also described on this figure.

The local Mach No's. and area ratios are described on Figure 3 where as shown the inlet is a converging, decelerating nozzle ($M_1 < M_\infty$, but both are supersonic), while the outlet is a diverging, accelerating nozzle. The overall appearance of this ejector is identical to low speed, low temperature ejectors of the first solution.

The Mollier Diagram shown on Figure 3, is simlar to that with subsonic mixing, but as a consequence of the larger entrainment ratio, the primary fluid has a larger decrease of specific entropy while the entrained flow has a smaller increase of specific entropy.

c. Second Solution (limit of subsonic mixing)

This point is a limit imposed by the Second Law of Thermodynamics at which the change of total entropy is zero, and where the thrust augmentation and the transfer of mechanical energy are considerably larger than at the other optimal conditions.

As illustrated on Figure 3, the large value of thrust augmentation at the point where the performance is limited by the Second Law is a result of the conversion of thermal energy from the energized flow to mechanical energy of the ejector flow. Propulsive efficiencies in excess of 100% are achieved under these conditions while overall efficiencies are extremely large but remain less than 100%. Thus there is no violation of the law of energy conservation.

As indicated on Figure 3, the total entropy change is zero and the entrainment ratio is not at its maximum under these conditions. The pressure and temperature at Station 2 are at a minimum at this condition and as shown on Figure 3, the Mach No. at Station 2 is a maximum. Thus the high Mach No. at Station 2 is achieved primarily by a static pressure reduction (or expansion).

Figure 3 illustrates the Mach No's. and area ratios required to achieve the flow characteristics previously described. As indicated the inlet must be of the converging/diverging, decelerating, De Laval Nozzle with subsonic induced flow at Station 1. The outlet which accelerates the flow from a supersonic value at Station 2 to a higher supersonic value at Station 3 is diverging and accelerating.

The Mollier Diagram for operation at this point is illustrated on Figure 3. It is somewhat similar to the corresponding diagram for the other optimal points at this conditions but since the change of total entropy is smaller (zero) the decrease of specific entropy of the energized fluid is larger and the increase of specific entropy of the induced flow is smaller in magnitude than those of the other optimal points, despite an entrainment ratio somewhat smaller than that corresponding to supersonic mixing.

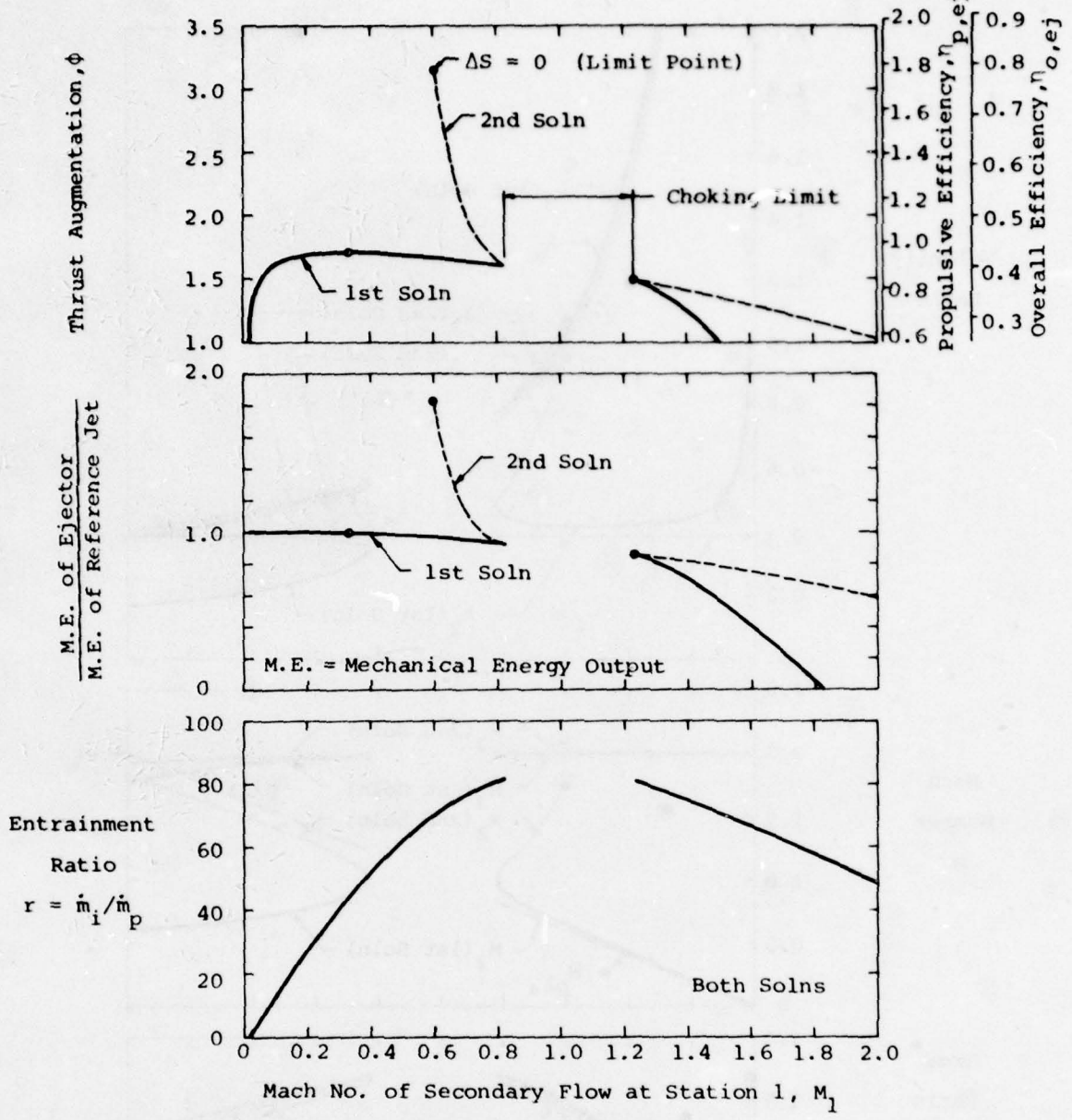

Condition: (Ram-jet)

$M_\infty = 2$; $\Delta P/p_\infty = 0$; $\Delta T/T_\infty = 10$; $\alpha_\infty = 20$

Figure 3. Ejector in High Speed Flight

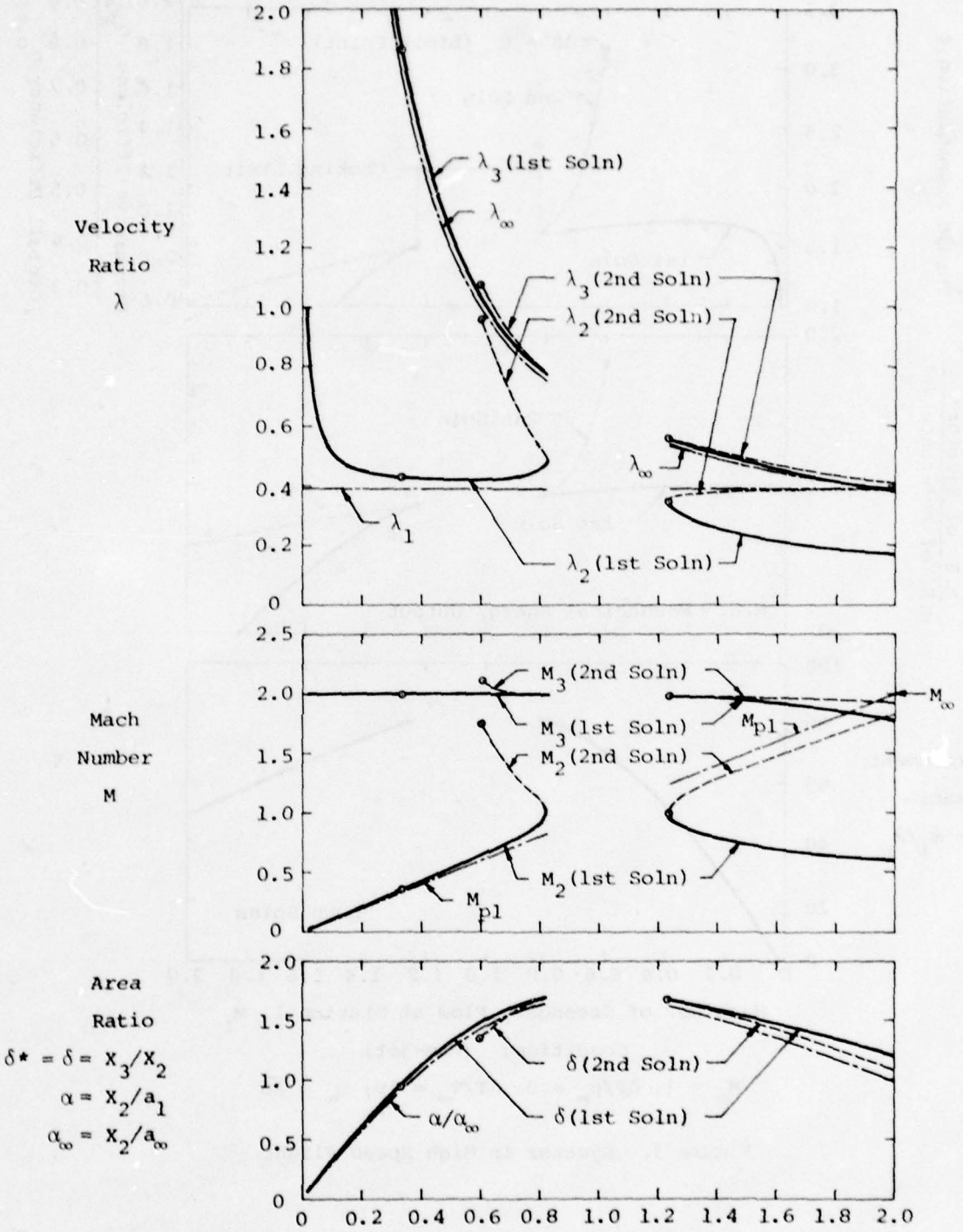

Condition: (Ram-jet)

$M_\infty = 2$; $\Delta P/p_\infty = 0$; $\Delta T/T_\infty = 10$; $\alpha_\infty = 20$

Figure 3 (continued)

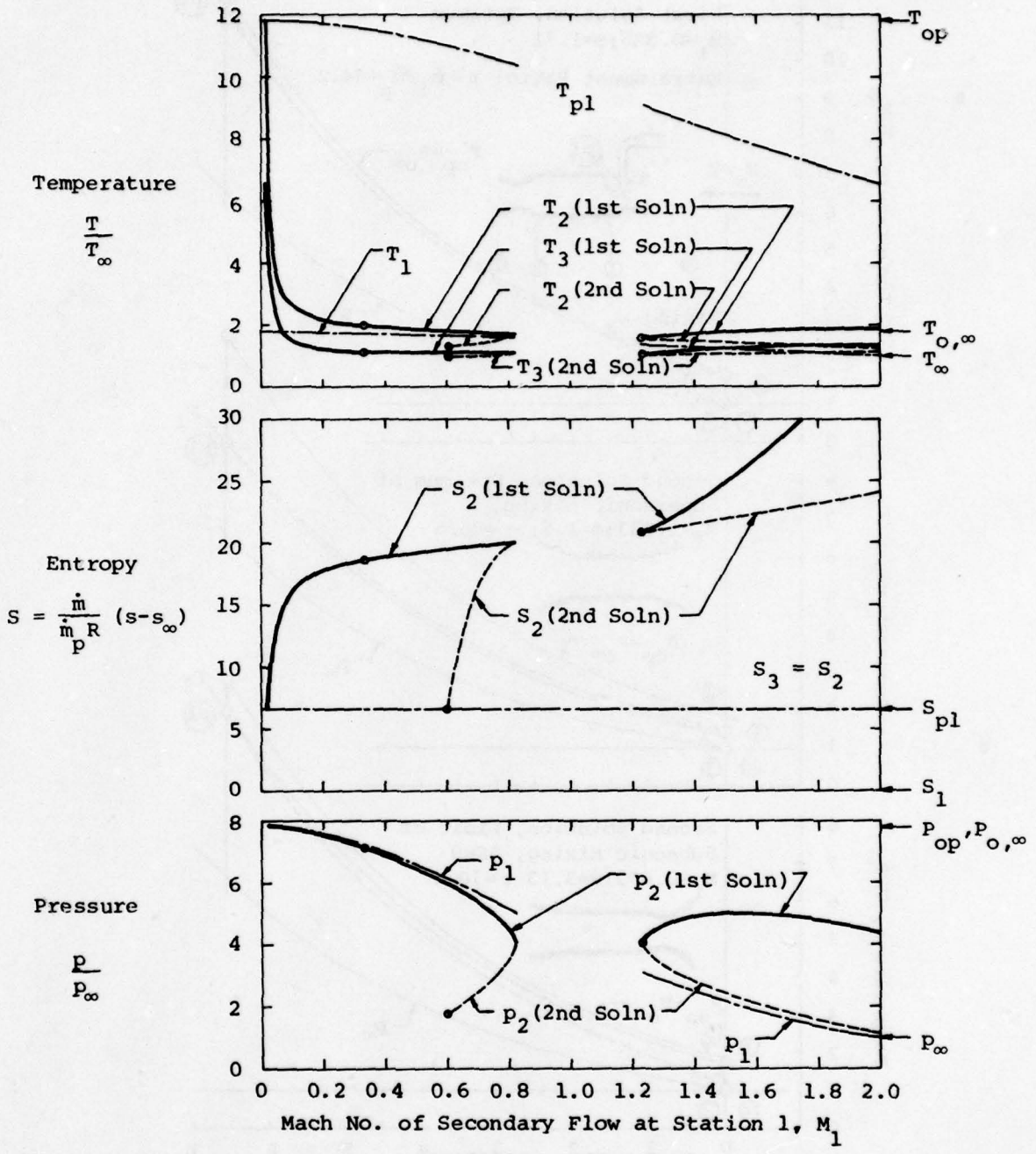

Condition: (Ram-jet)

$M_\infty = 2$; $\Delta P/p_\infty = 0$; $\Delta T/T_\infty = 10$; $\alpha_\infty = 20$

Figure 3 (continued)

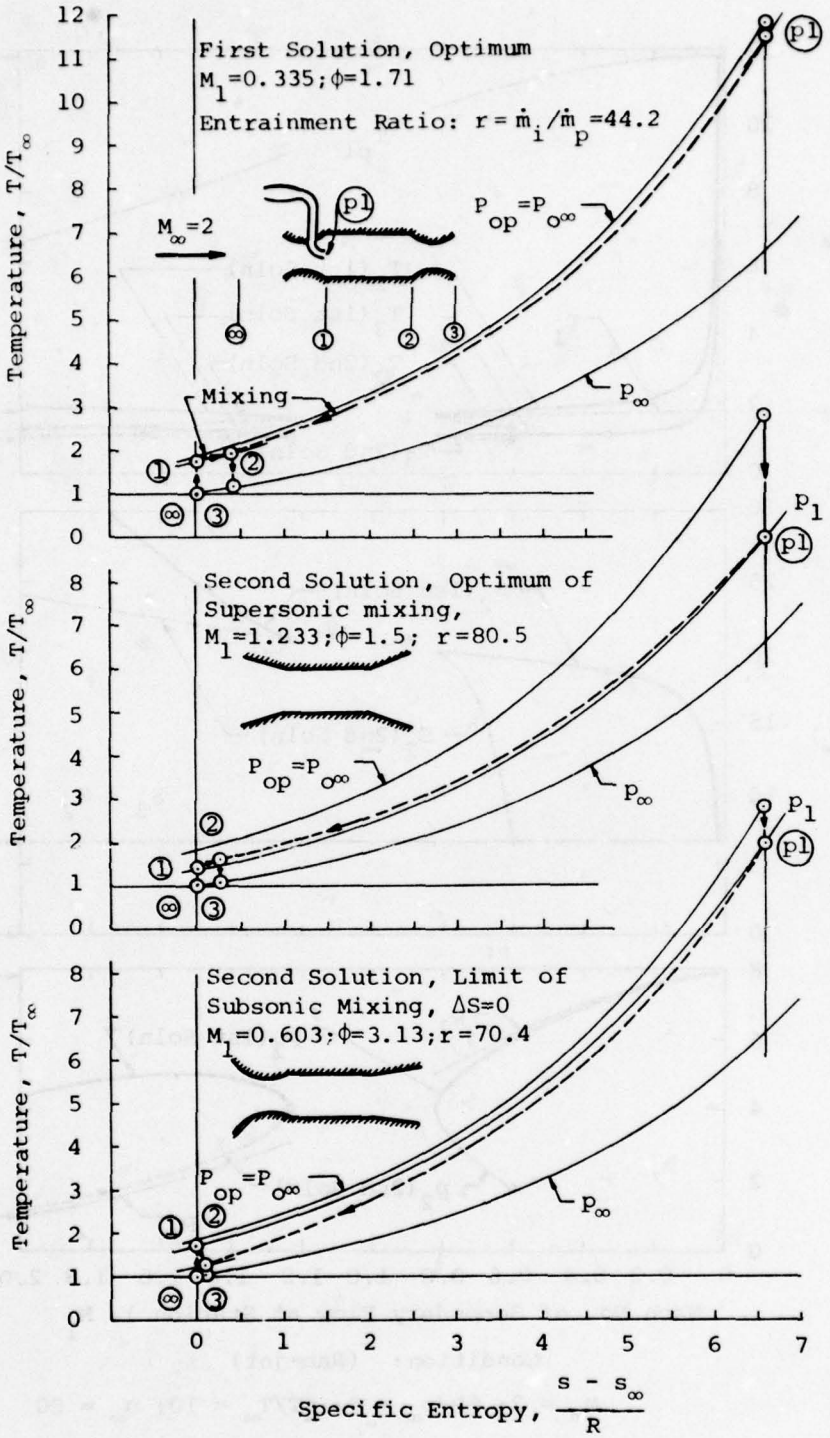

Condition: (Ram-jet)

$M_\infty = 2$; $\Delta P/p_\infty = 0$; $\Delta T/T_\infty = 10$; $\alpha_\infty = 20$

Figure 3 (concluded)

It is interesting to note that ejectors operating underwater or analyzed with the use of incompressible flow theory (References 2 and 3) always require accelerating (convergent) inlets and decelerating (divergent or diffusing) outlets to achieve optimal performance under the single realistic solution which exists. In contrast, the introduction of compressibility effects (variable temperature and density) into the analysis results in the existence of two distinct, realistic solutions representing ejectors which may require decelerating inlets and accelerating outlets. Depending upon the flight Mach No. and the characteristics of the injected gas, the ejector will require one of nine configurations. These nine configurations are the result of the possibility of a choice among three types of inlets (converging, diverging or De Laval Nozzle) and three types of outlets (converging, diverging or De Laval Nozzle).

The first of the two solutions to the compressible flow equations results in ejector configurations and flow patterns which at low flight speeds, powered by low temperature jets closely resemble those which are derived from the theory of incompressible flow. At high flight speeds or high temperature primary jets this solution indicates a radical departure from the ejector configurations derived from incompressible flow theory. High thrust augmentation can be achieved under this first solution over the entire range of flight speeds provided the ejector geometry and properties of the injected gas are properly selected, as will be shown on Figures 6 and 7.

The second solution with supersonic mixing and supersonic flight speeds requires an ejector configuration which geometrically resembles those derived from incompressible flow theory, but which perform the opposite function due to the difference between the supersonic and subsonic area/Mach No. relationship. At low flight speeds the geometry of the ejector differs considerably from those derived under incompressible flow theory, but the function can be similar to those derived under incompressible flow theory if powered by low temperature jets. With proper selection of the ejector geometry and the properties of the injected gas, the ejectors developed with the use of the second solution can produce better ejector performance than those derived under the first solution.

The importance of a careful selection of ejector geometry and injected gas characteristics cannot be overemphasized if high ejector performance is to be achieved during translatory conditions, under either of the two solutions to the flow equations.

The general features of these two solutions have been described in terms of two examples at two discrete operational conditions. It has been shown that in general, for a given condition, there exist three types of ejector or flow configurations which are of interest in the design of ejectors. Two of these configurations are the result of analysis using the second solution. One of these two exists when the induced flow is subsonic at the start of mixing, while the other exists when the induced flow is supersonic (or, in some special cases, slightly less than sonic) at the start of mixing. The third configuration of interest is the result of the analysis when the first solution is used and the induced flow is subsonic at the start of mixing.

Mollier diagrams illustrating the specific enthalpy as a function of the specific entropy for each of the selected design configurations are presented to describe the processes undergone by the primary, induced and mixed flows in the ejector. These diagrams are particularly useful in describing modifications to the basic gas generator thermodynamic cycle resulting from the use of ejector thrust augmentation.

To illustrate the feasibility of ejector propulsion, the thrust augmentation and propulsive efficiency of the reference jet have been shown for representative gas generator/ejector combination thrusters operating at the three design points over a range of flight Mach No's in the following section.

3. Combination Thrusters

The performance of combination thrusters over a range of flight Mach No's. from 0 to 3 has been evaluated for fanjet, ramjet, turbojet and rocket type gas generators. Each type of gas generator is of interest for different applications and under different operational conditions, depending upon the requirements of size, efficiency, etc. For example, the ideal performance of an ejector generally improves slowly with increasing values of the ratio of ejector mixing duct size (A_2) to primary jet (expanded to ambient pressure) size. In the examples described below, this ratio (α_∞) is maintained at a fixed value of 20, for discernment of the trend of performance as a function of flight Mach No. for each type of gas generator/ejector combination.

The calculation of performance of combination ejector thrusters is based upon fixed values of $\Delta P/p_\infty$, the ratio of pressure rise ($P_{or} - P_{o\infty}$) to the ambient pressure, and $\Delta T/T_\infty$, the ratio of temperature rise ($T_{op} - T_{o\infty}$) to the ambient temperature. In this manner the stagnation properties of the primary jet remain realistic with respect to flight Mach No. and altitude.

a. Fanjet/Ejector

The calculation of the fanjet/ejector performance is based upon the assumption that the compression is isentropic as previously described. Thus since the energized fluid contains only mechanical energy the overall efficiency is equal to the propulsive efficiency or in other words the thermal efficiency as defined in this document is 100%.

Figure 4 presents the thrust augmentation over a range of flight Mach No's, from zero to three when $\Delta P/p_\infty = 10$ and $\alpha_\infty = 20$. This represents one particular condition at which this device can operate and as indicated the thrust augmentation decreases rapidly with increasing flight Mach No. with all three types of optimal ejector configurations. However the ejector designed with subsonic mixing under the second solution provides superior performance to the other configurations over the entire range of operational conditions. As indicated, it is essential to use the design dictated by the second solution as a design criterion for transonic or supersonic ejectors powered by fanjets. Successful application of a fanjet ejector requires careful selection of the fanjet pressure. For example, at flight Mach Number of 0.3, the best range of $\Delta P/p_\infty$ for all three characteristic design points lies between 1 and 4 as shown on Figure 5 for an inlet area ratio (α_∞) of 20.

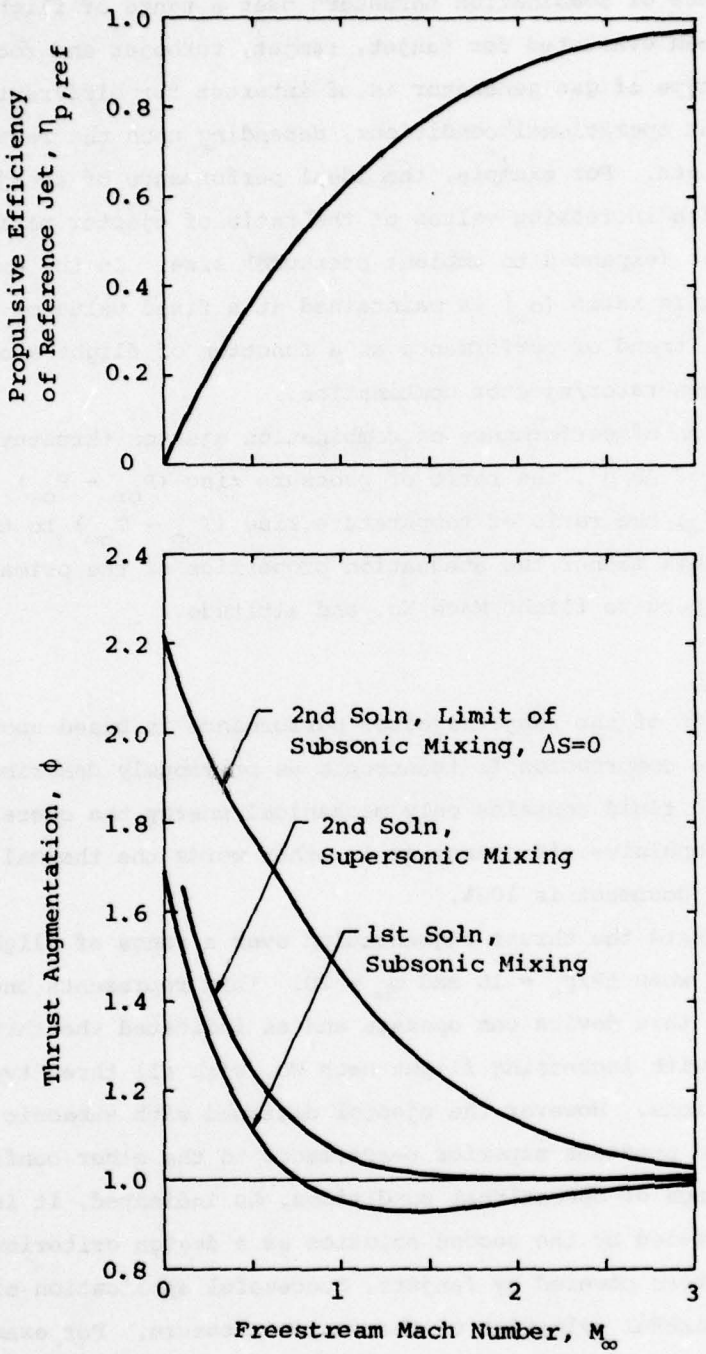

Figure 4. Fanjet/Ejector

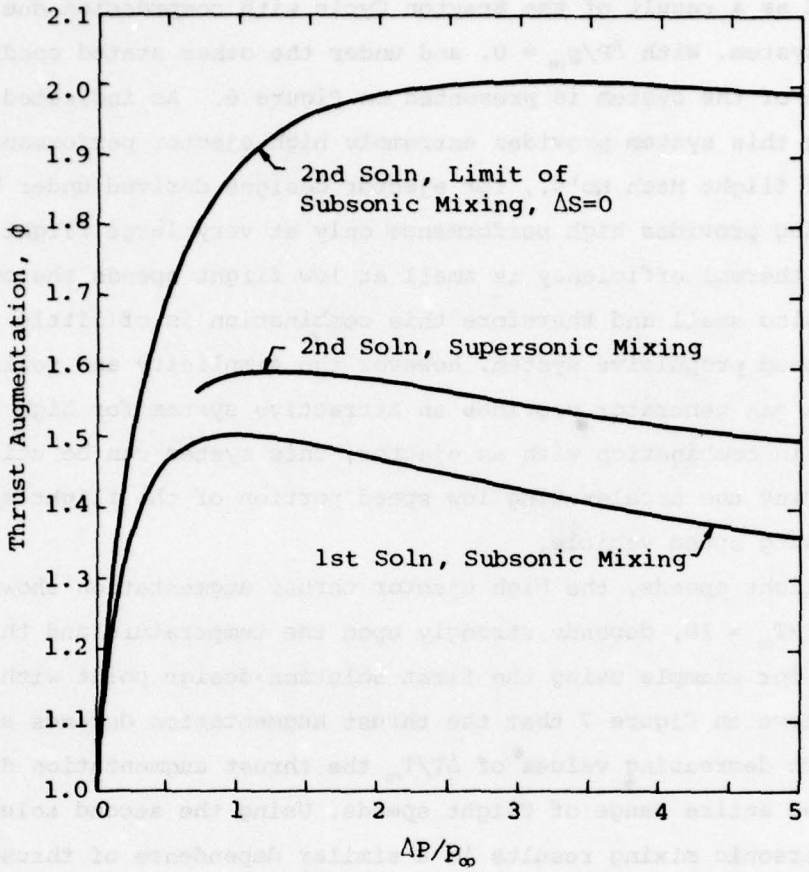

Condition: (Fan-jet)

$M_\infty = 0.3$; $\alpha_\infty = 20$

Figure 5. Influence of Pressure on Low Speed Ejector Performance

b. Ramjet/Ejectors

The ramjet/ejector combination thruster is a system in which the injected gas (efflux from a ramjet) contains large quantities of thermal and mechanical energy produced as a result of the Brayton Cycle with compression due to the motion of the system. With $\Delta P/p_\infty = 0$, and under the other stated conditions, the performance of the system is presented on Figure 6. As indicated, with subsonic mixing this system provides extremely high ejector performance over the entire range of flight Mach No's., for ejector designs derived under both solutions. Supersonic mixing provides high performance only at very large flight Mach No's.

Since the thermal efficiency is small at low flight speeds the overall efficiency is also small and therefore this combination is of little interest as a low cruise speed propulsive system. However the simplicity and reliability of the ramjet as a gas generator provides an attractive system for high speed propulsion and in combination with an ejector, this system can be utilized effectively during the accelerating low speed portion of the flight spectrum of a high cruising speed vehicle.

At high flight speeds, the high ejector thrust augmentation shown on Figure 6 for $\Delta T/T_\infty = 10$, depends strongly upon the temperature and the design configuration. For example using the first solution design point with subsonic mixing it is shown on Figure 7 that the thrust augmentation depends strongly upon $\Delta T/T_\infty$. With decreasing values of $\Delta T/T_\infty$ the thrust augmentation drops off rapidly over the entire range of flight speeds. Using the second solution design point with supersonic mixing results in a similar dependence of thrust augmentation upon the temperature (Figure 7), but good performance is achieved only at high flight speeds. This limitation at low speeds for the second solution with supersonic mixing is of little consequence however since as indicated above, the ramjet/ejector is not a practical system for cruise at these low speeds. With subsonic mixing the second solution also requires high temperature primary jets for high ejector performance. Thus it is evident that regardless of the design point utilized, the ramjet/ejector system operates effectively at high speeds and high temperatures. If low speed flight with this power plant is required, effective performance can only be achieved with subsonic mixing.

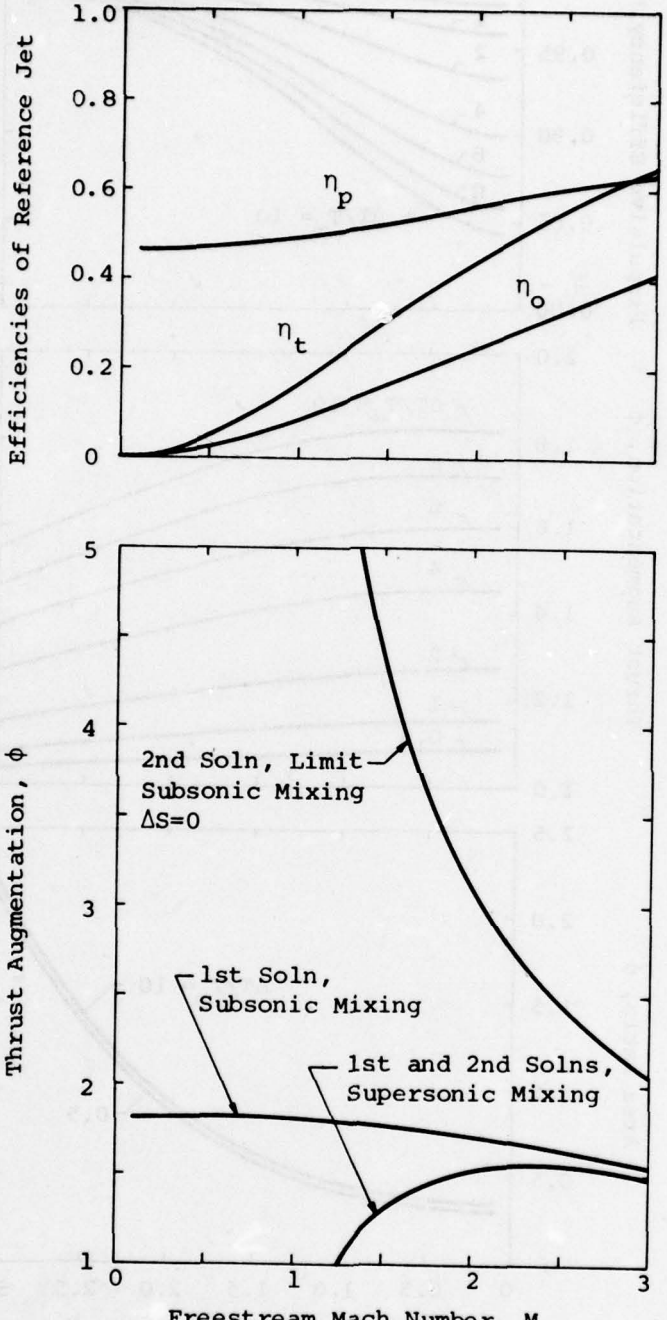

Condition: (Ram-jet)

$\Delta P/p_\infty = 0$; $\Delta T/T_\infty = 10$; $\alpha_\infty = 20$

Figure 6. Ramjet/Ejector

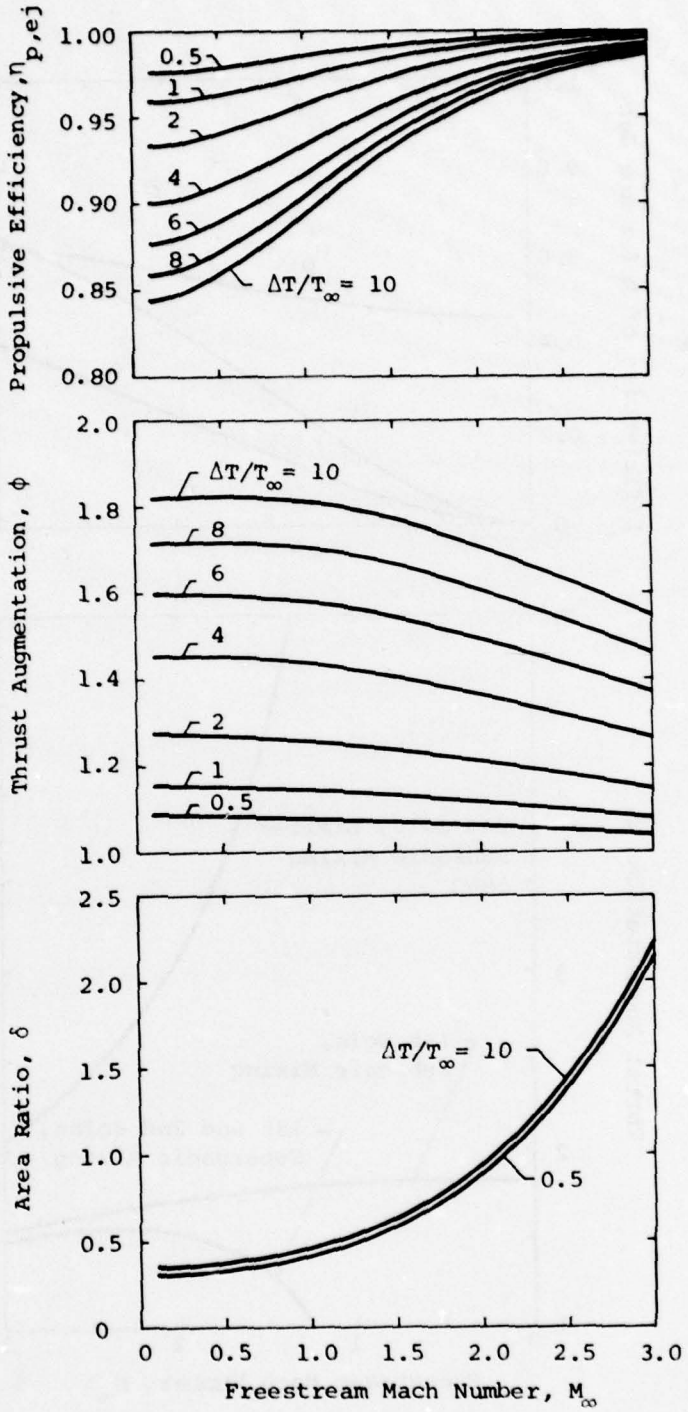

Condition: α_∞ = 20; $\Delta P/p_\infty$ = 0

Maximum Performance, First Solution, Subsonic Mixing

Figure 7. Influence of Temperature on Ramjet Ejector Performance

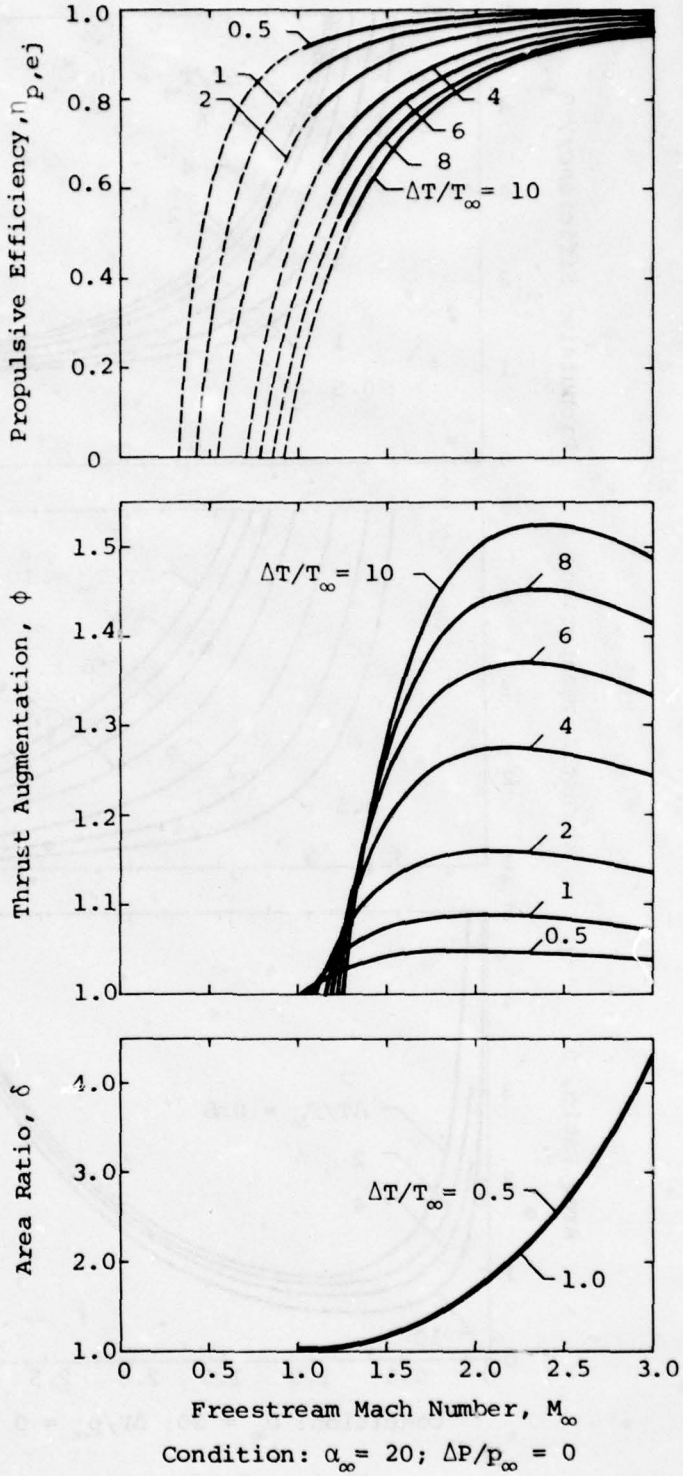

Condition: $\alpha_\infty = 20$; $\Delta P/p_\infty = 0$

Performance at Choking Limit
First and Second Solutions, Supersonic Mixing

Figure 7 (continued)

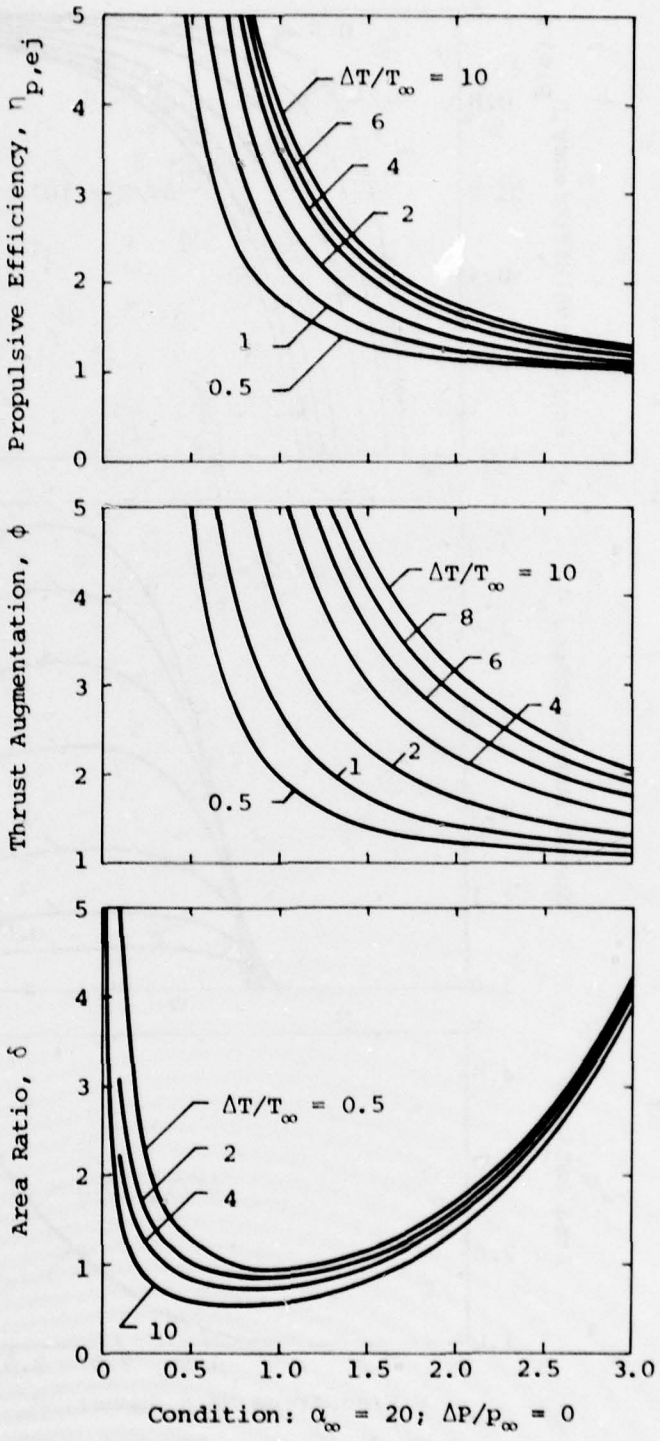

Maximum Performance
Limit of Second Solution, Subsonic Mixing (ΔS=0)

Figure 7 (concluded)

c. Turbojet/Ejector

Figure 8 illustrates the performance of a turbojet/ejector combination system over a range of flight Mach No's. from 0 to 3 with injected gas having high mechanical and thermal energies ($\Delta P/p_\infty = 10$, $\Delta T/T_\infty = 10$). As indicated, at high flight speeds the thrust augmentation is improved over the fanjet/ejector and is equivalent to the ramjet/ejector under these conditions. At low speeds the turbojet/ejector having the stated properties of the injected gas is competitive with the fanjet under all three design conditions.

At intermediate flight Mach Numbers (near 0.5), this turbojet/ejector having the properties stated above produces very low ejector performance, if designed according to the first solution, due to the fact that the design requirements for the use of hot and cold gas are in conflict. A cold gas high pressure ejector in this speed range requires a converging (accelerating) inlet and a diverging (decelerating) outlet, while a hot gas low pressure ejector requires a diverging (decelerating) inlet and a converging (accelerating) outlet. Thus the ejector having high pressure and temperature injected gas is at a conflicting design point where the best performing ejector is virtually a constant area duct. To counteract this difficulty it is possible to utilize ejector design criteria dictated by the second solution with subsonic mixing or to use a turbojet with small pressure ratio and high temperature as illustrated on Figure 9, or alternatively to use a high pressure ratio and low temperature effluent gas of the fanjet type.

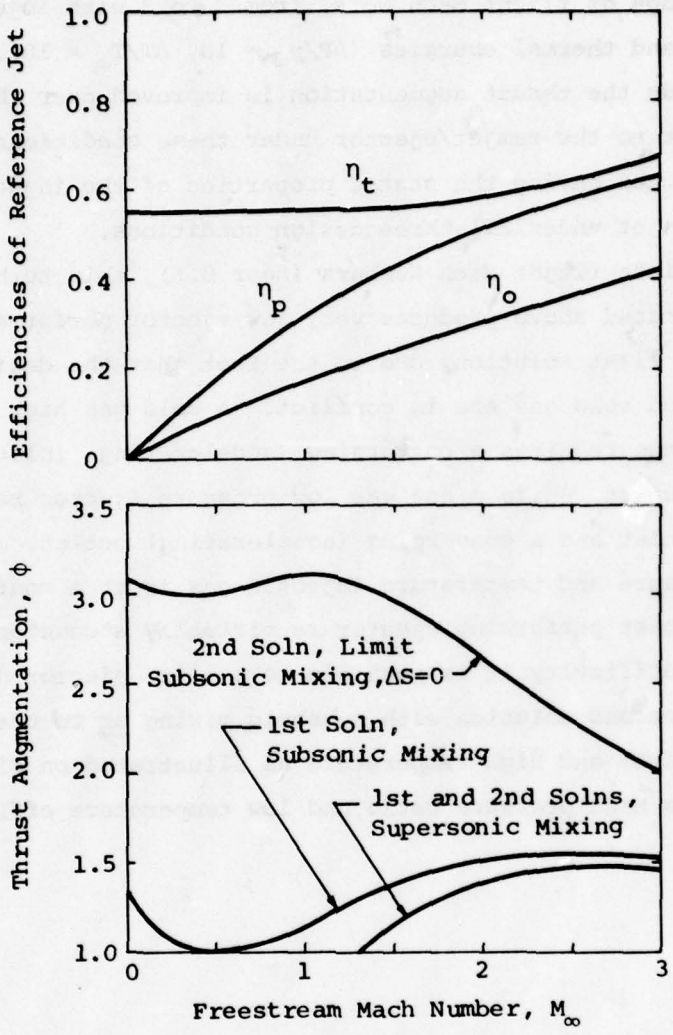

Condition: (Turbo-jet)

$\Delta P/p_\infty = 10$; $\Delta T/T_\infty = 10$; $\alpha_\infty = 20$

Figure 8. Turbojet/Ejector

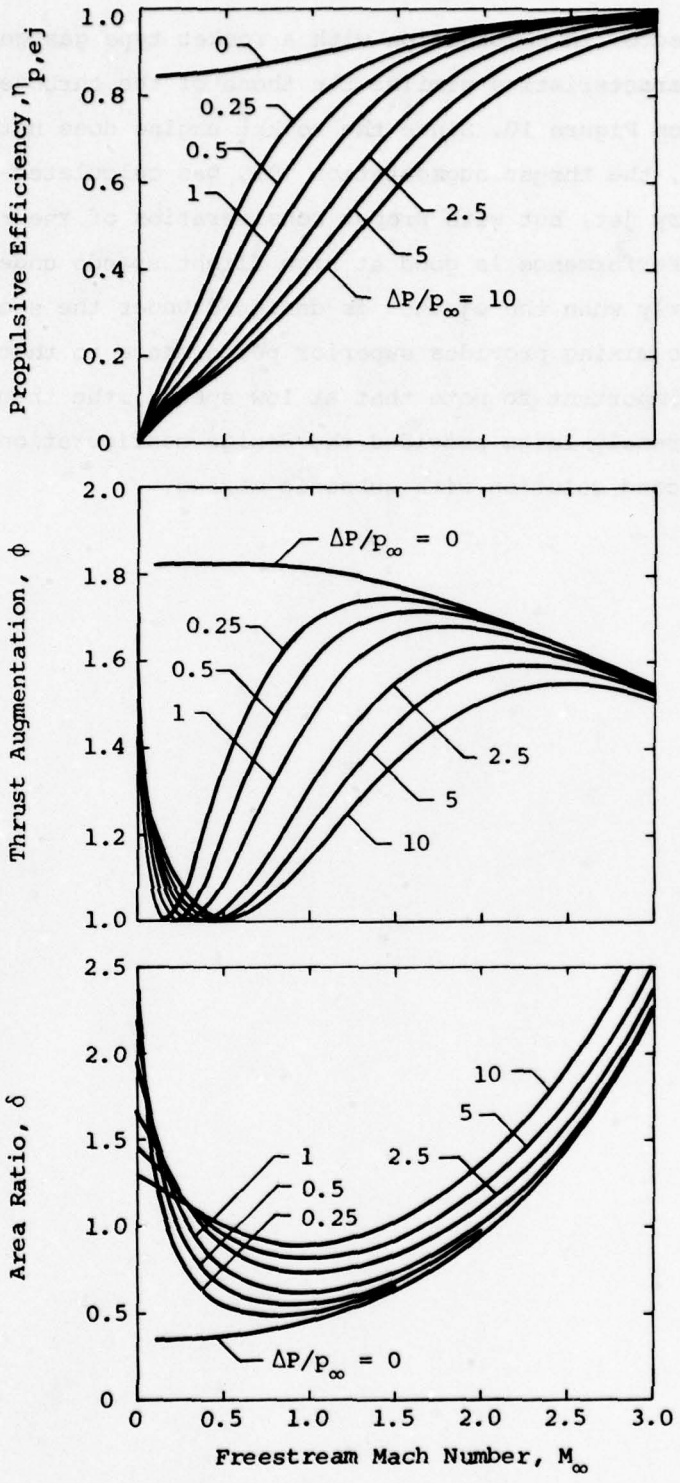

Condition: $\alpha_\infty = 20$; $\Delta T/T_\infty = 10$

Maximum Performance of the First Solution, Subsonic Mixing

Figure 9. Influence of Pressure on Turbojet/Ejector Performance

d. Rocket/Ejector

The use of an ejector in combination with a rocket type gas generator offers performance characteristics similar the those of the turbojet/ejector combination as shown on Figure 10. Since the rocket engine does not require intake of ambient air, the thrust augmentation (ϕ), was calculated without ram drag of the primary jet, but with proper consideration of the ram drag of the induced flow. Performance is good at high flight speeds under all design conditions, particularly when the ejector is designed under the second solution. As indicated, subsonic mixing provides superior performance to that with supersonic mixing. It is important to note that at low speeds, the thrust augmentation of this system is extremely large provided the design configuration is that which corresponds to the second solution with subsonic mixing.

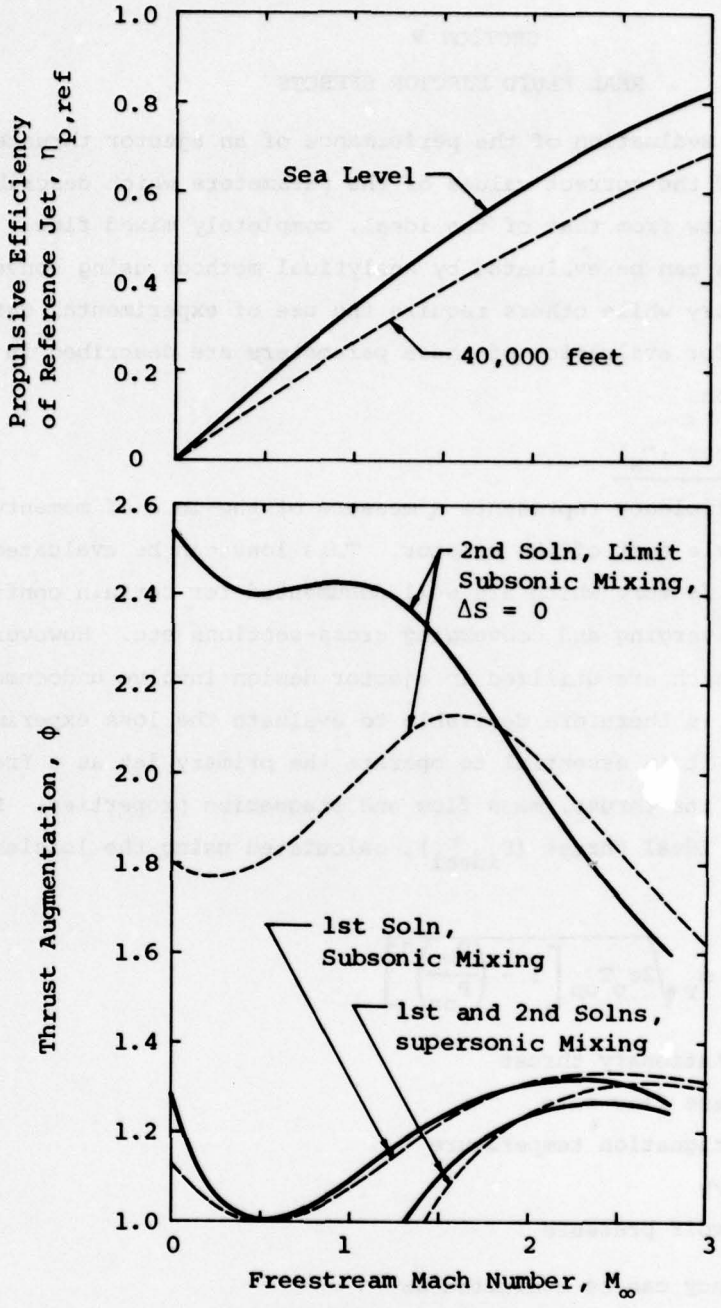

Condition: (Rocket Engine)
Chamber Pressure: 300 psia
Chamber Temperature: 6000°R
$\alpha_\infty = 20$

Figure 10. Rocket/Ejector

SECTION V

REAL FLUID EJECTOR EFFECTS

The realistic evaluation of the performance of an ejector thruster depends upon a knowledge of the correct values of the parameters which describe the deviation of the flow from that of the ideal, completely mixed flow. Certain of these parameters can be evaluated by analytical methods using conventional boundary layer theory while others require the use of experimental data. The methods available for evaluation of these parameters are described in the following discussion.

1. Nozzle efficiency (η_N)

The nozzle efficiency represents a measure of the loss of momentum occuring in the primary nozzle duct of the ejector. This loss can be evaluated using standard duct loss factors which are well documented for certain configurations such as corners, diverging and converging cross-sections etc. However certain types of nozzles which are utilized in ejector design involve undocumented configurations and it is therefore desirable to evaluate the loss experimentally. To accomplish this it is essential to operate the primary jet as a free stationary jet and to measure its thrust, mass flow and stagnation properties. From this experiment and the ideal thrust (F_{ideal}), calculated using the lossless reservoir pressure

$$F_{ideal} = \dot{m}_p \sqrt{2 c_p T_{op} \left[1 - \left(\frac{P_\infty}{P_{or}} \right)^n \right]} \tag{75}$$

where F = the stationary thrust

$\dot{m}_p$ = the mass flow rate

T_{op} = the stagnation temperature

n = $(\gamma-1)/\gamma$

P_{or} = reservoir pressure

the nozzle efficiency can be evaluated as

$$\eta_N = \frac{F_{exp}}{F_{ideal}} \tag{76}$$

When supercritical pressure ratios are utilized, the ejector requires a nozzle which is converging only since the expansion to the throat pressure can occur isentropically. In this case the ideal thrust of the nozzle as a free jet is

$$F^{*}_{ideal} = \dot{m}_p V'_{p^*} = \dot{m}_p \sqrt{2c_p T_{op}\left[1 - \left(\frac{p_*}{p_{or}}\right)^n\right]} \tag{77}$$

Measurement of the thrust, mass flow and stagnation temperature then can be utilized to determine η_N since

$$\eta_N = \frac{F_{exp}}{F^{*}_{ideal}} = \frac{F_{exp}}{\dot{m}_p \sqrt{2c_p T_{op}\left[1 - \left(\frac{p_*}{p_{or}}\right)^n\right]}} \tag{78}$$

where for air, $\frac{p_*}{p_{or}} = 0.5283$

If the primary jet is a wall jet, additional losses can occur due to skin friction which can be evaluated by employing boundary layer theory. Since the ejector performance ϕ, is almost directly proportional to η_N, using wall jets as primary jets should be avoided.

2. Inlet loss

The inlet loss of the induced flow occurs at the entrance to the ejector as a result of blockage, inlet separation and skin friction. Since in any real ejector these losses cannot in general be evaluated by analytical methods, it is necessary to utilize an experiment in which the distribution of pressures and temperature are measured at a station immediately downstream of the inlet. Then if at the survey station

p = static pressure

P_o = stagnation pressure

T_o = stagnation temperature

the average static pressure is

$$\bar{p} = \frac{1}{A_2} \iint p \, dy \, dz \tag{79}$$

the entrainment ratio is

$$r = \frac{\dot{m}_i}{\dot{m}_p} = \left\{ \frac{1}{\dot{m}_p} \iint p \sqrt{\frac{2}{nRT_o} \left(\frac{P_o}{p}\right)^n \left[\left(\frac{P_o}{p}\right)^n - 1\right]} \, dy \, dz \right\} - 1 \tag{80}$$

and the quantity

$$\overline{\rho U^2} = \frac{1}{A_2} \iint \frac{2p}{n} \left[\left(\frac{P_o}{p}\right)^n - 1\right] dy \, dz \tag{81}$$

With the knowledge of the primary jet characteristics, ($\dot{m}_p$, P_{op} (or P_{or} and η_N)) and the ejector geometry, the inlet area ratio is,

$$\alpha_\infty = \frac{A_2}{a_\infty} = \frac{p_\infty}{\dot{m}_p} \sqrt{\frac{2}{nRT_{op}} \left(\frac{P_{op}}{p_\infty}\right)^n \left[\left(\frac{P_{op}}{p_\infty}\right)^n - 1\right]} \, A_2 \tag{82}$$

The value of C_{di} can then be determined by an iterative solution of the following equations.

$$V_{p1} = \sqrt{2c_p T_{op} \left[1 - \left(\frac{p_1}{P_{op}}\right)^n\right]} \tag{83}$$

$$\alpha = \alpha_\infty \sqrt{\left(\frac{p_1}{p_\infty}\right)^{2-n} \frac{\left[(P_{op}/p_1)^n - 1\right]}{\left[(P_{op}/p_\infty)^n - 1\right]}} \tag{84}$$

$$\left(\frac{P_{o1}}{p_1}\right)^n = \frac{1}{2} + \sqrt{\frac{1}{4} + \left(\frac{P_{op}}{p_1}\right)^n \left[\left(\frac{P_{op}}{p_1}\right)^n - 1\right] \left(\frac{r}{\alpha - 1}\right)^2 \left(\frac{T_{o\infty}}{T_{op}}\right)} \tag{85}$$

$$U_1 = \sqrt{2\, c_p T_{o\infty} \left[1 - \left(\frac{p_1}{p_{o1}}\right)^n\right]} \tag{86}$$

$$p_1 = -\frac{\dot{m}_p}{A_2}\left(V_{p1} + rU_1\right) + \bar{p} + \overline{\rho U^2} \quad \text{(conservation of momentum)} \tag{87}$$

With the solution for p_1, $\left(\frac{P_{o1}}{p_1}\right)^n$ is also determined as shown above and

$$C_{di} = \frac{n\left(\frac{P_{o\infty}}{p_1} - \frac{P_{o1}}{p_1}\right)}{\left(\frac{P_{o1}}{p_1}\right)^n - 1}, \text{ since } \frac{P_{o\infty}}{p_1} = \frac{C_{di}}{n}\left[\left(\frac{P_{o1}}{p_1}\right)^n - 1\right] + \frac{P_{o1}}{p_1} \tag{88}$$

as described in Equation 8, if $U_e/U_\infty = 1$

Experimental determination of the inlet drag coefficient for the STAMP AJDE (Small Tactical Aerial Mobilitly Platform, Alperin Jet-Diffuser Ejector) was performed at FDRC, using an assumed uniform total temperature equal to the mass flow averaged total temperature of primary and induced flows. The results of this experimental analysis yielded inlet drag coefficients (C_{di}), ranging from 0.013 to 0.016, for the jet-diffuser ejector, depending upon primary nozzle design and attitude. Since the AJDE has throat dimensions of 10.16 cm x 38.1 cm, the two-dimensional value of C_{di} is about 0.010 to 0.013.

At supersonic flight speeds the inlet loss is primarily due to inlet shock waves, therefore it is more conveniently expressed as the inlet recovery factor

$$\eta_i = \frac{P_{o1}}{P_{o\infty}} \tag{89}$$

This factor depends upon the wave configuration of the inlet and its maximum acceptable value for decelerating inlets of the type used for engine inlets is specified by the conventional design requirement set forth in MIL-E-5007D, as

$$\eta_i = \frac{P_{o1}}{P_{o\infty}} = 1 - 0.075\ (M_\infty - 1)^{1.35} \tag{90}$$

for $1 < M_\infty < 5$.

Since ejectors translating at supersonic speeds may have subsonic or supersonic mixing (M_1 may be greater or less than 1.0), the inlet may be subject to the shock wave loss reflected in the factor (η_i) only when $M_1 < 1$. If the ejector is designed to utilize supersonic mixing ($M_1 > 1$), the inlet may be either decelerating or accelerating but in either case since a normal shock can be avoided the inlet loss is primarily comprised of skin friction and the value of C_{di} must be determined experimentally as described above.

The influence of η_i as given by MIL-E-5007D on the thrust augmentation of an ejector translating at a Mach No. of 2 with a ramjet type gas generator is illustrated on Figure 11, where as shown the performance remains high despite the large loss due to shock waves at the inlet. Under the first solution, the use of subsonic mixing provides superior ideal performance to that of supersonic mixing but shock losses required for subsonic mixing result in a reduction of the optimal value of M_1 and a degradation of performance which then becomes equivalent to that for supersonic mixing (see Figure 11).

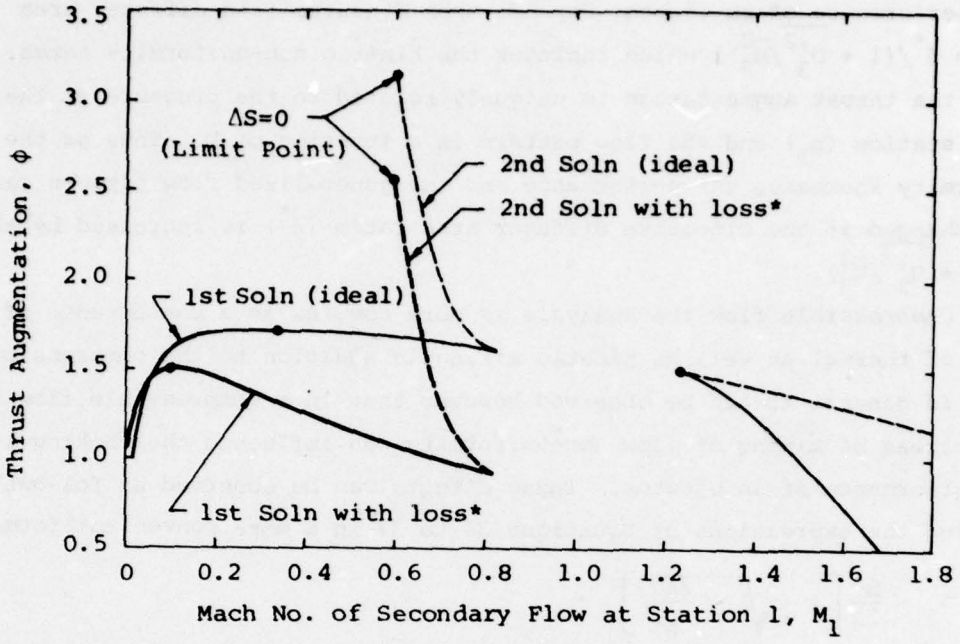

Condition: (Ram-jet) $M_\infty = 2$; $\Delta P/p_\infty = 0$; $\Delta T/T_\infty = 10$; $\alpha_\infty = 20$

*loss: MIL-E-5007D Inlet Recovery Factor

for $1 < M_\infty < 5$ is,

$$\eta_i = \frac{P_{o1}}{P_{o\infty}} = 1-0.075\ (M_\infty - 1)^{1.35}$$

Figure 11. Supersonic Ejector with Inlet Compression Loss

3. Flow non-uniformity due to incomplete mixing

Under the assumption of incompressibility it has been shown (Reference 3) that the performance of an ejector depends upon a generalized diffuser area ratio D [$= \delta^*/(1 + \overline{U_3'^2}/\bar{U}_3^2)$] which includes the kinetic non-uniformity terms. In that case the thrust augmentation is uniquely related to the pressure at the injection station (p_1) and the flow pattern is a function of D. Thus as the flow non-uniformity increases the performance and the generalized flow pattern can remain unchanged if the effective diffuser area ratio (δ^*) is increased by the factor $(1 + \overline{U_3'^2}/\bar{U}_3^2)$.

In a compressible flow the analysis is more complex as a consequence of the existence of thermal as well as kinetic mixing in addition to the compressibility effects. In general it can be observed however that in a compressible flow the varying degrees of mixing or flow non-uniformity can influence the choking limits and the performance of an ejector. These effects can be observed as follows.

Writing the expressions of Equations 34 to 37 in a more convenient form,

$$\lambda_2 = \frac{B}{2A}\left[1 \pm \sqrt{1 - \frac{4AC}{B^2}}\right] \tag{91}$$

where

$$\frac{4AC}{B^2} = \frac{J(1+r)^2(\gamma^2-1)}{\gamma^2\left[1 + r\lambda_1 + \frac{n\alpha}{2(T_{op}/T_{p1} - 1)}\right]^2}\left(1 + \frac{3-\gamma}{\gamma+1}\frac{\overline{U_2'^2}}{\bar{U}_2^2} + \frac{2}{\gamma+1}\frac{\overline{\rho_2' U_2'}}{\bar{\rho}_2 \bar{U}_2} + \frac{\gamma}{\gamma+1} C_F\right) \tag{92}$$

$$\frac{B}{2A} = \frac{\gamma\left[1 + r\lambda_1 + \frac{n\alpha}{2(T_{op}/T_{p1} - 1)}\right]}{(1+r)(\gamma+1)\left(1 + \frac{3-\gamma}{\gamma+1}\frac{\overline{U_2'^2}}{\bar{U}_2^2} + \frac{2}{\gamma+1}\frac{\overline{\rho_2' U_2'}}{\bar{\rho}_2 \bar{U}_2} + \frac{\gamma}{\gamma+1} C_F\right)} \tag{93}$$

It has previously been shown that at the choking limit the discriminant $(1 - 4AC/B^2)$ becomes zero. This implies that the non-uniformity terms in Equation 92 can influence the extent of the choked region. For example, since $\overline{U_2'^2}/\bar{U}_2^2$ and C_F are always positive an increase in their magnitude results in an increase in $4AC/B^2$ or a decrease in the magnitude of the discriminant. Obviously this results in a widening of the choked region or the requirement for operating the ejector at values of M_1 further from 1.0. Increasing thermal non-uniformity being directly related to the magnitude of $\overline{\rho_2' U_2'}/\bar{\rho}_2\bar{U}_2$, causes a decrease in the magnitude

of $4AC/B^2$ or an increase in the magnitude of the discriminant since $\overline{\rho_2' U_2'}/\bar{\rho}_2 \bar{U}_2$ is generally negative. This results in a narrowing of the choked region and the possibility of operating the ejector at values of M_1 closer to 1.0. Since the term B/2A includes the same non-uniformity term in its denominator its influence on λ_2 is opposite to that of $4AC/B^2$.

To examine the influence of flow non-uniformity on ejector thrust augmentation, it can be shown that from Equation 22 and 31

$$\frac{p_2}{p_\infty} = \frac{p_1}{p_\infty}\frac{2}{n\alpha}\left(\frac{T_{op}}{T_{p1}} - 1\right)\left[1 + r\lambda_1 + \frac{n\alpha}{2(T_{op}/T_{p1} - 1)}\right]\left\{1 - \frac{\gamma}{\gamma+1}\left(1 \pm \sqrt{1 - \frac{4AC}{B^2}}\right)\right.$$

$$\left. \times \left[1 + \frac{\gamma-1}{\gamma+1}\left(2\frac{\overline{U_2'^2}}{\bar{U}_2^2} + \frac{\overline{\rho_2' U_2'}}{\bar{\rho}_2 \bar{U}_2} - \frac{1}{2}C_F\right)\right]\right\}$$

$$\simeq \frac{p_1}{p_\infty}\frac{2}{n\alpha}\left(\frac{T_{op}}{T_{p1}} - 1\right)\left[1 + r\lambda_1 + \frac{n\alpha}{2(T_{op}/T_{p1} - 1)}\right]\left[1 - \frac{\gamma(\gamma-1)}{\gamma+1}\left(2\frac{\overline{U_2'^2}}{\bar{U}_2^2} + \frac{\overline{\rho_2' U_2'}}{\bar{\rho}_2 \bar{U}_2} - \frac{1}{2}C_F\right)\right]$$

$$\times \frac{1}{\gamma+1}\left\{1 \mp \gamma\sqrt{1 - \frac{4AC}{B^2}}\left[1 + (\gamma-1)\left(2\frac{\overline{U_2'^2}}{\bar{U}_2^2} + \frac{\overline{\rho_2' U_2'}}{\bar{\rho}_2 \bar{U}_2} - \frac{1}{2}C_F\right)\right]\right\}$$

and therefore,

$$\lambda_2\left(\frac{p_2}{p_\infty}\right)^{\frac{1}{\gamma}} = \frac{\gamma\left[\frac{2}{n\alpha}\left(\frac{T_{op}}{T_{p1}} - 1\right)\right]^{\frac{1}{\gamma}}\left[1 + r\lambda_1 + \frac{n\alpha}{2(T_{op}/T_{p1} - 1)}\right]^{\frac{\gamma+1}{\gamma}}\left(1 \pm \sqrt{1 - \frac{4AC}{B^2}}\right)}{(p_\infty/p_1)^{1/\gamma}(1 + r)(\gamma + 1)^{(\gamma+1)/\gamma}}$$

$$\times\left\{1 \mp \gamma\sqrt{1 - \frac{4AC}{B^2}}\left[1 + (\gamma-1)\left(2\frac{\overline{U_2'^2}}{\bar{U}_2^2} + \frac{\overline{\rho_2' U_2'}}{\bar{\rho}_2 \bar{U}_2} - \frac{1}{2}C_F\right)\right]\right\}^{\frac{1}{\gamma}}\left(1 - \frac{\overline{U_2'^2}}{\bar{U}_2^2} - \frac{\overline{\rho_2' U_2'}}{\bar{\rho}_2 \bar{U}_2} - \frac{1}{2}C_F\right) \quad (94)$$

Since $\gamma\sqrt{1 - 4AC/B^2}$ is generally small compared to 1, from Eq. C-5 of Appendix C

$$\left(1 \pm \sqrt{1 - \frac{4AC}{B^2}}\right)\left\{1 \mp \gamma\sqrt{1 - \frac{4AC}{B^2}}\left[1 + (\gamma-1)\left(2\frac{\overline{U_2'^2}}{\bar{U}_2^2} + \frac{\overline{\rho_2' U_2'}}{\bar{\rho}_2 \bar{U}_2} - \frac{1}{2}C_F\right)\right]\right\}^{\frac{1}{\gamma}}$$

$$= \left(\frac{1-\gamma}{2} + \frac{\gamma+1}{2}\frac{4AC}{B^2}\right) + \left[\mp\frac{(\gamma+1)(\gamma-1)}{3}\left(1 - \frac{4AC}{B^2}\right)^{3/2} - \frac{(\gamma+1)(\gamma-1)(2\gamma-1)}{8}\left(1 - \frac{4AC}{B^2}\right)^2 + \cdots\right]$$

$$+ (\gamma-1)\left[\mp\sqrt{1 - \frac{4AC}{B^2}} - \gamma\left(1 - \frac{4AC}{B^2}\right) + \cdots\right]\left(2\frac{\overline{U_2'^2}}{\bar{U}_2^2} + \frac{\overline{\rho_2' U_2'}}{\bar{\rho}_2 \bar{U}_2} - \frac{1}{2}C_F\right) + \cdots$$

In view of the fact that $(1 - 4AC/B^2) = O(\overline{U_2'^2}/\bar{U}_2^2)$ near the choking limit, the last two terms have orders of magnitude higher than $U_2'^2/\bar{U}_2^2$ and are neglected.

As shown in Appendix C, using the above approximation and Equation 92, the expression for $\lambda_2 (p_2/p_\infty)^{1/\gamma}$ near the choking limit becomes

$$\lambda_2 \left(\frac{p_2}{p_\infty}\right)^{\frac{1}{\gamma}} = \frac{\gamma\left[\frac{2}{n\alpha}\left(\frac{T_{op}}{T_{pl}} - 1\right)\right]^{1/\gamma}\left[1 + r\lambda_1 + \frac{n\alpha}{2(T_{op}/T_{pl} - 1)}\right]^{(\gamma+1)/\gamma}}{(p_\infty/p_1)^{1/\gamma}(1 + r)(\gamma + 1)^{(\gamma+1)/\gamma}}$$

$$\times \left\{\frac{1-\gamma}{2} + \frac{J(1 + r)^2(\gamma^2 - 1)(\gamma + 1)}{2\gamma^2\left[1 + r\lambda_1 + \frac{n\alpha}{2(T_{op}/T_{pl} - 1)}\right]^2}\right\}\left(1 - \frac{\gamma-1}{2}\frac{\overline{u_2'^2}}{\bar{u}_2^2} + \frac{\gamma-1}{2} C_F\right) \qquad (95)$$

From Equation 48

$$\lambda_3\left(1 + \frac{\overline{u_3'^2}}{\bar{u}_3^2} + \frac{\overline{\rho_3' u_3'}}{\bar{\rho}_3 \bar{u}_3}\right) = \sqrt{\frac{J}{1 + \frac{\overline{u_3'^2}}{\bar{u}_3^2}}\left[1 - \frac{\alpha\lambda_2\left(\frac{p_2}{p_\infty}\right)^{1/\gamma}}{\left(1 + r\frac{T_{o\infty}}{T_{op}}\right)\frac{T_{op}}{T_{pl}}\frac{p_1}{p_\infty}}\frac{\left(1 - \frac{1}{2}\frac{\overline{\rho_2'^2}}{\bar{\rho}_2^2}\right)}{\left(1 - \frac{1}{2}\frac{\overline{\rho_3'^2}}{\bar{\rho}_3^2}\right)}\right]} \qquad (96)$$

Examination of Equation 95 indicates that increases of non-uniformities decrease the term $\lambda_2 (p_2/p_\infty)^{1/\gamma}$, but the influence on $\lambda_3(1 + \overline{u_3'^2}/\bar{u}_3^2 + \overline{\rho_3' u_3'}/\bar{\rho}_3\bar{u}_3)$ is diminished by the non-uniformity terms at Station 3 in the denominator of Equation 96. Thus since the thrust augmentation is directly influenced by the term $\lambda_3(1 + \overline{u_3'^2}/\bar{u}_3^2 + \overline{\rho_3' u_3'}/\bar{\rho}_3\bar{u}_3)$, as indicated by Equation 56, the net effect of flow non-unformity on ϕ is small.

From Equation 52, for an isentropic ejector outlet,

$$\delta^* = \frac{1}{\lambda_3}\lambda_2\left(\frac{p_2}{p_\infty}\right)^{1/\gamma}\left(1 - \frac{1}{2}\frac{\overline{\rho_2'^2}}{\bar{\rho}_2^2}\right)\Big/\left(1 - \frac{1}{2}\frac{\overline{\rho_3'^2}}{\bar{\rho}_3^2}\right) \qquad (97)$$

Examination of Equation 97 in the light of Equation 95 indicates that increases in the kinetic non-uniformity at Station 2 results in a decreased value of the effective outlet area ratio (δ^*). Since the right hand side of Equation 96 is virtually independent of non-uniformity as discussed above, an increase of kinetic non-uniformity at Station 3 increases the required value of δ^* due to a decrease of λ_3. Thus for an ejector with a decelerating outlet, the non-uniformity term at Station 3 is larger than that at Station 2. This requires an increased value of δ^* with increasing kinetic non-uniformity. With an accelerating outlet this situation is reversed.

4. Correlation with Experiment

The influence of skin friction and incomplete mixing between Stations 1 and 2 are represented by the last three terms in the coefficient A of the solution for λ_2 as indicated by Equation 35. If it is assumed that a coefficient $\tilde{C}_f$ represents the entire influence of skin friction (which contributes to entropy production between Stations 2 and 3) and incomplete mixing between Stations 1 and 3, then Equation 35 takes the form

$$A = \frac{\gamma+1}{2\gamma} + \frac{1}{2}\tilde{C}_F \tag{98}$$

where,

$$\tilde{C}_F = 2\tilde{C}_f \ (\ell_T/X_2)$$

ℓ_T = total ejector length after injection

and, as a consequence of isentropic flow between station 2 and 3 ($\bar{\bar{s}}_3 = \bar{\bar{s}}_2$), Equation 48 can be expressed as

$$\lambda_3^2 = J\left[1 - \left(1 - \frac{\lambda_2^2}{J}\right)\left(\frac{p_\infty}{p_2}\right)^n\right] \tag{99}$$

and from Equation (28)

$$\frac{p_2}{p_\infty} = J\,\frac{1+r}{\alpha\,\lambda_2}\left(\frac{T_{op}}{T_{p1}} - 1\right)\left(1 - \frac{\lambda_2^2}{J}\right)\frac{p_1}{p_\infty} \tag{100}$$

Using this approximation, which incorporates the influence of incomplete mixing into the coefficient C_F, and applying the first solution to an ejector whose geometry, injected flow and nozzle characteristics correspond to those quoted in Reference 4 for the ARL Ejector provides excellent agreement between theory and Configuration F performance data of Reference 4, with $\tilde{C}_f = 0.006$. This high performing ejector had a diffuser in which the flow remained attached ($\delta^* = \delta$). Configuration D which is reported to have had the same length after injection as that of Configuration F but which had a longer mixing section and a shorter, wider angle diffuser displayed performance which was considerably lower than that of Configuration F and also lower than the above described analysis (at $\delta > 1.4$) as shown on Figure 12. Further the inception of diffuser separation is made evident by the drop in value of U_1 with increasing geometric diffuser area ratio shown in Reference 4. It can therefore be concluded that the Configuration D diffuser flow separated and that $\delta^* < \delta$.

Since the ARL ejectors had a throat dimension of 10" x 60", $\tilde{C}_f$ can be corrected to represent the coefficient of skin friction based on the wetted surface area. This value is 0.0051 (=0.006 x 6/7), which is very close to the coefficient of skin friction of a flat plat turbulent boundary layer over a wide range of Reynolds numbers near 10^6.

This example demonstrates that for a solid diffuser ARL ejector with length to throat ratio (ℓ_T/X_2) of 5, the mixing of the primary and the induced flow is adequate, and the ejector performance is controlled by factors η_N, C_{di}, skin friction (C_f) and most importantly, the effective diffuser area ratio δ^*.

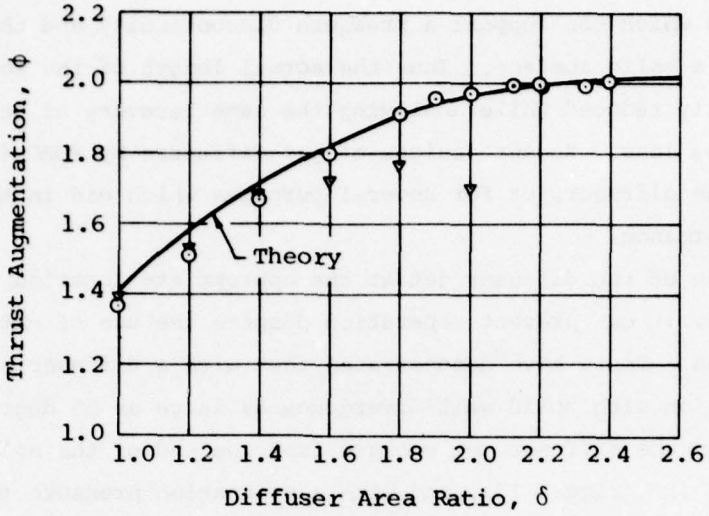

ARL Ejector (AIAA Paper 72-1174)

α = 25.3; η_N = 0.96; C_{di} = 0.025

$\tilde{C}_f$ = 0.006 P_{or}/p_∞ = 1.25 (fan-jet)

Theory assumes no separation

Configuration	Symbol	ℓ_T/X_2
D	▼	5
F	⊙	5

Figure 12. ARL Ejectors Compared to Theory

SECTION VI

JET DIFFUSER EJECTORS

Jet diffusers are as the name implies, diffusers which are comprised of fluid jet sheets which can support a pressure discontinuity and thereby perform the function of a solid surface. Thus the actual length of the solid surfaces can be drastically reduced while achieving the same recovery of jet kinetic energy or leaving loss. Recent designs of jet diffusers by FDRC (Reference 1), have utilized the diffuser jet for several purposes which aid in the improvement of ejector performance.

By injection of the diffuser jet at the appropriate location within the solid diffuser surface, it can prevent separation despite the use of extremely large divergence angles. Tests have demonstrated that with a diffuser jet it is possible to avoid separation with solid wall divergence as large as 60 degree half-angle. In addition, when the diffuser jet emerges from the end of the solid surface with a positive angle (β) (Figure 13), and with a stagnation pressure (P_{od}) greater than $P_{o\infty}$ it produces a jet diffuser which increases the effective diffuser area ratio (σ) to a value which is larger than the geometric diffuser area ratio (δ). A further indirect advantage accruing from the use of a diffuser jet is related to the increased effective length of the diffusion process which thereby permits the mixing of primary and induced flow to continue effectively downstream of the solid surfaces.

Jet diffusion has been shown to provide the above described advantages in subsonic flow and its mass flow and momentum requirements for optimal performance have been determined analytically (Reference 3) and experimentally (Reference 1). For an ideal jet diffuser ejector, the ejector flow will be fully mixed prior to the return to ambient pressure (far down stream of the ejector exit), therefore, the following analysis is based upon the assumption that the flow in the jet diffuser ejector is uniform, and introduces an empirical constant to correct the imperfection of the jet diffuser.

The governing equations upstream of station 2 are identical to those for a solid diffuser ejector, except,

1) flow is assumed uniform, non-uniformity terms vanishes,

2) $C_F = 0$, due to the non-existence of a mixing duct,

3) skin friction on solid surface of diffuser is accounted for in the momentum flux of the diffuser jet.

1. Jet-Diffuser

Previously, in the discussion of the flow through the ejector it has been assumed that the flow returned to ambient pressure at Station 3, which location coincided with the end of the effective diffusion process in a solid diffuser ejector. If however a jet diffuser is utilized, the flow returns to ambient pressure far downstream of the end of the solid surfaces. Between the end of the solid diffuser and the region where the flow returns to ambient pressure there exists a curved jet sheet called a diffuser jet. In this case the outlet end of the ejector appears as illustrated on Figure 13.

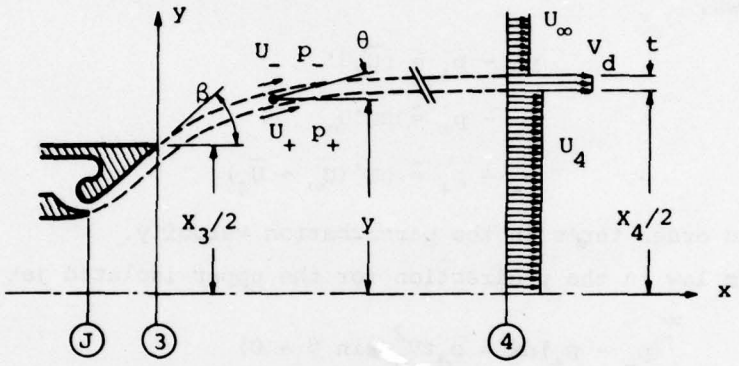

Figure 13. Jet-Diffuser

The diffuser jet is injected as a wall jet at Station J, and encounters a skin friction along the solid surface until Station 3 where the solid surface terminates at an angle β with respect to the axis of symmetry.

The momentum theorem between Stations 3 and 4 may be written as follows.

$$p_3 X_3 + 2 \int_{X_3/2}^{X_4/2} p_- dy + \dot{m}_c \bar{U}_3 + \dot{m}_d V_d \cos \beta = p_4 X_4 + \dot{m}_c \bar{U}_4 + \dot{m}_d V_d \tag{101}$$

or since $p_4 = p_\infty$, this may be expressed in a dimensionless form as

$$\frac{(p_3 - p_\infty) X_3}{\dot{m}_p V_{p1}} + \frac{2}{\dot{m}_p V_{p1}} \int_{X_3/2}^{X_4/2} (p_- - p_\infty) dy + (1 + r)(\lambda_3 - \lambda_4) - \frac{\dot{m}_d V_d}{\dot{m}_p V_{p1}} (1 - \cos \beta) = 0 \tag{102}$$

The integral involves p_- (the pressure on the external streamline of the diffuser jet), which equals p_∞ in the stationary case and in that situation the integral vanishes. However, in the translating case the integral can be evaluated by replacing the jet sheet with a vortex sheet as is done in jet flap theory.

Thus,

$$U_- = U_\infty - U' \tag{103}$$

$$U_+ = \bar{U}_4 + U'$$

where U' is assumed small compared to U_∞ and $\bar{U}_4$, and by applying Bernoulli's Equation to each side of the jet sheet, and assuming identical density for external and internal flows,

$$p_\infty - p_+ \cong \rho \bar{U}_4 U'$$

$$p_- - p_\infty \cong \rho U' U_\infty$$

and therefore,

$$p_- - p_+ \cong \rho U' (U_\infty + \bar{U}_4) \tag{104}$$

neglecting second order terms in the perturbation velocity.

The momentum law in the y-direction for the upper isolated jet sheet is

$$\int_x^\infty (p_- - p_+) dx = \rho_d t V_d^2 (\sin\theta - 0) \tag{105}$$

where

t = the jet sheet thickness

θ = the local angle w.r.t. the thrust direction (x).

Differentiation with respect to x yields

$$\frac{\rho_d t V_d^2}{R} = p_- - p_+ \tag{106}$$

R = Radius of curvature

since

$$\sin\theta = \frac{y'}{\sqrt{1 + y'^2}} \tag{107}$$

and

$$\frac{d \sin\theta}{dx} = \frac{y''}{(1 + y'^2)^{3/2}} = -\frac{1}{R} \tag{108}$$

Using Equations 104 and 106

$$\rho_d t V_d^2/R = \rho U'(U_\infty + \bar{U}_4) \tag{109}$$

and since $\dot{m}_d V_d = 2\rho_d t V_d^2$

V_d = velocity of diffuser jet

$\dot{m}_d$ = mass flow of diffuser jet (2 sides)

Therefore

$$U' = \frac{\dot{m}_d V_d}{2\rho\, R(\bar{U}_4 + U_\infty)} \tag{110}$$

Using Equation 110, the value of $p_- - p_\infty$ can be found from Equation 104 to be

$$p_- - p_\infty = \frac{\dot{m}_d V_d U_\infty}{2R(\bar{U}_4 + U_\infty)} \tag{111}$$

This permits integration of the integral in Equation 102.

$$\int_{X_3/2}^{X_4/2} (p_- - p_\infty)\,dy = \frac{\dot{m}_d V_d U_\infty}{2(\bar{U}_4 + U_\infty)} \int_{X_3/2}^{X_4/2} \frac{dy}{R} = \frac{\dot{m}_d V_d}{2} \frac{U_\infty}{\bar{U}_4 + U_\infty} (1 - \cos\beta) \tag{112}$$

Other terms in Equation 102 are expressed conveniently as follows. Similar to Equation (29) the p_3 term can be expressed as

$$\frac{p_3 X_3}{\dot{m}_p V_{p1}} = \frac{nJ}{2}(1 + r)\,\frac{1 - \frac{\lambda_3^2}{J}}{\lambda_3} \tag{113}$$

and noting that

$$\frac{p_\infty X_3}{\dot{m}_p V_{p1}} = \frac{n\alpha\delta}{2}\left(\frac{p_\infty}{p_1}\right)\Big/\left[\left(\frac{p_{op}}{p_1}\right)^n - 1\right]\ ; \quad \delta = \frac{X_3}{X_2} \tag{114}$$

Substituting Equations 112, 113 and 114 into Equation 102 results in the <u>ideal</u> jet diffuser equation which relates λ_4 to λ_3, or,

$$\lambda_4 = \frac{\gamma+1}{2\gamma}\lambda_3 + \frac{nJ}{2\lambda_3} - \frac{n\alpha\delta}{2(1+r)}\,\frac{\left(\frac{p_\infty}{p_1}\right)}{\left(\frac{p_{op}}{p_1}\right)^n - 1} - \frac{1}{1+r}\,\frac{\dot{m}_d V_d}{\dot{m}_p V_{p1}}(1 - \cos\beta)\left(1 - \frac{\lambda_\infty}{\lambda_4 + \lambda_\infty}\right) \tag{115}$$

where λ_3 can be calculated from λ_2 by Equation 50, if δ is known, or

$$\delta\,\lambda_3\left(1-\frac{\lambda_3^2}{J}\right)^{\frac{1}{\gamma-1}}=\lambda_2\left(1-\frac{\lambda_2^2}{J}\right)^{\frac{1}{\gamma-1}} \tag{116}$$

By substituting subsript 4 for subscript 3 in Equation 48 and under the uniform flow and isentropic outlet assumption

$$\lambda_4^2=J\left[1-\left(1-\frac{\lambda_2^2}{J}\right)\left(\frac{p_\infty}{p_2}\right)^n\right] \tag{117}$$

The effective diffuser area ratio σ can be obtained by assuming isentropic flow in the diffuser. Substituting σ for δ and subscript 4 for subscript 3 in Equation 50 neglecting all the non-uniformity terms, and noting that $\bar{\bar{s}}_4=\bar{\bar{s}}_2$, results in

$$\sigma=\frac{\lambda_2}{\lambda_4}\left\{\frac{1-\frac{\lambda_2^2}{J}}{1-\frac{\lambda_4^2}{J}}\right\}^{\frac{1}{\gamma-1}} \tag{118}$$

Combination of Equations 117 and 118 gives the relation between σ and λ_4, or,

$$\sigma\lambda_4=\lambda_2\left(\frac{p_2}{p_\infty}\right)^{1/\gamma} \tag{119}$$

Eliminating λ_4 from Equations 115 and 117 and noting that all other terms can be expressed in terms of (p_1/p_∞), gives the solution of the ideal jet-diffuser ejector problem.

In the realistic situation, imperfections do exist in the design of jet-diffusers. For example, in a three dimensional ejector, the peripheral variation of the diffuser jet thickness, and the non-uniform peripheral distribution of β, can degrade the performance of a jet-diffuser and result in a decrease of the effective diffuser area ratio (σ) and a premature termination of the effective mixing process which then decreases the entrainment capability of the ejector, and penalizes the ejector performance. Also the definition of outlet area ratio δ ($= X_3/X_2$) is arbitrary since the flow is highly two-dimensional (90° included angle in the AJDE) it is appropriate to introduce an empirical constant to relate the ejector geometry to the outlet area ratio.

The imperfections, attributable to the peripheral non-uniformity, two-dimensionality and three-dimensionality of the flow due to finite longitudinal dimensions can be described by an efficiency factor η_{dj}, in the form,

$$\eta_{dj} = \frac{\delta \text{ effective}}{\delta \text{ geometric}} \tag{120}$$

or replacing δ with $\delta\,\eta_{dj}$ in equation 115 and 116

$$\lambda_4 = \frac{\gamma+1}{2\gamma}\lambda_3 + \frac{nJ}{2\lambda_3} - \frac{n\alpha\delta\eta_{dj}\left(\frac{p_\infty}{p_1}\right)}{2(1+r)\left[\left(\frac{P_{op}}{p_1}\right)^n - 1\right]} - \frac{1}{1+r}\frac{\dot{m}_d V_d}{\dot{m}_p V_{p1}}(1-\cos\beta)\left(1 - \frac{\lambda_\infty}{\lambda_4+\lambda_\infty}\right) \tag{121}$$

and

$$\eta_{dj}\,\delta\,\lambda_3\left(1 - \frac{\lambda_3^2}{J}\right)^{\frac{1}{\gamma-1}} = \lambda_2\left(1 - \frac{\lambda_2^2}{J}\right)^{\frac{1}{\gamma-1}} \tag{122}$$

The complete solution of a jet-diffuser ejector can be obtained by eliminating λ_4 from equations 117 and 121 and solving for (p_1/p_∞) if δ is given, or solving for δ if (p_1/p_∞) is given.

If $P_{od} = P_{or}$ and $T_{od} = T_{op}$

$$\phi = \frac{(1+r)\lambda_4 + \frac{\dot{m}_d V_d}{\dot{m}_p V_{p1}} - r\lambda_e - \left(1 + \frac{\dot{m}_d}{\dot{m}_p}\right)\lambda_\infty}{\left(1 + \frac{\dot{m}_d}{\dot{m}_p}\right)\left(\frac{V_{p\infty}}{\eta_N V_{p1}} - \lambda_\infty\right)} \tag{123}$$

The ratio of diffuser jet to primary jet momentum which occurs in Equations 123 and 121 depends upon the degradation which occurs as a result of the skin friction encountered by the diffuser jet along the solid surface between Station J and Station 3. This skin friction force can be evaluated using the Blasius Law when the Reynolds number of the flow is less than 5×10^5 (laminar flow) or by using the Prandtl-Schlichting Law for Reynolds numbers greater than or equal to 5×10^5 (transition to turbulent flow).

The Reynolds number based upon length of wetted surface is (Reference 5)

$$Re/\ell_{dj} = \frac{\rho V_{d\infty}}{\mu_{d\infty}} = \frac{P_{od} M_{d\infty}}{\mu_{od}} \sqrt{\frac{\gamma}{(\gamma-1) c_v T_{od}}} \left(T_{od}/T_{d\infty}\right)^{\frac{\gamma-2}{\gamma-1}} \frac{(T_{d\infty}/T_{od}) + (198.6/T_{od})}{1 + (198.6/T_{od})} \tag{124}$$

$$M_{d\infty}^2 = [2/(\gamma - 1)][(P_{od}/p_\infty)^n - 1] \tag{125}$$

$$\mu_{od} = 2.270[T_{od}^{3/2}/(T_{od} + 198.6)] \times 10^{-8} \quad \frac{\text{lbf - sec}}{\text{ft}^2} \tag{126}$$

$$c_v = 4290 \text{ ft}^2/\text{sec}^2 \ {}^\circ\text{R} \tag{127}$$

To determine ℓ_{dj} we used the geometry of a family of jet diffuser ejector designed by FDRC whose geometry is described by,

$$\begin{aligned} \ell_{dj}/X_2 &= 0 && \delta \leq 1.0304 \\ \ell_{dj}/X_2 &= (1.0999\delta - 1.1333) && 1.0304 < \delta < 1.5855 \\ \ell_{dj}/X_2 &= (0.7071\delta - 0.5105) && \delta \geq 1.5855 \end{aligned} \tag{128}$$

$$X_2 = 4 \text{ in.} = 10.16 \text{ cm.}$$

Thus if P_{od} is in psia, X_2, ℓ_{dj} in inches, and T_{od} in ${}^\circ$R then for air

$$Re_\ell = 1.51 \times 10^7 (M_{d\infty} P_{od}/T_{od}) (\ell_{dj}/X_2) (T_{d\infty}/T_{od})^{1.5} [(T_{d\infty}/T_{od}) + (198.6/T_{od})] X_2$$

Then, according to the Blasius Law (Reference 6)

$$C_{fdj} = 1.328/\sqrt{Re_\ell} \qquad Re_\ell < 5 \times 10^5 \tag{129}$$

and according to Prandtl-Schlichting, (Reference 6)

$$C_{fdj} = 0.455/(\log Re_\ell)^{2.58} - (1613.8/Re_\ell) \qquad Re_\ell \geq 5 \times 10^5 \tag{130}$$

and the compressibility correction term is (Reference 6)

$$C_{fdj,comp} = C_{fdj,incomp} \div \{1 + 0.85(M_{d\infty}^2)[(\gamma - 1)/2]\} \tag{131}$$

Using C_{fdj} determined in this manner permits evaluation of $\dot{m}_d V_d/\dot{m}_p V_{pl}$ since

$$\begin{aligned} \dot{m}_d V_d/\dot{m}_p V_{pl} &= (\dot{m}_d V_{d\infty}/\dot{m}_p V_{pl})[1 - (\ell_{dj}/s_\infty) C_{fdj}] \\ &= (p_\infty/p_1)(s_\infty/a_1) \frac{(P_{od}/p_\infty)^n - 1}{(P_{op}/p_\infty)^n - 1} [1 - (\ell_{dj}/s_\infty) C_{fdj}] \end{aligned} \tag{132}$$

2. Correlation with Experiment

To illustrate the validity of this analysis, it was used to evaluate the performance of a series of jet-diffuser ejectors which were tested at FDRC under the STAMP (Small Tactical Aerial Mobility Platform) Program (Reference 1). These ejectors were three-dimensional, having widely diverging diffuser surfaces at the sides and flat, non-diverging end surfaces. The lack of divergence of the ends of the diffuser resulted in a collapse of the flow since the non-diverging diffuser jets could not sustain the pressure gradient. To delay this collapse, end plates of various sizes were added to extend the solid surfaces beyond the solid surfaces at the sides of the ejector as illustrated on Figure 14. Measurements of thrust augmentation were made for this series of end plate configurations with other geometric and thermodynamic parameters held constant. This data is also presented on Figure 14.

Using the geometric and thermodynamic parameters corresponding to those of the STAMP ejector tests, the values of C_{fdj} and η_{dj} were calculated using the above method. The improvement of jet diffuser efficiency (η_{dj}) with increasing size of the end plate is illustrated on Figure 15.

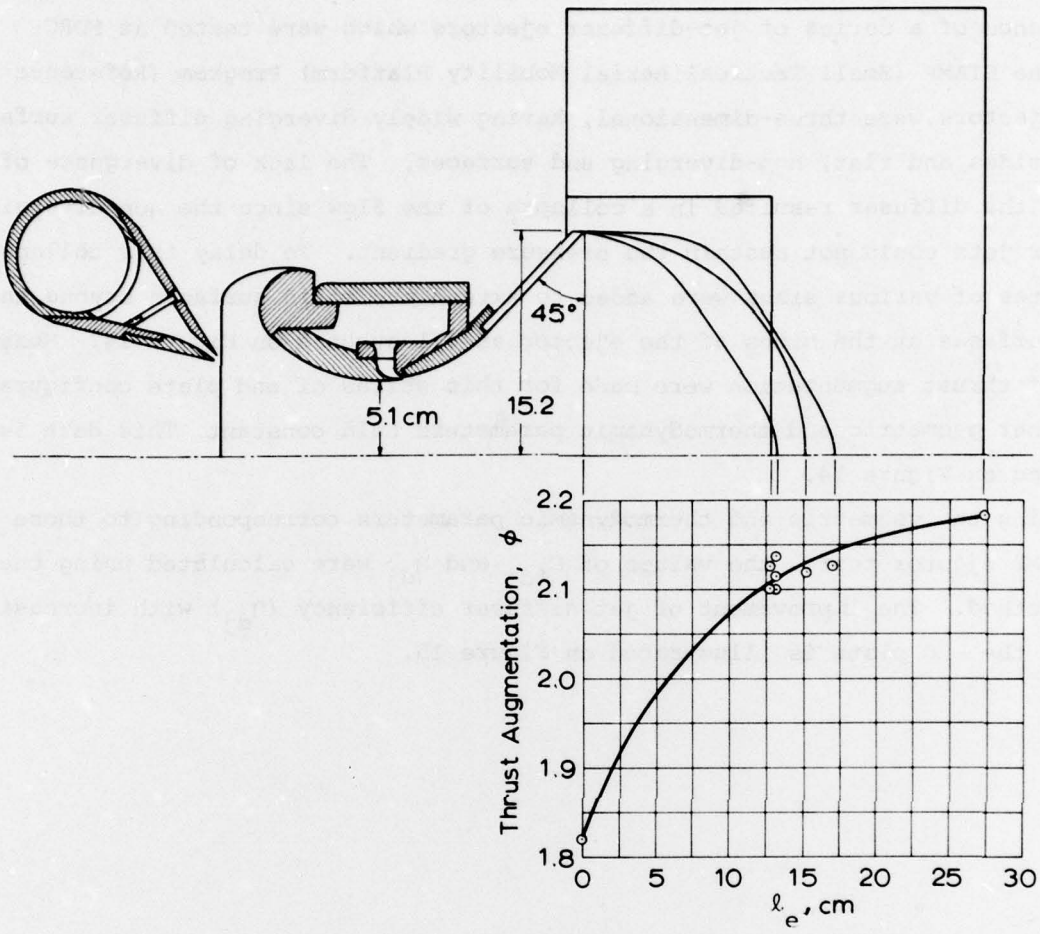

P_o = 24.3 kilopascals (3.52 psig)

$A_2/(s_\infty + a_\infty) = 21.6$; $s_\infty/a_\infty = 0.62$

Figure 14. End Plate Configurations and Performance, STAMP Ejector

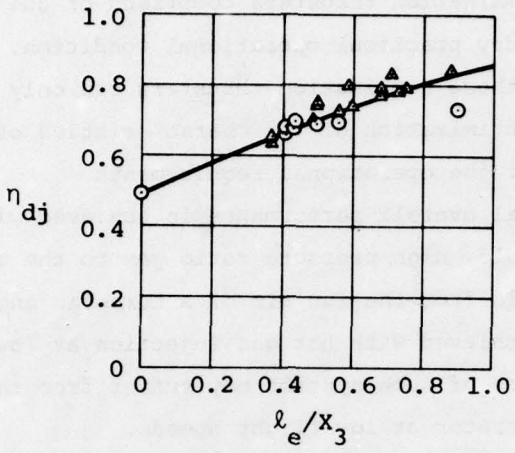

○ $\delta = 3$

▲ $1.6 \leq \delta \leq 3.1$

Assume, $\eta_N = 1$; $C_{di} = 0.016$

Figure 15. Jet-Diffuser Efficiency, STAMP Ejector
P_o = 24.3 kilopascals (3.52 psig)
$A_2/(s_\infty + a_\infty) = 21.6$; $s_\infty/a_\infty = 0.62$

SECTION VII

CONCLUSIONS AND REMARKS

The performance of systems which propel airborne vehicles can be greatly improved by the use of combination thrusters comprised of gas generators and ejectors, at any present day practical operational condition. The maximum advantage derivable from these combination thrusters can only be achieved as the result of a careful optimization of the characteristics of the gas generator and the ejector in view of the operational requirements.

At low speeds, optimal overall performance is achieved with gas generators which supply relatively cold, high pressure ratio gas to the ejector. Such gases can be obtained for example from the fan air of a turbofan engine. High ejector performance can also be achieved with hot gas injection at low pressure ratios but the overall performance of such systems may suffer from the poor thermal efficiency of the gas generator at low flight speeds.

At high subsonic or supersonic speeds, high overall performance can be achieved by combination thrusters which supply very hot injected gas to the ejector. This is a very practical arrangement since at these high speeds, a gas generator can supply hot effluent gas with high thermal efficiency and with an extremely simple and reliable gas generator of the ramjet type.

The performance degradation resulting from nozzle duct loss, inlet drag, skin friction and incomplete thermal and kinetic mixing has been considered in the analysis and methods have been discussed for evaluation of the loss coefficients. The performance of an ejector, after consideration of the losses, has been shown to agree very closely with experiments performed at ARL and FDRC under stationary conditions.

Since no data are available for translating ejectors, the relative importance of each loss coefficient during translational motion of the ejector cannot be evaluated. However, a complete treatment of the constant area mixing ejector was presented with all loss coefficients for future design and analysis of ejector problems.

A total of nine types of ejector configurations are required to accomodate the flow patterns which exist for optimal ejector performance under all conditions which have been examined. Only one configuration has been developed to date and

therefore only this one configuration has been used for comparison of theory and experiment. This configuration involves an acclerating, converging, subsonic inlet and a decelerating, diverging, subsonic outlet. Evaluation of the loss coefficients for other types of ejector configurations would require design, fabrication and testing of each type of ejector.

Using the design principle of the first solution, it has been shown that ejectors cannot operate effectively, in the medium subsonic speed range, when the injected gas contains both thermal and kinetic energy since the optimal ejector configurations for hot gas injection are very different from those for cold gas. Therefore it is essential that, in case of a turbofan engine, the efflux from the fan and the hot gas be injected into separate ejectors to achieve the best result.

As a result of the analysis based on the conservation laws of mass, momentum and energy within the Second Law of Thermodynamics, the use of ejectors in combination with gas generator engines has been shown to provide a means for producing more mechanical energy than that which is injected from its gas generator. This can only result from the conversion of injected thermal energy to mechanical energy in the ejector, in an amount in excess of the intrinsic loss resulting from the mixing process. Thus the otherwise wasted thermal energy of a free jet can be converted to mechanical energy similar to the Brayton cycle process. The conversion of lost mechanical energy (leaving loss) to useful energy has also been described in terms of the relative values of the propulsive efficiency of the free jet from the gas generator and the propulsive efficiency of the combination thruster.

It has been shown in References 2 and 3 that boundary layer ingestion has an effect on performance similar to that of a reduction of ram drag, and since ϕ is a monotonic function of $q/\Delta P$, in an incompressible fluid, a decrease of ingestion velocity results in an increase of thrust augmentation. Therefore in an incompressible fluid it is always desirable to locate the ejector at a region where boundary layer or wake can be ingested. In a compressible fluid, it has been shown that the performance depends upon temperature and pressure of the

energized fluid and does not always decrease with increasing flight Mach No.. Therefore ingestion of boundary layer or wake fluid while decreasing the ram drag also decreases the inlet compression which is required for high ejector performance under certain conditions. Therefore optimal ejector integration may require full usage of boundary layer ingestion or free stream ingestion. In the latter case the ejector may be better integrated upstream of the boundary layer or wake.

APPENDIX A

NORMAL SHOCK RELATION BETWEEN THE FIRST AND THE SECOND SOLUTION

In the ideal case when $C_F = 0$ and flow is uniform at Station 2, then, from Equations 34 to 37

$$\lambda_2 = \frac{B \pm \sqrt{B^2 - 4AC}}{2A} \tag{A-1}$$

where, $A = \frac{\gamma+1}{2\gamma}$ (A-2)

$$B = \frac{1 + r\lambda_1 + \frac{n\alpha}{2(T_{op}/T_{p1} - 1)}}{1 + r} \tag{A-3}$$

$$C = \frac{nJ}{2} = \frac{\gamma-1}{2\gamma} J \tag{A-4}$$

$$J = \frac{\bar{\bar{T}}_{o2}/T_{op}}{1 - T_{p1}/T_{op}} \tag{A-5}$$

Since, by definition,

$$U_2 = \lambda_2 V_{p1} \tag{A-6}$$

Therefore

$$\gamma R \, \bar{\bar{T}}_{o2} \left(\frac{T_2}{\bar{\bar{T}}_{o2}}\right) M_2^2 = \lambda_2^2 \, \gamma R \, T_{op} \left(\frac{T_{p1}}{T_{op}}\right) M_{p1}^2 \tag{A-7}$$

or

$$\frac{M_2^2}{1 - \frac{\gamma-1}{2} M_2^2} = \left(\frac{T_{op}}{\bar{\bar{T}}_{o2}}\right) \frac{M_{p1}^2}{1 + \frac{\gamma-1}{2} M_{p1}^2} \lambda_2^2 = \frac{\lambda_2^2}{\gamma C} \tag{A-8}$$

and

$$M_2^2 = \frac{\frac{1}{\gamma C} \lambda_2^2}{1 - \frac{\gamma-1}{2\gamma C} \lambda_2^2} \tag{A-9}$$

From Equation A-1

$$\frac{1}{\gamma C} \lambda_2^2 = \frac{(B^2 - 2AC) \pm B\sqrt{B^2 - 4AC}}{2\gamma C A^2} \tag{A-10}$$

Substituting Equation A-10 into A-9

$$M_2^2 = \frac{2}{\gamma-1} \frac{(B^2 - 2AC) \pm B\sqrt{B^2 - 4AC}}{\left[\frac{4\gamma C A^2}{\gamma-1} - (B^2 - 2AC)\right] \mp B\sqrt{B^2 - 4AC}} \tag{A-11}$$

Using Equation A-2 and A-4 to express C and A in terms of J and γ,

$$M_2^2 = \frac{2}{\gamma-1} \frac{\left(B^2 - \frac{\gamma^2-1}{2\gamma^2} J\right) \pm B\sqrt{B^2 - \frac{\gamma^2-1}{\gamma^2} J}}{\left(\frac{\gamma+1}{\gamma} J - B^2\right) \mp B\sqrt{B^2 - \frac{\gamma^2-1}{\gamma^2} J}} \tag{A-12}$$

Multiply the numerator and the denominator by

$$\left(\frac{\gamma+1}{\gamma} J - B^2\right) \pm B\sqrt{B^2 - \frac{\gamma^2-1}{\gamma^2} J}$$

and rearrange, the expression for M_2^2 becomes,

$$M_2^2 = \frac{1}{\gamma-1} \frac{\left(B^2 - \frac{\gamma-1}{\gamma} J\right) \pm B\sqrt{B^2 - \frac{\gamma^2-1}{\gamma^2} J}}{J - B^2} \tag{A-13}$$

If the first solution has a M_2 of M_{2I} and the second solution has a M_2 of M_{2II} then,

$$M_{2I}^2 = \frac{1}{\gamma-1} \frac{\left(B^2 - \frac{\gamma-1}{\gamma} J\right) - B\sqrt{B^2 - \frac{\gamma^2-1}{\gamma^2} J}}{J - B^2} \tag{A-14}$$

$$M_{2II}^2 = \frac{1}{\gamma-1} \frac{\left(B^2 - \frac{\gamma-1}{\gamma} J\right) + B\sqrt{B^2 - \frac{\gamma^2-1}{\gamma^2} J}}{J - B^2} \tag{A-15}$$

Then,

$$M_{2I}^2 \left[2\gamma M_{2II}^2 - (\gamma-1)\right]$$

$$= \frac{2\gamma}{(\gamma-1)^2} \left[\frac{\left(B^2 - \frac{\gamma-1}{\gamma} J\right)^2 - B^2\left(B^2 - \frac{\gamma^2-1}{\gamma^2} J\right)}{(J - B^2)^2}\right] - \frac{\left(B^2 - \frac{\gamma-1}{\gamma} J\right) - B\sqrt{B^2 - \frac{\gamma^2-1}{\gamma^2} J}}{J - B^2}$$

$$= 2 + (\gamma-1) M_{2II}^2$$

Therefore,

$$M_{2I}^2 = \frac{(\gamma-1)M_{2II}^2 + 2}{2\gamma M_{2II}^2 - (\gamma-1)} \tag{A-16}$$

which is a normal shock relation (Reference 5).

APPENDIX B

ENTROPY EXPRESSION FOR A NON-UNIFORM FLOW FIELD

Assumptions:

1. uniform pressure
2. density: $\rho = \overline{\rho} + \rho'; \quad \overline{\rho} = \frac{1}{X}\int_X \rho dy; \quad \rho' << \overline{\rho}$ (B-1)
3. velocity: $U = \overline{U} + U'; \quad \overline{U} = \frac{1}{X}\int_X U dy; \quad U' << \overline{U}$ (B-2)

The total entropy relative to its freestream value is,

$$S - S_\infty = \int_X c_v \ln \frac{p/p_\infty}{(\rho/\rho_\infty)^\gamma} d\dot{m}$$

$$= c_v \int_X \rho U \ln \frac{p/p_\infty}{(\rho/\rho_\infty)^\gamma} dy$$

$$= c_v \int_X (\overline{\rho} + \rho')(\overline{U} + U') \ln \frac{p/p_\infty}{\left[(\overline{\rho} + \rho')/\rho_\infty\right]^\gamma} dy$$

$$= c_v \overline{\rho}\,\overline{U} \int_X \left(1 + \frac{\rho'}{\overline{\rho}} + \frac{U'}{\overline{U}} + \frac{\rho'U'}{\overline{\rho}\,\overline{U}}\right)\left[\ln \frac{p}{p_\infty} - \gamma \ln \frac{\overline{\rho}}{\rho_\infty} - \gamma \ln\left(1 + \frac{\rho'}{\overline{\rho}}\right)\right] dy \quad \text{(B-3)}$$

Since,

$$\ln (1 + x) = x - \frac{x^2}{2} + \frac{x^3}{3} - \cdots\cdots \quad (\text{for } x^2 \leq 1) \quad \text{(B-4)}$$

then Equation B-3 becomes,

$$S - S_\infty = c_v \overline{\rho}\,\overline{U} \left\{\left(\ln \frac{p}{p_\infty} - \gamma \ln \frac{\overline{\rho}}{\rho_\infty}\right) \int_X \left(1 + \frac{\rho'}{\overline{\rho}} + \frac{U'}{\overline{U}} + \frac{\rho'U'}{\overline{\rho}\,\overline{U}}\right) dy \right.$$

$$\left. - \gamma \int_X \left(1 + \frac{\rho'}{\overline{\rho}} + \frac{U'}{\overline{U}} + \frac{\rho'U'}{\overline{\rho}\,\overline{U}}\right)\left(\frac{\rho'}{\overline{\rho}} - \frac{1}{2}\frac{\rho'^2}{\overline{\rho}^2} + \cdots\cdots\right) dy \right\} \quad \text{(B-5)}$$

Neglecting the terms with order of magnitude higher than 2, and integrate, Equation B-5 becomes,

$$S - S_\infty = c_v \overline{\rho}\,\overline{U}\, X \left[\left(1 + \frac{\overline{\rho'U'}}{\overline{\rho}\,\overline{U}}\right)\left(\ln \frac{p}{p_\infty} - \gamma \ln \frac{\overline{\rho}}{\rho_\infty}\right) - \frac{\gamma}{2}\left(\frac{\overline{\rho'^2}}{\overline{\rho}^2} + 2\frac{\overline{\rho'U'}}{\overline{\rho}\,\overline{U}}\right)\right]$$

$$\simeq c_v \overline{\rho}\,\overline{U}\, X \left(1 + \frac{\overline{\rho'U'}}{\overline{\rho}\,\overline{U}}\right)\left\{\ln \frac{p}{p_\infty} - \gamma\left[\ln \frac{\overline{\rho}}{\rho_\infty} + \frac{1}{2}\left(\frac{\overline{\rho'^2}}{\overline{\rho}^2} + 2\frac{\overline{\rho'U'}}{\overline{\rho}\,\overline{U}}\right)\right]\right\}$$

$$\simeq c_v \bar{\rho}\,\bar{U}\,X\left(1+\frac{\overline{\rho'U'}}{\bar{\rho}\,\bar{U}}\right)\left\{\ln\frac{p}{p_\infty}-\gamma\left\{\ln\frac{\bar{\rho}}{\rho_\infty}+\ln\left[1+\frac{1}{2}\left(\frac{\overline{\rho'^2}}{\bar{\rho}^2}+2\frac{\overline{\rho'U'}}{\bar{\rho}\,\bar{U}}\right)\right]\right\}\right\}$$

$$= c_v \bar{\rho}\,\bar{U}\,X\left(1+\frac{\overline{\rho'U'}}{\bar{\rho}\,\bar{U}}\right)\ln\frac{p/p_\infty}{\left\{\frac{\bar{\rho}}{\rho_\infty}\left[1+\frac{1}{2}\left(\frac{\overline{\rho'^2}}{\bar{\rho}^2}+2\frac{\overline{\rho'U'}}{\bar{\rho}\,\bar{U}}\right)\right]\right\}^{\gamma}} \qquad \text{(B-6)}$$

Since,

$$\dot{m} = \int_X \rho U dy$$

$$= \int_X (\bar{\rho}+\rho')(\bar{U}+U')dy$$

$$= \bar{\rho}\,\bar{U}\,X\left(1+\frac{\overline{\rho'U'}}{\bar{\rho}\,\bar{U}}\right) \qquad \text{(B-7)}$$

therefore Equation (B-6) can be expressed as

$$S - S_\infty = c_v\,\dot{m}\,\ln\frac{p/p_\infty}{\left\{\frac{\bar{\rho}}{\rho_\infty}\left[1+\frac{1}{2}\left(\frac{\overline{\rho'^2}}{\bar{\rho}^2}+2\frac{\overline{\rho'U'}}{\bar{\rho}\,\bar{U}}\right)\right]\right\}^{\gamma}} \qquad \text{(B-8)}$$

APPENDIX C

LINEARIZATION OF $\lambda_2 \left(\frac{p_2}{p_\infty}\right)^{\frac{1}{\gamma}}$ NEAR THE CHOKING LIMIT

Let,
$$x = \sqrt{1 - \frac{4AC}{B^2}} < \frac{1}{\gamma} \tag{C-1}$$

$$y = (\gamma-1)\left(2\frac{\overline{u_2'^2}}{\bar{u}_2^2} + \frac{\overline{\rho_2' u_2'}}{\bar{\rho}_2 \bar{u}_2} - \frac{1}{2} C_F\right) << 1 \tag{C-2}$$

$$z = \frac{J(1+r)^2(\gamma^2-1)}{\gamma^2\left[1 + r\lambda_1 + \frac{n\alpha}{2(T_{op}/T_{pl} - 1)}\right]^2} \tag{C-3}$$

Then, from Equation (92)

$$x^2 = 1 - \frac{4AC}{B^2} = 1 - z\left(1 + \frac{3-\gamma}{\gamma+1}\frac{\overline{u_2'^2}}{\bar{u}_2^2} + \frac{2}{\gamma+1}\frac{\overline{\rho_2' u_2'}}{\bar{\rho}_2 \bar{u}_2} + \frac{\gamma}{\gamma+1} C_F\right) \tag{C-4}$$

Expanding the term,

$$\begin{aligned}
&(1 \pm x)\left[1 \mp \gamma x(1+y)\right]^{1/\gamma} \\
&= (1 \pm x)\left[1 \mp x(1+y) - \frac{\gamma-1}{2}x^2(1+y)^2\right. \\
&\qquad \left. \mp \frac{(\gamma-1)(2\gamma-1)}{6}x^3(1+y)^3 - \frac{(\gamma-1)(2\gamma-1)(3\gamma-1)}{24}x^4(1+y)^4 + \cdots\right] \\
&= (1 \pm x)\left\{\left[1 \mp x - \frac{\gamma-1}{2}x^2 \mp \frac{(\gamma-1)(2\gamma-1)}{6}x^3 - \frac{(\gamma-1)(2\gamma-1)(3\gamma-1)}{24}x^4 + \cdots\right]\right. \\
&\quad \left. + y\left[\mp x - (\gamma-1)x^2 \mp \frac{(\gamma-1)(2\gamma-1)}{2}x^3 - \frac{(\gamma-1)(2\gamma-1)(3\gamma-1)}{6}x^4 + \cdots\right] + \cdots\right\} \\
&= \left[1 - \frac{\gamma+1}{2}x^2 \mp \frac{(\gamma+1)(\gamma-1)}{3}x^3 - \frac{(\gamma+1)(\gamma-1)(2\gamma-1)}{8}x^4 + \cdots\right] \\
&\quad + y\left[\mp x - \gamma x^2 + \cdots\right] + \cdots
\end{aligned} \tag{C-5}$$

Since near the choking limit, $O(x^2) = O(y) = O\left(\overline{u_2'^2}/\bar{u}_2^2\right)$, therefore the leading term of the above equation is,

$$\begin{aligned}
&(1 \pm x)\left[1 \mp \gamma x(1+y)\right]^{1/\gamma} \simeq 1 - \frac{\gamma+1}{2}x^2 \\
&= \frac{1-\gamma}{2} + \frac{\gamma+1}{2}z + z\left(\frac{3-\gamma}{2}\frac{\overline{u_2'^2}}{\bar{u}_2^2} + \frac{\overline{\rho_2' u_2'}}{\bar{\rho}_2 \bar{u}_2} + \frac{\gamma}{2} C_F\right) \\
&= \left(\frac{1-\gamma}{2} + \frac{\gamma+1}{2}z\right)\left[1 + \frac{z}{(1-\gamma)/2 + z(\gamma+1)/2}\left(\frac{3-\gamma}{2}\frac{\overline{u_2'^2}}{\bar{u}_2^2} + \frac{\overline{\rho_2' u_2'}}{\bar{\rho}_2 \bar{u}_2} + \frac{\gamma}{2} C_F\right)\right]
\end{aligned} \tag{C-6}$$

Near the choking limit, $x^2 = O\left(\overline{u_2'^2}/\bar{u}_2^2\right)$, and from Equation C-4,

$$z = 1 + O\left(\overline{u_2'^2}/\bar{u}_2^2\right) \tag{C-7}$$

therefore,

$$\frac{z}{(1-\gamma)/2 + z(\gamma+1)/2} = 1 + O\left(\overline{u_2'^2}/\bar{u}_2^2\right) \tag{C-8}$$

and Equation C-6 becomes,

$$(1 \pm x)\left[1 \mp \gamma x(1 + y)\right]^{1/\gamma}$$

$$\simeq \left(\frac{1-\gamma}{2} + \frac{\gamma+1}{2} z\right)\left(1 + \frac{3-\gamma}{2}\frac{\overline{u_2'^2}}{\bar{u}_2^2} + \frac{\overline{\rho_2' u_2'}}{\bar{\rho}_2 \bar{u}_2} + \frac{\gamma}{2} C_F\right) \tag{C-9}$$

Therefore,

$$\left(1 \pm \sqrt{1 - \frac{4AC}{B^2}}\right)\left\{1 \mp \gamma\sqrt{1 - \frac{4AC}{B^2}}\left[1 + (\gamma-1)\left(2\frac{\overline{u_2'^2}}{\bar{u}_2^2} + \frac{\overline{\rho_2' u_2'}}{\bar{\rho}_2 \bar{u}_2} - \frac{1}{2} C_F\right)\right]\right\}^{\frac{1}{\gamma}}$$

$$\simeq \left\{\frac{1-\gamma}{2} + \frac{J(1 + r)^2(\gamma^2 - 1)(\gamma + 1)}{2\gamma^2\left[1 + r\lambda_1 + \frac{n\alpha}{2(T_{op}/T_{p1} - 1)}\right]^2}\right\}\left(1 + \frac{3-\gamma}{2}\frac{\overline{u_2'^2}}{\bar{u}_2^2} + \frac{\overline{\rho_2' u_2'}}{\bar{\rho}_2 \bar{u}_2} + \frac{\gamma}{2} C_F\right) \tag{C-10}$$

and Equation (94) becomes (near the choking limit)

$$\lambda_2\left(\frac{p_2}{p_\infty}\right)^{\frac{1}{\gamma}} = \frac{\gamma\left[\frac{2}{n\alpha}\left(\frac{T_{op}}{T_{p1}} - 1\right)\right]^{1/\gamma}\left[1 + r\lambda_1 + \frac{n\alpha}{2(T_{op}/T_{p1} - 1)}\right]^{(\gamma+1)/\gamma}}{(p_\infty/p_1)^{1/\gamma}(1 + r)(\gamma + 1)^{(\gamma+1)/\gamma}}$$

$$\times \left\{\frac{1-\gamma}{2} + \frac{J(1 + r)^2(\gamma^2 - 1)(\gamma + 1)}{2\gamma^2\left[1 + r\lambda_1 + \frac{n\alpha}{2(T_{op}/T_{p1} - 1)}\right]^2}\right\}\left(1 - \frac{\gamma-1}{2}\frac{\overline{u_2'^2}}{\bar{u}_2^2} + \frac{\gamma-1}{2} C_F\right) \tag{C-11}$$

REFERENCES

1. Alperin, M., Wu, J. J. and Smith, Ch. A. "The Alperin Jet-Diffuser Ejector (AJDE) Development, Testing, and Performance Verification Report", Flight Dynamics Research Corporation, Naval Weapons Center, NWC TP 5853, February 1976.

2. Alperin, M. and Wu, J. J. "Underwater Ejector Propulsion, Theory and Applications", Flight Dynamics Research Corporation, FDRC 0812-11-76, October 1976.

3. Alperin, M. and Wu, J. J. "Underwater Jer-Diffuser Ejector Propulsion Real Fluid Effects", Flight Dynamics Research Corporation, FDRC 0294-8-78, August 1978.

4. Quinn, B. "Recent Developments in Large Area Ratio Thrust Augmentors", AIAA Paper No. 72-1174, AIAA/SAE 8th Joint Propulsion Specialist Conference, 1972.

5. Ames Research Staff, "Equations, Tables, and Charts for Compressible Flow", NACA Report 1135, 1953.

6. Schlichting, H., Boundary-Layer Theory, McGraw-Hill Book Company, 6th Ed., 1968.

*U.S.Government Printing Office: 1979 — 657-002/55